

MULTIVARIATE DATA ANALYSIS FOR FORCE-, DISPLACEMENT-, AND  
PERFORMANCE-BASED SEISMIC DESIGN OF REINFORCED MASONRY  
SHEAR WALLS

By

Ahmad Sabry Siam

B.Sc., M.Sc.

A Thesis Submitted to the School of Graduated Studies in Partial Fulfillment of  
the Requirements for the Degree Doctor of Philosophy

McMaster University  
©Copyright by Ahmad Siam  
June 2017

Doctor of Philosophy (2017)  
(Civil Engineering)

McMaster University  
Hamilton, Ontario

TITLE:                   MULTIVARIATE DATA ANALYSIS FOR FORCE-,  
DISPLACEMENT-, AND PERFORMANCE-BASED  
SEISMIC DESIGN OF REINFORCED MASONRY  
SHEAR WALLS

AUTHOR:                 Ahmad Sabry Siam  
                              B.Sc., M.Sc. (Cairo University)

SUPERVISORS:         Dr. Wael El-Dakhakhni  
                              Dr. Zoe Li

NUMBER OF PAGES:    xiii,193

## **Abstract**

Over the past decades, seismic analysis and design have been thoroughly addressed by the majority of international building codes and standards. Although seismic damage of structural components typically correlate better to displacement, rather than forces, current seismic codes adopt force-based seismic design (FBSD) approaches. However, in the past two decades, there has been a gradual shift from “strength” to “performance” through the introduction of performance-based seismic design (PBSD) of structural components that can be implemented with relative ease through displacement-based seismic design (DBSD) approaches. For reinforcement masonry shear wall (RMSW), several gaps still exist in implementing FBSD, DBSD and PBSD. Some of these gaps include: quantifying the reliability of the ductility-related parameters when a FBSD approach is adopted; quantifying a reliable maximum lateral load displacement when a DBSD approach is implemented; developing a backbone curve model so that different damage states can be identified when implementing PBSD approach. As such, this dissertation attempts to tackle these issues within the different seismic design approaches.

For FBSD, this study assesses the reliability of eight published plastic hinge models using a large database of experimentally tested RMSW. In addition to assessing model reliability in terms of displacement predictability, this dissertation also specifies calibration factors to further improve the evaluated models. For DBSD, multivariate data analysis technique through the principal component analysis (PCA) technique and partial least square (PLS) analysis technique is utilized to develop an experimentally calibrated RMSW displacement prediction expressions for both the maximum lateral load limit state and the ultimate displacement limit state. These expressions are further utilized to evaluate the parameters influencing RMSW displacement capacities. For PBSD, complete backbone curve model for RMSW under lateral loads is developed in this dissertation and subsequently utilized to generate an analytical RMSW performance database. This large database is further utilized to generate seismic fragility bands that are compared to the FEMA P-58 fragility curves in an effort to represent a more realistic means of quantifying RMSW performance and damage states under different seismic demand levels.

## **Dedications**

*To Sabry & Neibal,  
Magdi & Tahrir,  
Yasmine,  
Omar & Lina*

## **Acknowledgment**

*All praise and gratitude be to ALLAH the most Gracious, The Most Compassionate and the Most Merciful with the blessings Whom the good deeds are fulfilled.*

First, I would like to express my deep gratitude to my supervisor Dr. El-Dakhakhni. I was fortunate to work under an outstanding supervisor who is truly humble, honest, innovative, open minded, energetic, risk-taker, and more. This dissertation would have never materialized if it wasn't for his continuous guidance, support, patience, and encouragement. No words can describe how thankful I am to Dr. El-Dakhakhni. Sincere thanks and gratitude are also due to my co-supervisor Dr. Zoe Li for her advice and innovative ideas. I am especially grateful for the long discussions that significantly improved the quality of the dissertation.

Special thanks to my committee members, Dr. Lydell Wiebe and Dr. Peijun Guo, for their valuable advice and suggestions during the past four years. Their helpful comments and discussions during our meetings are greatly appreciated.

A word of thank is due to all my research teammates: Ahmed Ahmed (Yosri), Dr. Ahmed Ashour, Ahmed Ghith, Dr. Mustafa Siyam, Tarek El-Hashimy, Maysara Ghaith, and Dr. Yasser Khalifa. No words can express my gratified to them and their positive influence on my academic and personal life. Sincere thanks are also due to Shady Salem who is truly my buddy here in Hamilton. He has always been my de-stressor through our continuous academic and non-academic arguments. I would be remiss if I did not acknowledge my friend dear Dr. Mohammed Ezzeldin who has always been my mentor and edited the introduction and conclusion chapters of this dissertation.

At last, but by no means the least, I would like to express my sincere gratitude to my family for their unparalleled love and support. I am grateful to Yasmine (my wife) for being there for me. Her support, encouragement, patience, and unwavering love were undeniably the rock upon which my life has been built for the past six years. I will also be forever indebted to my parents for giving me the opportunities and experiences that made me who I am today. They selflessly encouraged me to explore new directions in life and seek my own destiny. This journey would have not been possible if not for them. Finally, special thanks to Amr Abdellatif, Raghad Abdellatif, Jouda Kuk, and Jennifer Hompoth for being my extended family here in Hamilton and for always keeping my family and I feel at home.

## **Co-Authorship**

This dissertation had been prepared in accordance with the regulation for a sandwich thesis format, a compilation of research paper stipulated by the faculty of graduate studies at McMaster University. This research presents analytical work carried out solely by Ahmad Siam. Dr. Wael El-Dakhakhni provided advice and guidance on Chapters 2, 3 and 4. Drs. Marwan Shedid and Yiping Guo provided additional advice and guidance on Chapter 2. Dr. Wessam Hussien provided additional advice and guidance on Chapter 3. Dr. Zoe Li provided additional advice and guidance on Chapter 4.

### **Chapter 2**

Siam A. S., Ezzeldin M., and El-Dakhakhani W. W. “Reliability of Displacement Capacity Prediction Models for Reinforced Concrete Block Shear Walls” *ASCE Journal of Structure Engineering*, submitted, April 2017

### **Chapter 3**

Siam, A. S., Hussein, W. M., and El-Dakhakhni, W. W. (2017). “Scoring Models for Reinforced Masonry Shear Wall Maximum Displacement Prediction under Seismic Loads.” *Engineering Structures*, 136, 511-522.

### **Chapter 4**

Siam, A., El-Dakhakhni, W., & Li, Z. (2017). “Seismic Risk Assessment of Reinforced Masonry Structural Wall Systems Using Multivariate Data Analysis.” *Engineering Structures*, 144, 58-72.

## TABLE OF CONTENTS

<b>1</b>	<b>INTRODUCTION .....</b>	<b>1</b>
<b>1.1</b>	<b>BACKGROUND AND MOTIVATION .....</b>	<b>1</b>
1.1.1	Seismic Design Approaches .....	2
1.1.2	Statistical Techniques .....	6
<b>1.2</b>	<b>RESEARCH OBJECTIVES.....</b>	<b>9</b>
<b>1.3</b>	<b>ORGANIZATION OF THE DISSERTATION .....</b>	<b>9</b>
<b>1.4</b>	<b>REFERENCE .....</b>	<b>11</b>
<b>2</b>	<b>RELIABILITY OF DISPLACEMENT CAPACITY PREDICTION MODELS FOR REINFORCED CONCRETE BLOCK SHEAR WALLS ..</b>	<b>17</b>
<b>2.1</b>	<b>ABSTRACT.....</b>	<b>17</b>
<b>2.2</b>	<b>INTRODUCTION.....</b>	<b>18</b>
<b>2.3</b>	<b>DISPLACEMENT CAPACITY PREDICTION MODELS .....</b>	<b>21</b>
2.3.1	Paulay And Priestley’s (1993) Model.....	23
2.3.2	Priestley And Calvi’s (1996) Model.....	23
2.3.3	Panagiotakos and Fardis’s (2001) Model .....	24
2.3.4	Euro Code 8’s (2005) Model .....	26
2.3.5	Priestley et al.’s (2007) Model.....	27
2.3.6	Bohl and Adebar’s (2011) Model .....	28
2.3.7	Kazaz’s (2013) Model.....	28
2.3.8	Shedid and El-Dakhakhni’s (2013) Model .....	29
<b>2.4</b>	<b>EXPERIMENTAL WALL SEISMIC PERFORMANCE DATABASE .....</b>	<b>31</b>
<b>2.5</b>	<b>ASSESSMENT OF CURRENT DISPLACEMENT CAPACITY MODELS .....</b>	<b>34</b>
<b>2.6</b>	<b>VALIDATION OF THE NORMALITY ASSUMPTION.....</b>	<b>37</b>
<b>2.7</b>	<b>DISCUSSION.....</b>	<b>38</b>
<b>2.8</b>	<b>MODEL PREDICTION CAPABILITY IMPROVEMENT .....</b>	<b>40</b>
<b>2.9</b>	<b>INFLUENCE OF DESIGN CHARACTERISTICS ON WALL DRIFT CAPACITIES... ..</b>	<b>43</b>
<b>2.10</b>	<b>CONCLUSIONS.....</b>	<b>46</b>
<b>2.11</b>	<b>ACKNOWLEDGMENTS.....</b>	<b>47</b>
<b>2.12</b>	<b>APPENDIX I.....</b>	<b>48</b>
2.12.1	Calculation of Yield and Ultimate Curvature .....	48
<b>2.13</b>	<b>NOTATION.....</b>	<b>49</b>
<b>2.14</b>	<b>REFERENCE .....</b>	<b>51</b>
<b>3</b>	<b>SCORING MODELS FOR REINFORCED MASONRY SHEAR WALL MAXIMUM DISPLACEMENT PREDICTION UNDER SEISMIC LOADS.....</b>	<b>73</b>
<b>3.1</b>	<b>ABSTRACT.....</b>	<b>73</b>
<b>3.2</b>	<b>INTRODUCTION.....</b>	<b>74</b>
<b>3.3</b>	<b>MODEL PARAMETERS .....</b>	<b>76</b>
3.3.1	Flexural Deformation.....	77
3.3.2	Shear Deformation Parameters .....	79

<b>3.4</b>	<b>EXPERIMENTAL DATABASE .....</b>	<b>81</b>
<b>3.5</b>	<b>MULTI VARIATE DATA ANALYSIS (MVDA) THEORY .....</b>	<b>83</b>
3.5.1	Principal Component Analysis (PCA) Background .....	83
3.5.2	Projection to Latent Structures (PLS) Background .....	84
<b>3.6</b>	<b>PCA IMPLEMENTATION ON THE EXPERIMENTAL DATABASE .....</b>	<b>86</b>
<b>3.7</b>	<b>PROPOSED SCORING MODEL .....</b>	<b>88</b>
<b>3.8</b>	<b>MODEL PERFORMANCE CHARTS.....</b>	<b>92</b>
3.8.1	Influence of Masonry Compressive Strength .....	93
3.8.2	Influence of Axial Load .....	95
3.8.3	Influence of Shear Reinforcement .....	96
3.8.4	Influence of Vertical Reinforcement .....	97
<b>3.9</b>	<b>DISCUSSION.....</b>	<b>99</b>
<b>3.10</b>	<b>CONCLUSIONS.....</b>	<b>100</b>
<b>3.11</b>	<b>ACKNOWLEDGMENTS.....</b>	<b>103</b>
<b>3.12</b>	<b>NOTATION.....</b>	<b>103</b>
<b>3.13</b>	<b>REFERENCE .....</b>	<b>105</b>
<b>4</b>	<b>SEISMIC RISK ASSESSMENT OF REINFORCED MASONRY STRUCTURAL WALL SYSTEMS USING MULTIVARIATE DATA ANALYSIS .....</b>	<b>127</b>
<b>4.1</b>	<b>ABSTRACT.....</b>	<b>127</b>
<b>4.2</b>	<b>INTRODUCTION.....</b>	<b>128</b>
<b>4.3</b>	<b>AVAILABLE BACKBONE PREDICTION MODELS.....</b>	<b>131</b>
<b>4.4</b>	<b>MODEL PREDICTION ASSESSMENTS .....</b>	<b>134</b>
4.4.1	Cracking Limit State .....	136
4.4.2	Yield Limit State .....	137
4.4.3	Maximum Strength Limit State .....	139
4.4.4	Ultimate Displacement Limit State (at 20% Strength Degradation)	141
4.4.5	Discussion .....	143
<b>4.5</b>	<b>MULTIVARIATE-BASED MODEL DEVELOPMENT.....</b>	<b>144</b>
4.5.1	Principal Component Analysis (PCA) .....	145
4.5.2	Partial Least Square (PLS) Analysis .....	148
<b>4.6</b>	<b>INFLUENCE OF DIFFERENT WALL DESIGN PARAMETERS ON BACKBONE CURVE.. .....</b>	<b>150</b>
<b>4.7</b>	<b>FRAGILITY BAND DEVELOPMENT.....</b>	<b>152</b>
<b>4.8</b>	<b>CONCLUSION .....</b>	<b>156</b>
<b>4.9</b>	<b>ACKNOWLEDGMENT .....</b>	<b>157</b>
<b>4.10</b>	<b>NOTATION.....</b>	<b>158</b>
<b>4.11</b>	<b>REFERENCES.....</b>	<b>160</b>
<b>5</b>	<b>SUMMARY, CONCLUSIONS, AND RECOMMENDATIONS .....</b>	<b>187</b>
<b>5.1</b>	<b>SUMMARY .....</b>	<b>187</b>
<b>5.2</b>	<b>CONCLUSIONS.....</b>	<b>188</b>
<b>5.3</b>	<b>RECOMMENDATION FOR FUTURE RESEARCH.....</b>	<b>192</b>

## List of Figures

Figure 1.1: (a) Equal energy (b) equal displacement approaches .....	15
Figure 1.2: Design acceleration response spectrum (Kowalsky et al. 1995)..	15
Figure 1.3: Effective stiffness for DBSD approach (Priestley et al. 2007) .....	16
Figure 1.4: Overview of PCA for three variables and two principle components.....	16
Figure 2.1: Typical Reinforced concrete block shear wall (RCBSW) configuration; a) Rectangular cross section; b) Elevation.....	64
Figure 2.2: Idealized representation of plastic hinge (Paulay and Priestley 1992).....	65
Figure 2.3: Sample linear regression plot of models; a) Paulay and Priestley (1993); b) Priestley and Calvi (1996).....	66
Figure 2.4: Linear regression lines for the eight models. ....	67
Figure 2.5: Sample residual plot of models; a) Paulay and Priestley (1993) (b) Priestley and Calvi (1996). ....	68
Figure 2.6: Normal probability plot of residuals. ....	69
Figure 2.7: Ranked residuals from different calibrated models.....	70
Figure 2.8: Influence of different wall characteristics on the drift capacity using the calibrated model of Shedid and El-Dakhakhni (2013); a) The masonry compressive strength; b) The axial load ratio. ....	71
Figure 3.1: Typical RMSW cross section and elevation.....	115
Figure 3.2: Extracting scores and loadings plot data for three variables....	116
Figure 3.3: Scatter plot to evaluate the applicability of using MVDA.....	117

<b>Figure 3.4: PCA for the RMSW database: (a) Scores plot; and (b) Loadings plot for all variables.....</b>	<b>118</b>
<b>Figure 3.5: PLS analysis of the RMSW database plain parameter: (a) scores plot; and (b) loadings plot.....</b>	<b>119</b>
<b>Figure 3.6: Variable important for projection (VIP) plot for PLS of the RMSW database. ....</b>	<b>120</b>
<b>Figure 3.7: PLS analysis of the RMSW database proposed model parameters: (a) Scores plot; and (b) loadings plot .....</b>	<b>121</b>
<b>Figure 3.8: Actual to predicted RMSW database drifts.....</b>	<b>122</b>
<b>Figure 3.9: Influence of masonry compressive strength on scenario RMSW drift capacities.....</b>	<b>123</b>
<b>Figure 3.10: Influence of axial load on scenario RMSW drift capacities. ...</b>	<b>123</b>
<b>Figure 3.11: Influence of shear reinforcement on scenario RMSW drift capacities: (a) constant spacing with different bar diameters; and (b) constant bar diameter with different spacing .....</b>	<b>124</b>
<b>Figure 3.12: Influence of vertical reinforcement on scenario RMSW drift capacities: (a) constant spacing with different bar diameters; and (b) constant bar diameter with different spacing. ....</b>	<b>125</b>
<b>Figure 3.13: Bounds of scenario RMSW drift capacities. ....</b>	<b>126</b>
<b>Figure 4.1: Experimental versus analytical predictions of drifts at the yield limit state. ....</b>	<b>170</b>
<b>Figure 4.2: Push and pull experimental drifts at the maximum strength limit state. ....</b>	<b>171</b>
<b>Figure 4.3: Experimental versus analytical predictions of drifts at the maximum strength limit state.....</b>	<b>172</b>
<b>Figure 4.4: Model prediction evaluation at the maximum strength limit state: (a) push direction; and (b) pull direction. ....</b>	<b>173</b>

<b>Figure 4.5: Push and pull experimental drifts at the ultimate displacement limit state. ....</b>	<b>174</b>
<b>Figure 4.6: Experimental versus analytical predictions of drifts at the ultimate displacement limit state. ....</b>	<b>175</b>
<b>Figure 4.7: Model prediction evaluation at the ultimate displacement limit state: (a) push direction; and (b) pull direction. ....</b>	<b>176</b>
<b>Figure 4.8: (a) Score plot for all database (b) Loading plot for all variables .....</b>	<b>177</b>
<b>Figure 4.9: PLS, (a)score plot. (b) loading plot .....</b>	<b>178</b>
<b>Figure 4.10: (a) Score plot and (b) loading plot for the proposed model.....</b>	<b>179</b>
<b>Figure 4.11: Proposed model drifts compare to experimental data limits.</b>	<b>180</b>
<b>Figure 4.12: Influence of changing the axial stress ratio and masonry compressive strength on wall backbone curves. ....</b>	<b>181</b>
<b>Figure 4.13: Backbone curves and DS variation for different wall aspect ratio. (L=2,400 mm, default scenario).....</b>	<b>182</b>
<b>Figure 4.14: Effect of <math>f'_m</math> variability on the fragility curves.....</b>	<b>183</b>
<b>Figure 4.15: Effect of axial stress variability on the fragility curves. ....</b>	<b>184</b>
<b>Figure 4.16: Effect of <math>\rho_{sh}</math> variability on the fragility curves.....</b>	<b>185</b>
<b>Figure 4.17: Effect of <math>\rho_v</math> variability on the fragility curves. ....</b>	<b>186</b>

## List of Tables

<b>Table 2.1: Characteristics of experimental wall database .....</b>	<b>56</b>
<b>Table 2.2: Yield, ultimate curvatures, and drift capacities of wall database</b>	<b>59</b>
<b>Table 2.3: Plastic hinge and displacement capacity models.....</b>	<b>62</b>
<b>Table 2.4: Regression analysis results.....</b>	<b>62</b>
<b>Table 3.1: Characteristics of wall database.....</b>	<b>111</b>
<b>Table 3.2: Coefficients of the proposed ultimate displacement prediction model .....</b>	<b>114</b>
<b>Table 3.3: Range of wall characteristics for the performance chart scenarios and default wall scenario.....</b>	<b>114</b>
<b>Table 4.1: The experimental RMSW database .....</b>	<b>166</b>
<b>Table 4.2: Average ratio between model predictions and experimental drifts .....</b>	<b>168</b>
<b>Table 4.3: Proposed model calibration coefficient.....</b>	<b>169</b>
<b>Table 4.4: Design parameters and default scenario for the analytical wall database .....</b>	<b>169</b>

## **CHAPTER 1**

### **INTRODUCTION**

#### **1.1 BACKGROUND AND MOTIVATION**

The poor performance of *unreinforced* masonry structures during earthquakes [e.g. Napier in Hawke's Bay, New Zealand (1931) and El Centro in California, USA (1940)] has clearly illustrated their vulnerability as a seismic force resisting system (SFRS). As such, North American codes require masonry buildings in seismic zones, to be fully- or partially grouted and detailed with horizontal and vertical reinforcement to improve the buildings performance during seismic events. However, similar to other SFRS, it is not economical to design reinforced masonry shear wall (RMSW) systems to remain elastic under seismic events. Subsequently, similar to other international seismic design provisions, North American codes allow some damages to occur within localized zones of the SFRS (Paulay and Priestly 1992), provided that such damage would not result in a structural collapse and would develop in a ductile manner. In this respect, three alternative design approaches (force-, displacement-, performance-based seismic design) are commonly used for SFRS, including those constructed of RMSW to meet different performance objectives. These approaches will be explained next as they are directly related to the scope and objectives of the dissertation.

### 1.1.1 Seismic Design Approaches

Force-based seismic design (FBSD) approach (Housner 1956 and Tabinashi 1956) adopts seismic response/force modification factors (e.g.  $R_d$  in Canada) to account for the reduction in the seismic forces on the inelastic SFRS relative to its equivalent elastic counterpart (NBCC 2015). Such factors usually relate the inelastic displacement of the SFRS to the corresponding expected displacement of the elastic system and, as such, these factors depend on the *ductility* of the structure under consideration. The ductility is defined by Park (1989) as “*the ability of a structure to undergo large deformations in the inelastic range without a substantial reduction in strength*”. As such, the displacement ductility,  $\mu_\Delta$ , of a structure can be used as a possible measure of system ductility. Regardless of the measure, the provision of ductility will, in turn, allow such a SFRS, with proper reinforcement detailing, to sustain large inelastic deformations without a major loss of strength and stiffness. In this respect, two different assumptions are studied by researchers to estimate this ductility and subsequently the associated response modification factors (Lu et al. 2001). First, the *equal energy* assumption depends on the energy imposed on an elastic structure that could be similarly dissipated by an equivalent (i.e. of equal elastic stiffness) inelastic system, as shown in Figure 1.1(a). According to this assumption, the relationship between  $R_d$  and  $\mu_\Delta$  is given by:  $R_d = \sqrt{2\mu_\Delta - 1}$ . However, the assumption of dissipating equal energy might require the inelastic structure to have significantly high displacement capacity. Therefore,

several researchers argued that the elastic and inelastic systems would not possess the same energy capacity, and, instead, they would have the same displacement capacity (Newmark and Hall 1969, Lai and Biggs 1980). The *equal displacement* assumption equates the displacement of an elastic system to that of the corresponding inelastic (elastic-perfect-plastic) system (Veletsos and Newmark 1960), which yields to  $R_d = \mu_\Delta$ , as shown in Figure 1.1(b). The choice either of these two assumptions, during the design stage, depends mainly on the period of the structure under consideration, as shown Figure 1.2 (Kowalsky et al. 1995), whereas the *equal energy* assumption is typically used for relatively short period structures, because the inelastic displacements are usually greater than the those of the corresponding elastic one with the same stiffness. As the period of the structures increases, the inelastic and inelastic responses become equivalent, leading to the adoption of the equal displacement assumption (Kowalsky et al. 1995).

FBSD procedure assumes that the stiffness of the structure is essentially independent of its strength (Priestley 2000). More specifically, the structure is expected to maintain the same period as its fundamental *elastic* one, irrespective of the seismic base shear demand imposed on the structure, which often pushes the structure beyond its elastic response range. However, Smith and Tso (2002) showed that stiffness and strength are coupled for several reinforced concrete components (i.e. piers, flexural shear walls, and ductile moment resisting frames). This finding led to inconsistency between the assumed and the actual stiffness of the structure being considered. Subsequently, this inconsistency would affect the estimated

displacement ductility demand and thus the seismic displacement using the FBSD approaches. As such, the displacement-based seismic design (DBSD) approach focuses on the displacements as the basis for the design through specifying a target displacement rather than a displacement limit. Within this approach, stiffness is not an input variable but is instead the end result or the output (Kowalsky et al. (1995), Calvi and Kingsley (1995), Priestley and Calvi (1997), Priestley and Kowalsky (2000), and Priestley et al. (2007)).

The DBSD approach characterizes the structure by a secant stiffness,  $K_e$ , at a target displacement,  $\Delta_{Q_{\max}}$ , associated with the maximum strength limit,  $Q_{\max}$ , and equivalent viscous damping ratio,  $\zeta_{eq}$ , as shown in Fig 1.3. This approach is iterative as it aims at reaching an appropriate design that has the ability to achieve the target displacement. The first step in this iterative approach is to specify the target displacement by either the serviceability criterion or the ultimate lateral displacement criterion (e.g. the code drift limits). Then, after calculating the yield displacement,  $\Delta_y$ , the corresponding displacement ductility,  $\mu_\Delta$ , and the effective equivalent viscous damping ratio,  $\zeta_{eq}$ , can be evaluated. Afterwards, the effective period of the structure can be obtained,  $T_e$ , from the displacement response spectrum and subsequently the effective stiffness,  $K_e$ , can be evaluated as well. Finally, the design base shear is evaluated by multiplying the effective stiffness  $K_e$  by the corresponding displacement (Priestley et al. 2007). One of the major requirements of the DBSD approach is defining the yield- and the maximum lateral

load limit states. As such, a reliable load-displacement relationship is key to identify the yield limit state and the maximum target displacement that RMSW can be designed for.

Finally, the performance-based seismic design (PBSD) approach has the capability to design buildings with a realistic and reliable understanding of the risk to life, occupancy, and economic loss that may occur as a result of future seismic hazard events (Priestley 2000). This approach has been introduced over the past three decades by several researchers (Wallace and Moehle 1992; Moehle 1992; Priestley 1993; Priestley 2000; and Priestley et al. 2007). In addition, various guidelines recently adopted PBSD to analyze and design new SFRS [e.g. SEAOC Vision (2002) (1995), ATC-40 (1996), FEMA 356 (2000), FEMA 445 (2006)]. Improvement in the SFRS performance, through the adoption of PBSD approach, has been highlighted also by several researchers (Chandler and Lam 2001). Moreover, the next generation of seismic codes and standards is expected to enable codifying paradigm shift from “strength- and displacement-” to “performance-” based design (Bommer and Pinho 2006). In PBSD, the desired performance level is selected by the stakeholder(s). Afterwards, a numerical model of the structure is subjected to an input ground motion or earthquake hazard level and is subsequently evaluated to achieve this desired performance. Finally, the structure is continuously altered, by changing its design parameters, until an acceptable performance level is achieved. Assessment of structures in this approach is currently expressed in terms of discrete performance levels (e.g. Operational, Immediate Occupancy, Life

Safety, and Collapse Prevention) whereas these levels can be quantified/related to the lateral displacement capacities (FEMA P-58 2012).

Overall, and regardless of which RMSW seismic design approaches are adopted, several knowledge gaps, pertaining to several aspects, are highlighted by several researchers. For example, in FBSD, an estimation of the response modification factor requires a reliable evaluation of the equivalent plastic hinge length of the wall to accurately calculate the inelastic displacement and subsequently the wall ductility. Also, in DBSD approach, the quantification of a reliable  $\Delta_{Q_{max}}$  is of a great interest to many researchers to identify the wall load-displacement relationship envelope. In addition, for the PBSO approach, different RMSW require linkage to corresponding engineering demand parameters (e.g. drift limits) or damage states. In order to address some of the challenges pertaining to FBSD, DBSD, and PBSO, different statistical techniques are introduced in this dissertation to analyze the seismic response RMSW. These techniques are utilized to develop an accurate and reliable load-displacement relationship (e.g. backbone curve) that can be used when different design approaches of flexurally dominated RMSW are adopted.

### **1.1.2 Statistical Techniques**

Statistics can be defined as the method of collecting, analyzing, interpreting, and drawing conclusions from data (Dixon and Massey 1969, Agresti and Finlay

1999). As different statistical techniques (e.g. linear regression and multivariate data analysis) will be used throughout the dissertation, a brief overview on these techniques is presented in this section.

### 1.1.2.1 Linear regression analysis

Regression analysis is typically used to evaluate the relationship between one or more dependent and independent variables (Montgomery et al. 1992). There are three main types of regression analysis (Draper 1966): 1) *simple linear regression* assumes a linear relationship between the dependent variable and the independent variable; 2) *multiple linear regression* assumes that the dependent variable is a linear function of more than one independent variable; 3) *nonlinear regression* assumes a nonlinear relationship between dependent and independent variables.

Within the aforementioned types of regression analyses, *residual analysis* is always required to evaluate the deviation of the dependent value from its expected value. This deviation (error) is usually assumed to be normally distributed with zero mean and constant variance (Montgomery et al. 1992). The normality assumption is validated using the normal probability paper. In addition to the normality validation, the residual plot and the relative root mean square error are implemented to obtain a better assessment of the regression model.

### 1.1.2.2 Multivariate data analysis (MVDA)

In regression analysis, one of the implicit assumptions is that independent variables are both statically independent and uncorrelated. However, applying multivariate data analysis (MVDA) to datasets overcomes this assumption. Multivariate data contains much more observed and measured datasets than univariate datasets (Lattin et al. 2003). MVDA manipulates datasets to express the datasets information in a comprehensible way. Afterwards, MVDA results are interpreted to relate the scientific technical content to the objectives of the investigation. This dissertation uses two different MVDA methods: 1) principal component analysis (PCA); and 2) partial least squares/projections to latent structures (PLS). The PCA linearly transforms a set of variables into a substantially smaller set of uncorrelated variables, representing most of the information in the original set (Jackson 1993). Figure 1.4 shows a graphical representation of the simple case of three variables and two principal components. As can be seen in the figure, two PCs form a plane that represents a *viewing window* into the multidimensional space. PCA is limited to capture only the characteristics of the independent variables (explanatory variables). Subsequently, the PCA method is incapable of answering how much independent variable may be related to the dependent variable (response variable) per se. On the other hand, the PLS method does not only overcome the PCA limitations (Wold et al 1984), but also provides a mathematical model that relates the dependent- to independent variables (Maitra and Yan 2008).

## **1.2 RESEARCH OBJECTIVES**

This dissertation aims at quantifying reliable parameters to be employed within different seismic design approaches (FBSD, DBSD, and PBSB) of RMWS. To achieve this goal, the following objectives are identified:

- 1) Assessing the reliability of RMWS displacement ductility models available in literature, when the FBSD approach is adopted. Subsequently proposing improvement to such models and evaluating the different impact of RMSW design characteristics on model response.
- 2) Developing an analytical model that can quantitatively evaluate the displacement associated with the peak lateral load for RMSW, when the DBSD approach is adopted, and evaluating the model response to different geometrical and mechanical RMSW characteristics.
- 3) Developing an analytical model, for RMSW backbone curve prediction, that accounts for both the flexural and shear deformation components using MVDA, and linking the model to different damage states associated with PBSB. Subsequently, the model is used to develop RMSW fragility *bands* as an alternative to the fragility *curves*, currently adopted in the FEMA P-58.

## **1.3 ORGANIZATION OF THE DISSERTATION**

This section summarizes the content of each of the five chapters in the dissertation as follows:

- Chapter 1 introduces the background and the objectives of the research work as well as an overview of the different statistical techniques implemented in this dissertation.
- Chapter 2 presents the evaluation of RMSW ductility, within the FBSD framework, through performing reliability analysis of eight relevant models available in the literature. These models have been originally proposed to evaluate reinforced concrete shear walls or RMSW plastic displacements utilizing the idealized plastic hinge concept. The analysis is facilitated using a collected experimental database by applying both linear regression and residual analyses.
- Chapter 3 utilizes MVDA methods to develop a reliable model that can be used, within the DBSD approach, to estimate the displacement associated with RMSW peak lateral load. The developed model evaluates the displacements using the wall geometrical and mechanical parameters. The model is also capable of quantifying the flexural and shear displacement components separately. In addition, the model can be used with any consistent set of units (i.e. dimensionless). Finally, the model is utilized to evaluate the geometrical and mechanical parameters influencing RMSW response.
- Chapter 4 presents the development of a RMSW backbone curve, as it relates to the PBSB approach. The FEMA P-58 (2012) defines different damage states linked to lateral wall drift levels. As such, this chapter

assesses four published backbone models relative to an experimental RMSW database results. Afterwards, this chapter develops a reliable experimentally calibrated backbone curve (model) using PCA and PLS approaches. The model is further utilized to obtain different damage states and develop alternative concepts for seismic fragility prediction.

- Chapter 5 presents summary, conclusions, and recommendation for future work related to the work presented in this dissertation.

#### **1.4 REFERENCE**

- Agresti A, Agresti BF. *Statistical Methods for the Sciences*. Upper Saddle River, NJ. 1999.
- ATC A. 40, *Seismic evaluation and retrofit of concrete buildings*. Applied Technology Council, report ATC-40. Redwood City. 1996.
- Bommer JJ, Pinho R. Adapting earthquake actions in Eurocode 8 for performance-based seismic design. *Earthquake Engineering & Structural Dynamics*. 2006 Jan 1;35(1):39-55.
- Calvi GM, Priestley MJ, Kowalsky MJ. Displacement-based seismic design of structures. In: *3rd National Conference on Earthquake Engineering and Engineering Seismology*; 2008.
- Chandler AM, Lam NT. Performance-based design in earthquake engineering: a multi-disciplinary review. *Engineering structures*. 2001 Dec 31;23(12):1525-43.
- Dixon WJ, Massey FJ. *Introduction to statistical analysis*. New York: McGraw-Hill; 1969.

- Draper NR, Smith H, Pownell E. Applied regression analysis. New York: Wiley; 1966 Mar.
- Estados Unidos Federal Emergency Management Agency. FEMA.. Prestandard and commentary for the seismic rehabilitation of buildings. FEMA; 2000.
- FEMA 306. Evaluation of Earthquake Damaged Concrete and Masonry Wall Buildings. Applied Technology Council, Washington, DC, 1998.
- FEMA-445, Next-generation performance-based seismic design guidelines-program plan for new and existing building. Applied Technology Council, Washington, DC, 2006.
- FEMA P-58. Seismic Performance Assessment of Buildings. Applied Technology Council, Washington, D.C, 2012.
- FEMA P-58/BD-3.8.10. Damage State and Fragility Curves for Reinforced Masonry Shear Walls. FEMA P-58/BD-3.8.10, Applied Technology Council, Washington, DC, 2009.
- Housner GW. Limit design of structures to resist earthquakes. InProc. of 1st WCEE 1956 (pp. 5-1).
- Jackson DA. Stopping rules in principal components analysis: a comparison of heuristical and statistical approaches. Ecology. 1993 Dec 1;74(8):2204-14.
- Kapoi CM. Experimental performance of concrete masonry shear walls under in-plane loading (Doctoral dissertation, Washington State University) 2012.
- Kowalsky MJ, Priestley MN, Macrae GA. Displacement-based design of RC bridge columns in seismic regions. Earthquake engineering & structural dynamics. 1995 Dec 1;24(12):1623-43.
- Lai SS, Biggs JM. Inelastic response spectra for aseismic building design. Journal of the Structural Division. 1980 Jun;106(6):1295-310.
- Lattin JM, Carroll JD, Green PE. Analyzing multivariate data. Pacific Grove, CA: Thomson Brooks/Cole; 2003 Jan.

- Lu Y, Hao H, Carydis PG, Mouzakis H. Seismic performance of RC frames designed for three different ductility levels. *Engineering Structures*. 2001 May 31;23(5):537-47.
- Maitra S, Yan J. Principle component analysis and partial least squares: Two dimension reduction techniques for regression. *Applying Multivariate Statistical Models*. 2008 Jun 15;79.
- Moehle JP. Displacement-based design of RC structures subjected to earthquakes. *Earthquake Spectra* 1992;8(3):403–28.
- Montgomery DC, Peck EA, Vining GG. *Introduction to linear regression analysis*. John Wiley & Sons; 1992.
- NBCC. 2015. *National Building Code of Canada*. Institute for Research in Construction, National Research Council of Canada, Ottawa, Ont.
- Newmark NM, Hall WJ. Seismic design criteria for nuclear reactor facilities. In *Proceedings of the 4th World Conference on Earthquake Engineering* 1969 Jan 13 (Vol. 4, pp. 37-50).
- Paulay T., and Priestly, M. *Seismic design of reinforced concrete and masonry buildings*. Wiley, New York 1992.
- Priestley MJ, Calvi GM. Concepts and procedures for direct displacement-based design and assessment. In *Proc. International Conference on Seismic Design Methodologies for the Next Generation of Codes* 1997 Jun 24 (pp. 171-182).
- Priestley MN. Myths and fallacies in earthquake engineering—conflicts between design and reality. *Bull New Zealand Natl Soc Earthquake Eng* 1993;26(3):329–41.
- Priestley MJ. Performance based seismic design. *Bull New Zealand Soc Earthquake Eng* 2000;33(3):325–46.
- Priestley MJN, Calvi GM, Kowalsky MJ. *Displacement-based seismic design of structures*. Pavia, Italy: IUSS Press; 2007.

- SEAOC Vision 2000 Committee. Performance-based seismic engineering.” Structural Engineers Association of California, Sacramento, California. 1995.
- Smith RS, Tso WK. Inconsistency of force-based design procedure. *Journal of Seismology and Earthquake Engineering*. 2002 Jan 1;4(1):47.
- Tanabashi R. Studies on the nonlinear vibrations of structures subjected to destructive earthquakes. In *World Conference on Earthquake Engineering 1956* Jun.
- Tomazevic M. *Earthquake-resistant design of masonry buildings*. World Scientific; 1999 Jul 5.
- Veletsos AS, Newmark NM. Effect of inelastic behavior on the response of simple systems to earthquake motions. In *Proceedings of the 2nd world conference on earthquake engineering 1960* Jul 11 (Vol. 2, pp. 895-912).
- Wallace JW, Moehle JP. Ductility and detailing requirements of bearing wall buildings. *Journal of Structural Engineering*. 1992 Jun;118(6):1625-44.
- Wold S, Ruhe A, Wold H, Dunn, III WJ. The collinearity problem in linear regression. The partial least squares (PLS) approach to generalized inverses. *SIAM Journal on Scientific and Statistical Computing*. 1984 Sep;5(3):735-43.

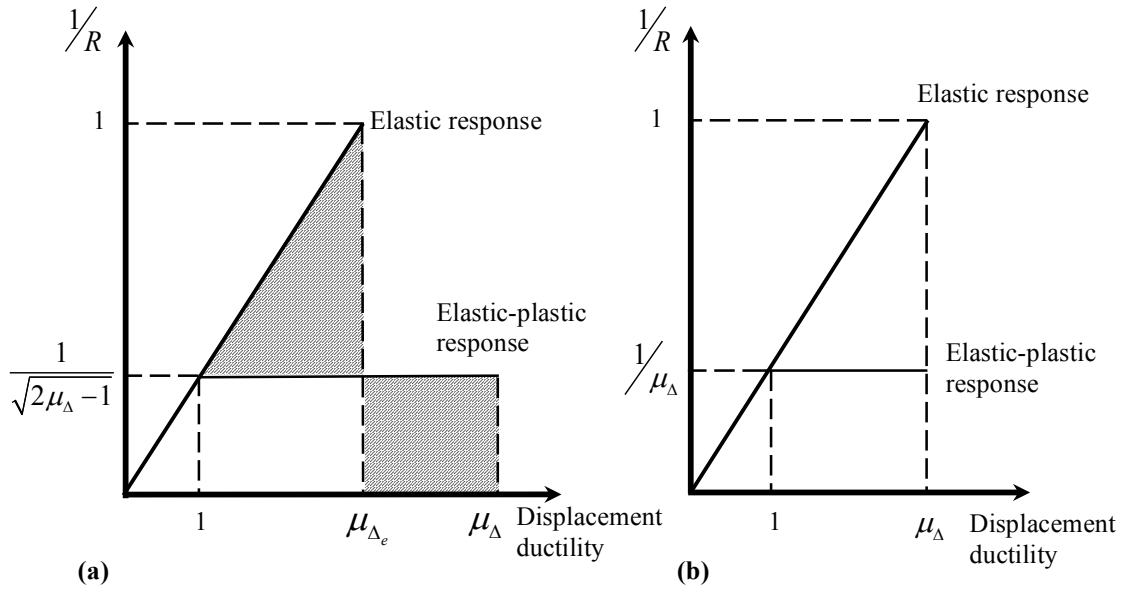


Figure 1.1: (a) Equal energy (b) equal displacement approaches

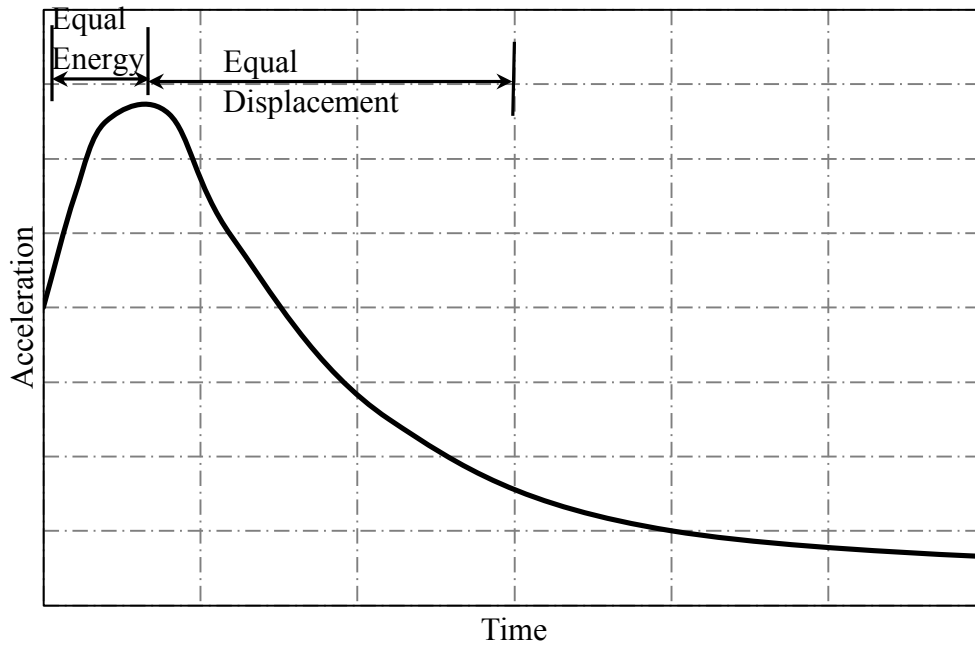


Figure 1.2: Design acceleration response spectrum (Kowalsky et al. 1995)

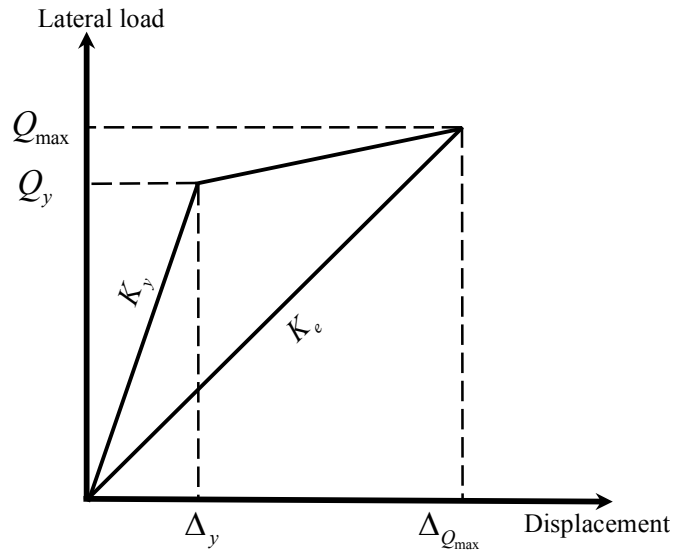


Figure 1.3: Effective stiffness for DBSD approach (Priestley et al. 2007)

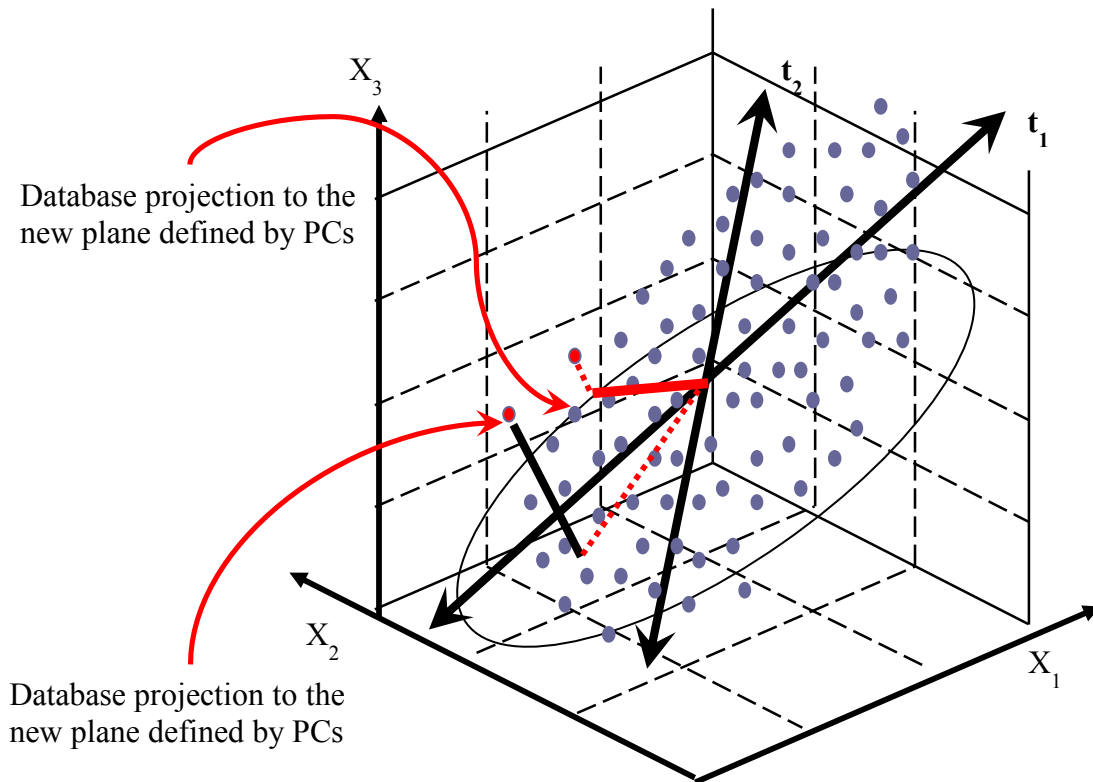


Figure 1.4: Overview of PCA for three variables and two principle components.

## **CHAPTER 2**

### **RELIABILITY OF DISPLACEMENT CAPACITY PREDICTION MODELS FOR REINFORCED CONCRETE BLOCK SHEAR WALLS**

#### **2.1 ABSTRACT**

Reinforced concrete block (masonry) shear wall construction presents an economic solution for seismic resistant low- and mid-rise buildings throughout North America. In this respect, wall displacements are output, based on wall characteristics, when force-based seismic design approaches are used. In displacement-based seismic design approaches, however, target displacements are the key input needed within the wall design process. As large displacement demands develop within the building seismic force resisting systems (SFRS), inelastic strain, curvature, and rotation demands develop within specific wall zones idealized as equivalent plastic hinges. In this study, eight different models are utilized to predict the maximum displacement capacities of reinforced concrete block shear walls (RCBSW). Experimental results of eighty-one RCBSW have been used to evaluate the reliability of the eight models. According to the analysis performed in this study, none of the eight models was found to be reliable in terms of predicting the maximum displacement capacity when compared to the corresponding experimental results. To further improve the predictability of these models, calibration coefficients are introduced and the corresponding improved results are presented. Based on its capability of capturing the experimental results,

one of these calibrated models is selected and further utilized to investigate the influence of altering the wall design characteristics on their maximum displacement capacities. This study aims at improving the displacement capacity predictions of RCBSW-SFRS in an effort to facilitate the development of relevant displacement-based design provisions in future seismic codes.

## **2.2 INTRODUCTION**

Recent research studies have highlighted the drawbacks of force-based seismic design (FBSD) approaches (Wallace and Moehle 1992; Moehle 1992; Priestley 1993; Priestley 2000; and Priestley et al. 2007) and clearly emphasized the needed shift towards performance-based seismic design (PBSD) philosophy by adopting displacement-based design (DBSD) approaches. Nevertheless, almost all current international seismic design provisions are still based on FBSD. In FBSD, displacements are considered only as output of the design process (Paulay and Priestley 1992; Park 1997; and Tomaževic 1999). Conversely, in DBSD, displacements are the key input required to initiate the design process (Calvi and Kingsley 1995; Medhekar and Kennedy 2000; Priestley et al. 2007 and others). Regardless of the design approach used, PBSD depends on accurate quantification of the structural component displacement capacities in order to identify their damage states and subsequently, the expected overall building performance. At large displacement demands, the critical zones of the building seismic force

resisting systems (SFRS) typically experience inelastic strains, curvatures, and rotations. These zones are idealized during analysis, design, and detailing stages as equivalent plastic hinges to facilitate applying capacity design principles and using prescribed code-detailing requirements (Paulay and Priestley 1992).

The seismic response of cantilever reinforced concrete block shear walls (RCBSW) with rectangular cross section, as shown in Fig. 2.1, is highly influenced by the shear span ratio, the magnitude of the applied axial load, and the distribution and the amount of horizontal and vertical reinforcements (Park 1975; Shing et al. 1989; Shing et al. 1990; Drysdale et al. 1994; and Thomsen and Wallace 2004). As such, the aforementioned geometrical and material characteristics are key aspects during seismic design because they control the wall failure mechanisms. Seismic design typically aims at ensuring that wall failure is flexurally dominated rather than being governed by shear due to the ductile nature and the accompanying high energy dissipation of the former behavior. A flexural failure mechanism is typically characterized by tensile yielding of the vertical reinforcement, formation of a plastic hinge zone as well as masonry crushing at critical wall locations (Clough et al. 1965; Paulay 1972; Blakeley et al. 1975; Paulay and Spurr 1977; Priestley 1981; Priestley and Elder 1982; Priestley 1982, and Park 1989). Under higher displacement demands, formation of plastic hinge zone accompanied by face shell spalling and crushing of the grout columns occur within the wall toe regions (Shedid et al. 2008). More severe toe crushing with a reduced wall ductility is observed with increased axial stress on the wall cross section (Sherman 2011).

Flexural wall ductility is also adversely affected by increased vertical reinforcement ratios, which might also correspond to decreased displacement capacities and can result in severe strength degradations (Eikanas 2003).

When analyzing a cantilever wall subjected to a top lateral load utilizing idealized plastic hinge models, top displacements are obtained as the summation of three displacement components: 1) wall flexural displacement,  $\Delta_f$ , which is the sum of the yield displacement,  $\Delta_y$ , and the plastic displacement,  $\Delta_p$ , contributions (Park 1989); 2) wall shear displacement,  $\Delta_{sh}$ ; and 3) sliding displacement,  $\Delta_{sl}$ , along the interface between the wall and its foundation. Sliding can be prevented by adopting adequate detailing and, as such, most wall displacement predictive models in the literature focus on the flexural contribution to the overall wall displacement capacity ignoring the relatively small shear deformation contribution, especially in flexurally dominated seismically-detailed walls. Therefore, the focus of this study is to assess and calibrate available flexural displacement capacity predictive models through: 1) compiling relevant wall displacement models available in the literature; 2) briefly describing the experimental database and the statistical tools used to assess the available models; 3) calibrating the models to further improve their predictability; and 4) utilizing the most reliable (calibrated) model to further study the influence of the different wall characteristics on the maximum displacement capacities.

### 2.3 DISPLACEMENT CAPACITY PREDICTION MODELS

It is not economical to design SFRS to behave elastically under moderate to large earthquakes. Therefore, inelastic behavior through ductile response is expected where damage can be localized in pre-specified zones without causing collapse. Park (1989) defined ductility as “*the ability of a structure to undergo large deformations in the inelastic range without a substantial reduction in strength.*” As such, the wall displacement ductility can be defined as the ratio between the total displacement capacity and the yield displacement. When FBSD approaches are adopted, the wall displacement ductility capacity is key as it is directly related to the code-prescribed force modification factor (Paulay and Priestley 1992). Displacement-based seismic design (DBSD) approaches, on the other hand, focus on identifying target design displacements that correspond to specific damage/performance level and, as such, displacement is the main design input in the DBSD procedure. DBSD also requires quantifying the secant stiffness corresponding to that target displacement as well as hysteretic damping and ductility level. Although outside the scope of the current study, developing accurate predictive models for such parameters is also needed.

To predict wall plastic displacements and the corresponding displacement ductility, idealized equivalent plastic hinge lengths (i.e. zones), over which plastic strains, curvatures and rotations are (ideally) assumed constant, will need to be

quantified. Subsequently, the equivalent plastic hinge length could be considered as one of the key parameters in both FBSD and DBSD approaches.

For the typical loading and boundary conditions of a cantilever wall (see Fig. 2.2), the top wall displacement corresponding to the first yield of the outermost vertical reinforcement is defined as the yield displacement,  $\Delta_y$ . This displacement can be calculated by double-integrating the curvature profile distribution along the height of the cantilever wall. Displacement beyond  $\Delta_y$  is defined as plastic displacement,  $\Delta_p$ , which can be calculated by multiplying the plastic rotation,  $\theta_p$ , at the base by the height above the center of the assumed equivalent plastic hinge. This top displacement can be expressed using Eq. 1 (Paulay and Priestley 1992):

$$\Delta_u = \Delta_y + \Delta_p = \frac{H_w^2 \phi_y}{3} + (\phi_u - \phi_y) L_p (H_w - 0.5 L_p) \quad (2.1)$$

In Eq. 1, the plastic rotation is represented by the term  $(\phi_u - \phi_y) L_p$ , where  $L_p$  is the equivalent plastic hinge length,  $\phi_u$  and  $\phi_y$  are the ultimate and yield curvatures, respectively (the formulae used for calculations of curvatures evaluation are provided in Appendix I). The plastic rotation is assumed in Eq. 2.1 such that the plastic curvatures are uniform over the height of the equivalent plastic hinge (Paulay and Priestley 1992), as shown in Fig. 2. Finally, the displacement capacity of the wall, corresponding to the wall's maximum lateral load, can be evaluated by the summation of the yield and plastic displacements.

In the next sections, eight different models will be utilized to estimate the equivalent plastic hinge length (used in Eq. 2.1) and/or the wall displacement capacity to assess the models' reliability using the experimental database utilized in this study. In the following section, each of the eight models will be presented along with its assumptions, limitations and definitions of its required input parameters.

### **2.3.1 Paulay And Priestley's (1993) Model**

Based on experimental results of reinforced concrete walls subjected to simulated earthquake loading combined with theoretical consideration of fundamental structural behavior, Paulay and Priestley (1993) proposed the following expression to evaluate the equivalent plastic hinge length:

$$L_p = 0.2L_w + 0.044H_w \quad (2.2)$$

It is noteworthy to mention that this model, from Paulay and Priestley's point of view, is on the conservative side for estimating the equivalent plastic hinge length.

### **2.3.2 Priestley And Calvi's (1996) Model**

Priestley and Calvi (1996) discussed the capacity design principles where it is necessary to identify, during the conceptual design stage, the potential locations of

inelastic behavior (plastic hinge locations) and their corresponding plastic rotation capacities. These plastic rotation capacities, and hence the wall ductility capacity, depend on the wall cross-section geometry and its transverse reinforcement. More specifically, transverse reinforcement provides the dual functions of confining the concrete core, thus sustaining higher compressive strain, and restraining the longitudinal compression reinforcement against buckling. According to Priestley and Calvi (1996), the equivalent plastic hinge length is evaluated using

$$L_p = \begin{cases} 0.08H_w + 0.022d_b f_y, & \text{if } L_p \geq 0.044d_b f_y \\ 0.044d_b f_y, & \text{if } L_p \leq 0.044d_b f_y \end{cases} \quad (2.3)$$

where  $H_w$  is the wall height, and  $d_b$  is the vertical bar diameter. Equation 2.3 introduces an additional rotation term in the plastic hinge region resulting from the strain penetration of the longitudinal reinforcement in the foundation.

### 2.3.3 Panagiotakos and Fardis's (2001) Model

Panagiotakos and Fardis (2001) reported the experimental results of several reinforced concrete members (i.e. beams, columns and walls) subjected to uniaxial bending, with and without axial loads, to derive expressions for deformations at yielding and failure in terms of the geometrical and mechanical properties of the structural members. The same authors reported the results obtained from 1,032 specimens subjected to monotonic or cyclic loadings (266 beams, 705 columns, and

61 walls). Based on these results, the following expression was developed to evaluate the total rotation at failure,  $\theta_u$  :

$$\theta_u = \frac{\phi_y L_w}{3} + (\phi_u - \phi_y) L_p \left( 1 - \frac{L_p}{2L_w} \right) \quad (2.4)$$

Utilizing expressions for the yield and ultimate curvatures combined with Eq. 4, the total rotations at failure were used to develop formulae for the plastic hinge length prediction that provided the best fit to the experimental data. In this respect, the data were categorized into two types according to the loading condition (monotonic or cyclic) used throughout the test. Therefore, two models, Eqs. (2.5) and (6), were introduced to evaluate the equivalent plastic hinge length for cyclic and monotonic loading conditions, respectively.

$$L_{p,cy} = 0.12L_w + 0.014a_{sl}d_b f_y \quad (2.5)$$

$$L_{p,mon} = 1.5L_{p,cy} = 0.18L_w + 0.021a_{sl}d_b f_y \quad (2.6)$$

In Eqs. (2.5) and (2.6),  $L_{p,cy}$  is the equivalent plastic hinge under cyclic loadings,  $L_{p,mon}$  is the equivalent plastic hinge under monotonic loading,  $a_{sl}$  denotes a zero-one variable which is equal to either 1.0 if slippage of the longitudinal reinforcement is possible or zero if slippage is not possible, and  $f_y$  is the yield stress of the tension reinforcement in MPa.

As the data obtained in the current study for shear walls tested under cyclic loading only, the ultimate rotation given by Eq. (2.4) will be calculated using the plastic hinge length formula given by Eq. (2.5) only.

#### 2.3.4 Euro Code 8's (2005) Model

Another equivalent plastic hinge length model is included in the current Euro code EC8. In Annex A of EC8 Part 3 (CEN, 2005) a plastic hinge length equation, in which the member geometry, tension shift and strain penetration components are included, is given as:

$$L_p = \frac{L_v}{30} + 0.2L_w + 0.11 \frac{d_b f_y}{\sqrt{f'_c}} \quad (2.7)$$

With the length and strain limits defined in EC8 (CEN, 2005), the displacement capacity of the RCBSW can be evaluated. The first term in Eq. 7 accounts for the spread of plasticity along the wall and was hence chosen to be dependent on the ratio between moment and shear (shear span ratio), represented by  $L_v$ , at the plastic hinge location. The second term in Eq. 2.7,  $0.2L_w$ , accounts for the tension shift, while the third term in the same equation accounts for the strain penetration as a function of the longitudinal bar diameter,  $d_b$ .

### 2.3.5 Priestley et al.'s (2007) Model

Priestley et al. (2007) proposed a plastic hinge model to meet specific serviceability and damage control performance levels. The model accounts for the tension shift due to diagonal shear cracks and the strain penetration into foundation (as functions of bar diameter and the ratio between the ultimate and yield strengths of the flexural reinforcement). The corresponding expression proposed to evaluate the plastic hinge length is:

$$L_p = k.H_w + 0.1L_w + L_{sp} \quad (2.8)$$

In Eq. 2.8, the tension shift presents 10% of wall length, the ratio between the ultimate and yield strengths to bar being represented by  $k = 0.2 \left( \frac{f_u}{f_y} - 1 \right)$ , where  $k$  factor should not exceed 0.08, and the strain penetration depth,  $L_{sp}$ , is expressed as:

$$L_{sp} = 0.022f_y d_b \quad (2.9)$$

There are some cases where the ultimate tensile strength,  $f_u$ , is not reported while the yield strength,  $f_y$ , is known from the database. As such, an approach proposed by Bannister et al. (2000) is followed. This approach indicates that reinforced steel bars produced via controlled manufacturing processes generally have yield to ultimate tensile strengths ratio ranging from 0.8 to 0.95, with an average of about 0.875. Therefore, the ultimate tensile strength is evaluated in the

current study using the following expression  $f_u = 1.14 \times f_y$  (based on the yield strength values reported in the corresponding study).

### 2.3.6 Bohl and Adebar's (2011) Model

Bohl and Adebar (2011) investigated the profile of inelastic curvatures that should be used to estimate the flexural displacement capacity of reinforced concrete shear walls using a nonlinear finite element model. A model that is capable of predicting the equivalent plastic hinge length, as expressed in Eq. 2.10, was subsequently developed based on the range of reinforced concrete shear walls with different shear span ratios, wall lengths, and axial compression levels.

$$L_p = \begin{cases} \left(0.2L_w + 0.05 \frac{M}{V}\right) \left(1 - 1.5 \frac{P}{f_c A_w}\right), & \text{if } L_p \leq 0.8L_w \\ 0.8L_w, & \text{if } L_p \geq 0.8L_w \end{cases} \quad (2.10)$$

In Eq. 10,  $M/V$  is the shear span ratio,  $A_w$  is the gross area of the wall cross section, and  $P$  is the axial load.

### 2.3.7 Kazaz's (2013) Model

This model evaluated the length of the equivalent plastic hinge in terms of several variables such as wall length, shear span ratio, axial load ratio ( $P/A_w f_c$ ), and the

ratio of horizontal web reinforcement ( $\rho_{sh}$ ). The equation proposed by Kazaz (2013) for the plastic hinge length prediction is

$$L_p = 0.27L_w \left(1 - \frac{P}{A_w f'_c}\right) \left(1 - \frac{f_y \rho_{sh}}{f'_c}\right) \left(\frac{M/V}{L_w}\right)^{0.45} \quad (2.11)$$

This model was developed based on the regression analysis of the aforementioned variables and was also calibrated based on a finite element shear wall model utilizing the Turkish seismic code (TCS 2007) provisions. Two different methods were adopted to evaluate the length of the plastic hinge zone given in Eq. 2.11. The first method was based on the ultimate curvature profile calculated from analyzing the wall-cross sectional strain profile when the outer tension steel reached a strain of 0.06. In the second method, the curvature profile was calculated using the shell element strains introduced in the finite element model at the wall's two ends at the same height (i.e. in the same horizontal level). As such, the vertical strains at the compression,  $\varepsilon_c$ , and tension,  $\varepsilon_t$ , wall toes were evaluated from the finite element model without specifying numerical limits to the corresponding calculated curvatures as  $\phi = (\varepsilon_c + \varepsilon_t) / L_w$ .

### 2.3.8 Shedid and El-Dakhakhni's (2013) Model

Most available plastic hinge models, including all the models discussed above, are originally developed for reinforced concrete shear walls. Conversely, Shedid and

El-Dakhakhni (2013) adopted and modified the Priestley et al.'s (2007) model to quantify the top displacement of experimentally tested RCBSW. The mechanics-based analytical model assumes that the curvature profile over the height of flexural dominant RCBSW is linear up to the yield limit. The plastic hinge length,  $L_p$ , in this model is presented as the distance from the base of the wall to the yield curvature along the wall.  $L_p$  in turn is divided into three parts; the first part represents the strain penetration inside the foundation, while the second part indicates the spread of plasticity due to inclined cracks, and the third part reflects the effect of the extent of plasticity spread up to the yield point. Top displacement capacity is expressed in terms of  $L_1$ ,  $L_2$ , and  $L_3$  for the above three parts respectively as:

$$\Delta_u = \Delta_y + (\phi_u - \phi_y)L_2 \left( H_w - \frac{L_2}{2} \right) + \phi_u L_1 \left( H_w + \frac{L_1}{2} \right) + \frac{1}{4}(\phi_u - \phi_3)L_3 \left( H_w - L_2 - \frac{L_3}{3} \right) \quad (2.12)$$

$$\phi_3 = \phi_y \frac{H_w - L_2}{H_w} \quad (2.13)$$

$$L_1 = 0.03f_y d_b \quad (2.14)$$

$$L_3 = \left( 1 - \frac{M_y}{M_u} \right) H_w - L_2 \quad (2.15)$$

All the models/formulation discussed in the current study utilized SI units and do not explicitly account for the shear deformations. Nonetheless, these models

were assessed and further calibrated using different experimental results where the contributions of the shear and flexural deformations are essentially lumped together in the different model displacement predictions. Moreover, all the models discussed in the current study were developed to quantify the displacement at the maximum load only. As such, the current study is not focused on extending the use of these models to predict other displacement limit states (e.g. cracking, yielding, and 80% strength degradation) on the wall pushover curve.

#### **2.4 EXPERIMENTAL WALL SEISMIC PERFORMANCE DATABASE**

The current concrete and masonry seismic code provisions identify limits to distinguish between wall behavior in terms of being flexurally dominated (slender) or shear dominated (squat) walls, based on the wall's shear span ratio. Both the ACI 318-14 clause 18.10.6.2 and the CSA A23.3-14 clause 21.5.1.4 (for concrete design) adopt a value of 2.0 for this ratio. However, the TMS 402/ACI 530/ ASCE5 clause 8.3.4.4, and CSA S304-14 clause 7.10.2.2 (masonry design standards) adopt a value of 1.0 for the shear span ratio. In addition, the pre-standard supplement document of the seismic performance assessment proposed by the federal emergency management agency, FEMA P-58/VBD-3.8.10 (FEMA 2012), utilizes several walls with aspect ratio of 1.0 to define damage states and fragility curves for flexurally dominated RCBSW. It should be noted that, although there are code-specified threshold values for the shear span ratio that separate shear- from

flexurally-dominated walls, real (experimentally tested) walls do not suddenly switch from one response to another at a specific shear span ratio value. Instead, wall behavior would be influenced by several other parameters (e.g. steel ratios) and would change gradually from being mainly flexural- to mostly shear-dominated as walls become *squatter*. Within the scope of the current study, all walls selected within the experimental database in the current study are flexurally dominated in terms of experiencing one or more flexural response behavior (if not all) including horizontal cracks, yielding, buckling, and fracture of the vertical (flexural) steel reinforcement, masonry crushing at wall toes, and/or the out-of-plane buckling in the compression zone.

The experimental database utilized in the current study consists of 81 walls extracted from several studies reported in the literature (Shing et al. 1990; Pilakoutas and Elnashai 1995; Thomson and Wallace 2004; Voon and Ingham 2006; Shedid et al. 2008; Dazio et al. 2009; Sherman 2011; Kapoi 2012; and Ahmadi 2014). In the current study, the walls investigated are all flexurally dominated with aspect ratios varying from 0.8 to 3.0. The walls were subjected to axial compressive stress that varied from 0% (no external axial load except the walls' own weights) to 15% of the masonry compressive strength. In addition, these walls have vertical and horizontal reinforcement ratios,  $\rho_v$  and  $\rho_{sh}$ , respectively, varying from 0.16% to 1.3% and 0.05% to 0.625%, respectively, as illustrated in Table 2.1. As can be seen also in Table 2.1, the yield strength of vertical

reinforcement,  $f_y$ , used in walls varied between 318 MPa and 624 MPa, while the masonry compressive strength,  $f'_m$ , ranged from 12 MPa to 31 MPa. It should be noted that within 81 available experimental data point, only six walls had  $f'_m$  values evaluated using the Canadian standards. As such, Canadian code-based  $f'_m$  value is normalized to the corresponding USA code-based value. Moreover, the elastic-perfectly plastic steel material behavior is adopted for the vertical reinforcement with respect to the ultimate curvature analysis. Finally, the equivalent rectangular stress block approach is also used in this study to evaluate both the yield and ultimate curvatures.

Table 2.2 presents both yield and the ultimate curvatures of all the walls calculated based on the following assumptions: 1) plane sections remain plane (Euler-Bernoulli's theory) under flexure; 2) vertical reinforcement bars in the compression zone of the wall cross section contribute to the yield and ultimate flexural capacity; 3) the steel Young's modulus is 200 GPa; 4) vertical reinforcement bars stress strain relationship are elastic-perfectly-plastic; 5) the masonry elastic module (used in yield curvature analysis only) is taken equal to  $900f'_m$  where  $f'_m$  in MPa; 6) the walls' own weight is taken into account in calculating the applied axial stress; 7) the yield stage is evaluated at the yield onset of the outermost vertical rebar within the tension side of the wall's cross section; and 8) the masonry compression strain at the ultimate stage is equal to 0.003.

Shedid and El-Dakhakhni (2013) model has the capability to quantify directly the maximum displacement due to flexural. However, Pangioyakos and Fardis (2001) model evaluate the ultimate rotation then the calculation of maximum displacement is the multiplication of the ultimate rotation by wall height. Therefore, both models do not need the adaptation presented in Eq. 2.1. For all other models, both yield and ultimate curvatures estimates, presented in Table 2.2, are combined with the predicted equivalent plastic hinge length of each model independently (see Table 2.3), using its corresponding parameters and assumptions, to evaluate the maximum displacement using the formula given in Eq. 2.1. Afterwards, a direct comparison is facilitated and presented in the next section between all the models in terms of predicting the wall drift capacity (i.e. percentage of top wall maximum lateral displacement normalized by its height), shown in Table 2.2.

## **2.5 ASSESSMENT OF CURRENT DISPLACEMENT CAPACITY MODELS**

Several statistical tools are available to assess the reliability of numerical or analytical models in terms of predicting the experimental results. In this study, linear regression and residual analyses are selected as powerful tools to facilitate understanding the relationships between the different parameters among the data being studied. Several researchers and text books (e.g. Montgomery et al. 1992) described these statistical techniques and, as such, the theory behind their use will not be discussed in detail in this section. Instead, this section presents general

description of the same techniques within the assessment of the current (eight) models in predicting displacement capacities of all walls within the experimental database, as discussed earlier.

Linear regression determines the statistical relationship between the predictor or regressor (drift capacity observed from the experiment) and the response variable (drift capacity evaluated using the selected model) using the following equation:

$$y = \beta_0 + \beta_1 x + \varepsilon \quad (2.16)$$

where  $y$  is the response variable,  $\beta_0$  and  $\beta_1$  are the coefficients in the linear relationship,  $x$  is the predictor, and  $\varepsilon$  is the prediction error. Since the relationship between observed and predicted displacement capacity requires that the regression line goes through the origin ( $\beta_0 = 0$  in this study). This is intentionally adopted so that the regression model is correct for the case of zero displacement. The linear regression model assumes that the errors are mutually independent and normally distributed with a zero mean and a variance represented as  $\sigma^2$ . The validity of this assumption is checked using the normal probability paper (Montgomery et al. 1992) as will be discussed in the next section.

Figure 2.3 show the results of the regression analysis for the models of Paulay and Priestley's (1993) and Priestley and Calvi's (1996) as examples, while Fig. 2.4 and Table 2.4 present the regression lines and coefficients, respectively, for all eight models. The regression coefficients of 0.52 and 0.46 for the models of Paulay and Priestley's (1993) and Priestley and Calvi's (1996), respectively, indicate that these

models estimate the displacement capacity, on average, as approximately 52% and 46%, respectively, of the corresponding measured values. The Panagiotakos and Fardis's (2001) model has almost the same trend as the Priestley and Calvi's (1996) model with only 3% difference in the slopes of the regression lines (or regression coefficients). Table 2.4 also shows that the Euro Code 8's (2005) model tends to underestimate the drift capacity by 27%, while the Priestley et al.'s (2007) model underestimates the drift capacity by 39%. The Bohl and Adebar's (2011) and Kazaz's (2013) models have similar prediction capabilities with 52% and 55% as their respective regression coefficients. The Shedid and El-Dakhkhni's (2013) model has a regression coefficient of 78% which is slightly higher than that of the Euro Code 8 (2005) model.

Residuals from the regression analysis may be viewed as the deviation between the data and the fit, and can be calculated as

$$\varepsilon_i = y_i - \hat{y}_i, \quad i = 1, 2, \dots, n \quad (2.17)$$

where  $\varepsilon_i$  is the  $i^{\text{th}}$  error or residual in a sample of size  $n$ ,  $y_i$  and  $\hat{y}_i$  are the corresponding  $i^{\text{th}}$  observed and predicted values. It is important to note that the residuals also measure the variability that cannot be explained by the regression model. As such, analysis of the residuals is an effective tool for discovering several types of model deficiencies. In this respect, the residual plot for the Paulay and Priestley's (1993) model, shown in Fig. 2.5a, shows that the model has a trend of underestimating the drift capacity with the maximum and minimum relative errors

of 69% and -77%, respectively; and for only four walls out of the 81 walls included in the database, the drift capacities are overestimated by more than 20%. The Priestley and Calvi's (1996) model has the maximum and minimum relative errors equaling to 20% and -77%, respectively, as shown in Fig. 5b.

## 2.6 VALIDATION OF THE NORMALITY ASSUMPTION

A probability plot is a graphical technique for assessing the data assumption of following a theoretical distribution. In a probability plot, the data are plotted against a theoretical distribution in such a way that the points should form an approximate straight line. Departures from this straight line indicate departures from the theoretical distribution. In this study, the residuals from a regression analysis are plotted in ascending order on the horizontal axis, the medians of corresponding order statistics from a normal distribution (referred to as the normal order statistic medians) are plotted on the vertical axis. The normal order statistic medians are calculated as  $\phi^{-1}[F_{\varepsilon}(\varepsilon_{(i)})]$ , where  $\phi^{-1}$  is the inverse of the cumulative distribution function of the standard normal variate and  $F_{\varepsilon}(\varepsilon_{(i)})$  is the empirically determined cumulative probability associated with an individual residual  $\varepsilon_{(i)}$ . With all the residuals of a regression analysis ranked in an ascending order,  $F_{\varepsilon}(\varepsilon_{(i)})$  can be calculated as  $\frac{i}{(n+1)}$  (Seber and Wild 1977) where  $i$  is the rank of  $\varepsilon_{(i)}$  (i.e.,  $\varepsilon_{(i)}$ )

is the  $i^{\text{th}}$  largest residual) and  $n$  is the total number of residuals from one regression analysis. Figure 6 shows the normal probability plot of the eight models to evaluate the distribution of their residuals. As can be seen in Fig. 6, residuals from all models approximately follow the normal distribution, where plotted data points are almost clustered around a straight line. This reveals that the results of the regression analysis executed for all the models can be relied on.

The regression analyses indicates that all model predictions are generally inaccurate, and on average, the model predicted drift capacities that range from approximately 46% (i.e. Priestley and Calvi 1996) to 78% (i.e. Shedid and El-Dakhakhni 2013) of the corresponding experimental measured values. As such, all the models are further investigated to analyze their limited capabilities in predicting the drift capacity, as will be discussed in the next section.

## **2.7 DISCUSSION**

The Priestley and Calvi (1996) equivalent plastic hinge model (see Table 3) is based only on three wall characteristics including the wall height, vertical bar diameter, and yield strength of the vertical bar. The model is thought to be too simple as it does not have the capability of capturing the changes in both the wall geometrical and material characteristics. The Panagiotakos and Fardis (2001) model is as simple as the Priestley and Calvi (1996) model, but uses the wall length instead of the wall height to describe the wall characteristics. It is also different in terms of introducing

a zero-one parameter for the slippage concept. Moreover, the Panagiotakos and Fardis (2001) model is based on a large dataset of structural elements including beams, columns, and walls. As such, the model is not specifically developed for wall behavior prediction per se. The Paulay and Priestley (1993) model is the simplest one among the eight models with only two parameters: the wall length and the wall height. The Priestley et al. (2007) model can be considered an evolution from the Paulay and Priestley (1993) model through introducing a new term,  $L_{sp}$ , that considers the strain penetration depth and the spread of plasticity along the wall height. Also, the first term in the model depends on the ratio between the ultimate and yield strengths of the vertical reinforcement. The Paulay and Priestley (1993) and Priestley et al. (2007) models, however, do not take into account several wall characteristics such as the change of the axial load effect which is introduced in the Bohl and Adebar (2011) model. Also, the Bohl and Adebar (2011) model explicitly presents the shear span as a factor in addition to the wall length.

None of the models listed above considers the shear reinforcement as a factor contributing to the wall displacement except the model by Kazaz (2013) where it reflects the influence of axial load, amount of shear reinforcement, and the ratio between shear span and wall length. One drawback of the Kazaz (2013) model is that the equivalent plastic hinge length is related only to the wall length. The Euro Code 8 (2005) model account for the shear span, tension shift, and strain penetration which are the same as those used in the Priestley et al. (2007) model, but the two models adopt different coefficients, also the implementation of the strain

penetration is dissimilar where the Priestley et al. (2007) model introduces the square root of the concrete compressive strength.

While all the previous models are developed for reinforced concrete shear walls, the Shedid and El-Dakhakhni (2013) model is the only model adopted for RCBSW, which might attribute for its higher regression coefficient (i.e. 78%) compared to all other models. This model decomposes the plastic displacement into three terms that consider the strain penetration ( $L_1$ ), the spread of plasticity ( $L_2$ ), and the extent of plasticity to the yield point ( $L_3$ ). The shortcoming of the Shedid and El-Dakhakhni (2013) model is that the model does not account for both the shear reinforcement and axial load, although it can be argued that the axial load is represented implicitly within the wall cross section curvature evaluations. Despite all the limitations discussed above in this section, all models are further calibrated to enhance their prediction capabilities, as will be presented in the next section.

## **2.8 MODEL PREDICTION CAPABILITY IMPROVEMENT**

The results of the regression and residual analyses reveal that all models can benefit from further improvement by calibrating the different factors used in the models. The least squares parameter estimation method is used to quantify the calibration coefficient  $c_j$  with  $j = 1, 2$  and  $3$  introduced according to number of terms constituting each model. This method estimates the calibration coefficients so that

the average squared residuals or the sum of squared residuals are minimized. One of the methods for carrying out this minimization is to differentiate Eq. (2.18) with respect to  $c_j$ , equate the derivatives to zero, and solve the resulting equations for the calibration factor, as given in Eq. (19).

$$\sum_{i=1}^n \varepsilon_i^2 = \sum_{i=1}^n (y_i - \hat{y}_i)^2 \quad (2.18)$$

$$\frac{\partial}{\partial c_j} \sum_{j=1}^n \varepsilon_j^2 = 0 \quad j=1, 2, 3 \quad (2.19)$$

where  $\varepsilon_i$  is the residual of displacement capacity for individual wall,  $n$  is the number of walls available in the experimental database, and  $c_j$  with  $j = 1, 2$  and  $3$  is the calibration coefficient evaluated for each term in the enhanced models, as shown in Table 2.5.

For the Shedid and El-Dakhakhni (2013) model as an example, however all the calibrated model factors are shown in Table 2.5, the calibration analysis using the least square errors method provides three calibration factors to enhance the model predictability for the plastic displacement component keeping in mind the yield component is not included in the enhancement in this study. The first term, which accounts for the strain penetration, is recommended to be decreased to 0.01 of its original value. Whereas with the calibration factor for the second term which accounts for the spread of plasticity, it proposes a 2.71 amplification. The third term, implements the extend of plasticity to the yield point, is increased to 2.32. Assessing the modified Shedid and El-Dakhakhni (2013) model is expressed as:

$$\Delta_u = \Delta_y + 0.01(\phi_u - \phi_y)L_2\left(H_w - \frac{L_2}{2}\right) + 2.71\phi_u L_1\left(H_w + \frac{L_1}{2}\right) + \frac{2.32}{4}(\phi_u - \phi_3)L_3\left(H_w - L_2 - \frac{L_3}{3}\right)$$

(2.20)

The ranked values of the residuals for the eight calibrated models are plotted in Fig. 7, while the maximum (i.e. overestimation) and minimum (i.e. underestimation) errors are given in Table 5 for the same models. The calibrated Kazaz 2013 model overestimates and underestimates the maximum drifts by 2.2% and 5.6% difference than the experimental drifts, respectively. Conversely, the calibrated models (Bohl and adebar 2011) and (Shedid and El-Dakhakhni 2013) have the least difference between the predicted and experimental drifts, in compared to all other models, with maximum of errors approximately 1.38% and 1.22%, as shown in Table 5, respectively.

To verify the results discussed above, the root mean square (RMS) error (RMSE) analysis (Montgomery et al. 1992) has been performed to measure the performance of all prediction models. For the case of our study, it can be calculated as:

$$RMSE = \sqrt{\frac{1}{n} \sum_{i=1}^n (\Delta_{u_i} - \Delta_{u(\text{exp})_i})^2}$$

(2.21)

where  $\Delta_{u_i}$  is the  $i^{\text{th}}$  predicted drift capacity and  $\Delta_{u(\text{exp})_i}$  is the corresponding  $i^{\text{th}}$  experimentally determined drift capacity in the database. The RMS errors for the eight models range from 0.51 to 0.82, as shown in Table 2.5. The RMS errors

analysis is concise with the residual analysis in terms of quantifying the effectiveness of the calibrated models. More specifically, the errors analysis does not only confirm that the calibrated model (Kazaz 2013) has the highest RMS errors of 0.82, but also shows that the calibrated models (Bohl and adebar 2011) and (Shedid and El-Dakhakhni 2013) tend to have the lowest RMS errors of 0.57 and 0.51, respectively, when compared to all other models. Since Shedid and El-Dakhakhni (2013) calibrated model has the lowest RMS error among all the calibrated models, it is selected to be utilized to demonstrate the effect of altering the design characteristics on wall maximum drift capacities, as will be presented in the next section.

## **2.9 INFLUENCE OF DESIGN CHARACTERISTICS ON WALL DRIFT CAPACITIES**

This section presents the influence of both geometrical and material characteristics on the maximum drifts capacity using the Shedid and El-Dakhakhni (2013) calibrated model for different wall aspect ratios. As such, a default wall is introduced within the maximum and the minimum range of different characteristics following masonry construction practice in North America. This wall has vertical and horizontal spacing of reinforcement of 400 mm, while the yield strength will be kept constant for both reinforcement, and is equal to 400 MPa. The compressive strength of masonry is 13.5 MPa with S type mortar. The wall length, height and thickness are considered constant and are equal to 2,400 mm, 6,000 mm and 190

mm, respectively. A summary of the selected default wall characteristics is given in Table 2.6. A first principle (mechanics) analysis is executed for each wall scenario to evaluate its yield and ultimate curvatures, and subsequently its drift capacity.

The calibrated model is first used to capture the influence of altering the wall aspect ratio and the masonry strength on the maximum drift of the wall. At low wall aspect ratios, the differences between the maximum drifts are smaller compared to the high aspect ratio walls, as shown in Fig. 2.8a. For example, the maximum drift capacities difference between the type of compressive strengths are 0.20%, 1.10%, and 5.00% for wall with aspect ratios of 1.00, 2.25, and 3.75, respectively. In addition, the drift capacity increases from 0.12% to 0.85% for aspect ratios 1.00 and 3.75, respectively, for a masonry compressive strength of 10.0 MPa. Similar overall trend is observed for all the remaining compressive strengths (i.e. 13.5 MPa and 17.0 MPa).

As can be seen in Fig. 8b, the model is consistent with mechanics regarding the effect of axial load being inversely proportioned with the drift capacity of RCBSW. For example, at an aspect ratio of 2.25, the wall drift capacities are 1.37%, 1.12%, and 0.79% at the 1.0%, 2.5%, and 10.0% axial load ratio, respectively. For approximately no axial load (axial load of 1% of  $f'_m A_g$ ), the drift capacity increases from 0.82% to 2.05% for aspect ratios 1.00 and 3.75, respectively, while for axial

load ratio equals to 5% of  $f'_m A_g$  (i.e. default wall), the drift capacity ranges between 0.55% and 1.32%.

The vertical reinforcement is a key parameter that significantly changes the behavior of RCBSW. The vertical reinforcement influence can be quantified using two different factors. The first factor is the spacing between the bars, while the bar diameter is the second factor. Overall, the analysis reveals the influence of the former factor on the wall drift capacities is higher than that of the later factor. Figure 8c depicts the influence of altering the vertical reinforcement bar diameter on the wall drift capacities as a function of the wall aspect ratios. Within the same wall aspect ratio, the differences between the drift capacities when changing the vertical bar diameter are minimal with a maximum value of approximately 6% for all bar diameters. However, changing the spacing of the vertical reinforcement does not follow a similar trend of drift capacities to that of changing bar diameter as shown in Figure 8d where the differences between the wall drift capacities for low and high aspect ratio walls are not negligible. For example, keeping all material and geometric characteristics the same for wall aspect ratio of 1.00, the drift capacities can range between 0.63% and 0.47% by varying the vertical reinforcement ratio between 0.175% and 0.526%, respectively.

## 2.10 CONCLUSIONS

Current seismic design codes adopt force-based seismic design approaches that require displacement check at the end of the design process based on perceived SFRS ductility capacities. However, accurate quantification of the top displacement of RCBSW under seismic loadings is directly related to wall damage, and thus to performance-based seismic design provisions. The response of a ductile flexurally dominated RCBSW under lateral seismic loads is similar to that of a vertical cantilever and can be characterized by an idealized plastic hinge at the base. As such, top flexural displacement can be assumed as the sum of yield and plastic displacements. Literature shows that different models have been proposed to evaluate the plastic displacement component utilizing the idealized plastic hinge concept. It is clear that the eight models evaluated within the paper are developed solely based on wall flexural behaviors. As such, the focus of this study is assessing the reliability of the existing eight predictive models and calibrating one of the most reliable models within the available database of 81 flexurally-dominated RCBSW test results.

This study concludes that the eight considered models would benefit from improvement through introducing calibration factors for different terms used in each model in order to improve their predictability. This proposed prediction enhancement modification based on the current analyses, would still only *implicitly* account for shear deformation contributions to the overall wall displacement. This fact should be also taken into consideration when predicting the overall

displacement of walls with characteristics outside the range of those evaluated within the currently available dataset. The proposed prediction enhancement resulted in RMS errors of 0.51 for the most reliable model. This calibrated model is selected to study the influence of altering the wall design characteristics on their maximum drift capacities. The results show that the influence of the axial load and vertical bar spacing is higher compared to the masonry compressive strength and vertical bar diameter on wall drift capacities.

This paper presents a comprehensive assessment to the available models in terms of predicting the displacement capacities of reinforced concrete block shear walls through powerful statistical tools. Although the experimental database used in this paper contains large number of flexurally-dominated shear walls with different configurations, the experimental results of more reinforced concrete block shear walls (i.e. flexurally- and/or shear-dominated) are expected to further improve the predictability of these models, and subsequently facilitate the development of prescriptive design requirements for the next generation of seismic design codes.

## **2.11 ACKNOWLEDGMENTS**

Financial support has been provided by the Natural Sciences and Engineering Research Council (NSERC) of Canada and the Canada Masonry Design Centre (CMDC). Additional support has been provided by the McMaster University

Centre for Effective Design of Structures (CEDs) funded through the Ontario Research and Development Challenge Fund (ORDCF), a program of the Ontario Ministry of Research and Innovation (MRI).

## 2.12 APPENDIX I

### 2.12.1 Calculation of Yield and Ultimate Curvature

The calculation of the yield curvature is based on onset yield of the outermost vertical reinforcement bar in the tension side. This is conducted considering Bernoulli's assumption that plane sections remain plane after bending. The yield curvature can be calculated as below:

$$\phi_y = \frac{\varepsilon_y}{d_1 - c_y}$$

$$\varepsilon_y = \frac{f_y}{E_s}$$

$$P = C_m + C_s - T_s$$

$$C_m = 0.5 \varepsilon_m E_m t_w c_y$$

$$C_s = \sum A_s f'_s, \quad \text{where } 0 \leq f'_s \leq f_y$$

$$T_s = \sum A_s f_s, \quad \text{where } 0 \leq f_s \leq f_y$$

$$T_i = A_s \frac{d_i - c_y}{d_1 - c_y} f_y$$

$$\varepsilon_m = \frac{\varepsilon_y c_y}{d - c_y}$$

The determination of the ultimate curvature is based on ultimate strain for the reinforced masonry taken in this study equals to 0.003 following the CSA S304

Clause 10.2.2 (CSA, 2014) using the stress block method. The following set of equations shows the sequence adopted to quantify of the ultimate curvature:

$$\phi_u = \frac{0.003}{c_u}$$

$$P = C_m + C_s - T_s$$

$$C_m = 0.85 f'_m t_w (0.8 c_u)$$

$$C_s = \sum A_s f'_s, \quad \text{where } 0 \leq f'_s \leq f_y,$$

$$f'_s = \frac{c_u - d_i}{c_u} 0.003 E_s < f_y$$

$$T_s = \sum A_s f_s, \quad \text{where } 0 \leq f_s \leq f_y,$$

$$f_s = \frac{d_i - c_u}{c_u} 0.003 E_s < f_y$$

### 2.13 NOTATION

$A_w$  = Cross sectional area of the wall

$c_j$  = calibration coefficients ( $j=1, 2, 3$ )

$a_{sl}$  = Zero-one variable. It is equal to 1.0 if slippage of the longitudinal reinforcement is possible and zero if it is not possible.

$C_m$  = Compression force in cross section of a masonry wall

$C_s$  = Compression fore in the vertical reinforcement

$c_u$  = Length of compression zone corresponding to ultimate load

$c_y$  = Length of compression zone at first yield of vertical reinforcement in cross section

$d_l$  = Distance from the extreme compression fiber in cross section to the first vertical tension bar

$d_b$  = Bar diameter of vertical reinforcement

$d_i$  = Distance from the extreme compression fiber to the location of vertical reinforcement

$d_{sh}$  = Diameter of shear (horizontal) reinforcement

$E_s$  = Modulus of elasticity for steel reinforcement

$F_\varepsilon(\varepsilon_i) = i^{\text{th}}$  empirical cumulative probability density function

$f_c^i$  = Concrete Compressive strength  
 $f_m^i$  = Masonry Compressive strength  
 $f_s^i$  = Compressive stress in vertical reinforcement  
 $f_s$  = Tensile stress in vertical reinforcement  
 $f_u$  = Ultimate strength for reinforcement steel bars  
 $f_y$  = Yield strength for reinforcement steel bars  
 $f_{y,sh}$  = Yield strength of shear (horizontal) reinforcement  
 $H_w$  = Wall height  
 $i$  = Wall rank  
 $L_p$  = Equivalent plastic hinge length  
 $L_{p,cy}$  = Equivalent plastic hinge under cyclic loading  
 $L_{p,mon}$  = Equivalent plastic hinge under monotonic loading,  
 $L_{sp}$  = Strain penetration length in the foundation in Priestley et al. (2007) model  
 $L_v$  = Moment to shear ratio at the section of plastic hinge formation  
 $L_w$  = Wall length  
 $L_1$  = Strain penetration length inside the foundation in Shedid and El-Dakhakhni (2013) model  
 $L_2$  = Spread of plasticity length due to inclined cracks  
 $L_3$  = the extent of the plasticity spreading to the yield point  
 $M_u$  = Ultimate moment at the base of the wall  
 $M_y$  = yield moment at the base of the wall  
 $n$  = total number of walls in the database  
 $P$  = Axial compressive load  
 $T_s$  = Tensile force in vertical reinforcement in cross section in masonry wall  
 $t_w$  = Wall thickness  
 $V$  = Shear load at the base of the wall  
 $y$  = Response corresponding to regressor variable  
 $y_i = i^{\text{th}}$  actual observed response  
 $y_i = i^{\text{th}}$  predicted response from regression analysis  
 $x$  = Regressor variable  
 $\Delta_{(exp)i} = i^{\text{th}}$  experimental displacement capacity  
 $\Delta_f$  = Flexural displacement (mm)  
 $\Delta_p$  = Plastic displacement (mm)  
 $\Delta_{sh}$  = Shear displacement  
 $\Delta_{sl}$  = Sliding displacement  
 $\Delta_{(u)i}$  = displacement capacity for  $i^{\text{th}}$  wall  
 $\Delta_u$  = Maximum displacement capacity  
 $\Delta_y$  = Yield lateral displacement

$\beta_0$  and  $\beta_1$  = Regression coefficients

$\varepsilon_i$  =  $i^{\text{th}}$  regression error

$\varepsilon_c$  = Compression strain in the outermost fiber in wall cross section

$\varepsilon_t$  = Tension strain in the outermost reinforcement bar

$\varepsilon_m$  = Compression strain in the outermost masonry compression fiber

$\varepsilon_y$  = Yield strain in the vertical reinforcement bar in cross section

$\theta$  = Section rotation

$\theta_p$  = Plastic rotation

$\theta_u$  = Ultimate rotation

$\rho_{sh}$  = Horizontal reinforcement ratio

$\rho_v$  = Vertical reinforcement ratio

$\phi_3$  = Curvature at the end of the spread of plasticity  $L_3$

$\phi_y$  = Yield curvature of the wall section

$\phi_u$  = Ultimate curvature of the wall section

## 2.14 REFERENCE

ACI Committee, American Concrete Institute, & International Organization for Standardization. (2014). "Building code requirements for structural concrete (ACI 318-14) and commentary." American Concrete Institute.

Ahmadi, F., Hernandez, J., Sherman, J., Kapoi, C., Klingner, R. E., and McLean, D. I. (2014). "Seismic Performance of Cantilever-Reinforced Concrete Masonry Shear Walls." *Journal of Structural Engineering*.

Bannister, A. C., J. Ruiz Ocejo, and F. Gutierrez-Solana. "Implications of the yield stress/tensile stress ratio to the SINTAP failure assessment diagrams for homogeneous materials." *Engineering Fracture Mechanics* 67.6 (2000): 547-562.

Banting, B., and El-Dakhakhni, W. W. (2014) "Normal Strain-adjusted Shear Strength Expression (NSSSE) for Reinforced Masonry Structural Walls" *ASCE Journal of Structural Engineering* Vol. 140, No. 3, CID: 04013075.

Bentz, E. C., Vecchio, F. J., & Collins, M. P. (2006). "Simplified modified compression field theory for calculating shear strength of reinforced concrete elements." *ACI Structural Journal*, 103(4), 614.

- Blakeley, R. W. G., Cooney, R. C., and Megget, L. M. (1975). "Seismic shear loading at flexural capacity in cantilever wall structures." *Bulletin of the New Zealand National Society for Earthquake Engineering*, 8(4), 278-290.
- Bohl, A., and Adebar, P. (2011). "Plastic hinge lengths in high-rise concrete shear walls." *ACI Structural Journal*, 108(2).
- Calvi, G. M., and Kingsley, G. R. (1995). "Displacement- based seismic design of multi- degree- of- freedom bridge structures." *Earthquake engineering and structural dynamics*, 24(9), 1247-1266.
- Canadian Standards Association. "CSA S304. 1-14: Design of Masonry Structures." Mississauga, ON, Canada.
- Clough, R. W., Benuska, K. L., and Wilson, E. L. (1965, January). "Inelastic earthquake response of tall buildings." In *Proceedings, Third World Conference on Earthquake Engineering, New Zealand (Vol. 11)*.
- Dazio, A., Beyer, K., and Bachmann, H. (2009). "Quasi-static cyclic tests and plastic hinge analysis of RC structural walls." *Engineering Structures*, 31(7), 1556-1571.
- Drysdale, R. G., Hamid, A. A., and Baker, L. R. (1994). "Masonry structures: behavior and design." Prentice Hall.
- Eikanas, I. K. (2003). "Behavior of concrete masonry shear walls with varying aspect ratio and flexural reinforcement." Diss. Washington State University, 2003.
- European Committee for Standardization (CEN). (2005). "Eurocode 8: Design of structures for earthquake resistance: Part 3: Assessment and retrofitting of buildings." BS EN 1998-3, Brussels, Belgium.
- FEMA (Federal Emergency Management Agency). (2012). "Damage states and fragility curves for reinforced masonry shear walls." FEMA P-58/BD-3.8.10, Washington, DC.
- Hernandez, J. F. (2012). "Quasi-Static Testing of Cantilever Masonry Shear Wall Segments" Master of Science Thesis, Texas University, 2012. Texas University Press: Texas 2012.
- Kapoi, C. M. (2012). "Experimental Performance of Concrete Masonry Shear Walls Under In-Plane Loading." Master-Thesis, Washington University, 2012. Washington University Press: Washington 2012.

- Kazaz, İ. (2013). “Analytical Study on Plastic Hinge Length of Structural Walls.” *Journal of Structural Engineering*, 139(11), 1938-1950.
- Masonry Standards Joint Committee. (2011). “Building Code Requirements for Masonry Structures (TMS 402-11/ACI 530-11/ASCE 5-11).” The Masonry Society, Boulder, CO.
- Medhekar, M. S., and Kennedy, D. J. L. (2000). “Displacement-based seismic design of buildings—theory.” *Engineering structures*, 22(3), 201-209.
- Moehle, J. P. (1992). “Displacement-based design of RC structures subjected to earthquakes.” *Earthquake spectra*, 8(3), 403-428.
- Montgomery, D. C., Peck, E. A., and Vining, G. G. (1992). “Introduction to linear regression analysis.” *Wiley series in probability and statistics* Show all parts in this series.
- Panagiotakos, T. B., and Fardis, M. N. (2001). “Deformations of reinforced concrete members at yielding and ultimate.” *ACI Structural Journal*, 98(2).
- Park, R. (1989). “Evaluation of ductility of structures and structural assemblages from laboratory testing.” *Bulletin of the New Zealand National Society for Earthquake Engineering*, 22(3), 155-166.
- Park, R. (1997). “A static force-based procedure for the seismic assessment of existing reinforced concrete moment resisting frames.” *Bulletin of the New Zealand National Society for Earthquake Engineering*, 30(3), 213-226.
- Paulay, T. (1972). “Some aspects of shear wall design.” *Bulletin of New Zealand Society for Earthquake Engineering*, 5(3).
- Paulay, T., and Spurr, D. D. (1977, January). “Frame-Shear Wall Assemblies Subjected to Simulated Seismic Loading.” In *Proceedings of Sixth World Conference on Earthquake Engineering*, New Delhi.
- Paulay T., and Priestley M. J. N. (1992). “Seismic Design of Reinforced Concrete and Masonry Buildings.” Wiley, New York.
- Paulay, T., and Priestley, M. J. N. (1993). “Stability of ductile structural walls.” *ACI Structural Journal*, 90(4).
- Pilakoutas, K., and Elnashai, A. (1995). “Cyclic behavior of RC cantilever walls, part I: experimental results.” *ACI Structural Journal*, 92(3).
- Priestley, M. J. N. (1981). “Ductility of Unconfined Masonry Shear Walls.” *Bulletin*, 12-20.

- Priestley, M. J. N., and Elder, D. M. (1982). "Cyclic loading tests of slender concrete masonry shear walls." *Bulletin of the New Zealand National Society for Earthquake Engineering*, 15(1), 3-21.
- Priestley, M. J. N. (1982). "Ductility of Confined Concrete Masonry Shear Walls." *Bulletin of the New Zealand National Society for Earthquake Engineering*, 15(1), 22-26.
- Priestley, M. N. (1993). "Myths and fallacies in earthquake engineering - conflicts between design and reality." *Bulletin of the New Zealand National Society for Earthquake Engineering*, 26(3), 329-341.
- Priestley, M. N., and Calvi, G. M. (1996). "Seismic design and retrofit of bridges." John Wiley and Sons.
- Priestley, M. J. N. (2000). "Performance based seismic design." *Bulletin of the New Zealand Society for Earthquake Engineering*, 33(3), 325-346.
- Priestley, M. J. N., Clavi, G. M., and Kowalsky, M. J. (2007). "Displacement-based Seismic Design of Structures." IUSS Press, Pavia, Italy.
- Seber, G. A. F., and Wild, C. J. (1977). "Nonlinear regression." *Wiley Series in Probability and Mathematical Statistics. Applied Probability and Statistics Section (EUA)*.
- Shedid, M., Drysdale, R., and El-Dakhkhni, W. (2008) "Behavior of Fully Grouted Reinforced Concrete Masonry Shear Walls Failing in Flexure: Experimental Results." *J. Structure. Eng.*, 134(11), 1745-1767.
- Shedid, M. T., and El-Dakhkhni, W. W. (2013). "Plastic hinge model and displacement-based seismic design parameter quantifications for reinforced concrete block structural walls." *Journal of Structural Engineering*, 140(4).
- Sherman, J. D. (2011). "Effect of Key Parameters on the Performance of Concrete Masonry Shear Walls Under In-Plan Loading." *PhD-Thesis, Washington University, 2011. Washington University Press: Washington 2011.*
- Shing, P. B., Noland, J. L., Klamerus, E., and Spaeh, H. (1989). "Inelastic behavior of concrete masonry shear walls." *Journal of Structural Engineering*, 115(9), 2204-2225.
- Shing, P. B., Schuller, M., and Hoskere, V. S. (1990). "In-plane resistance of reinforced masonry shear walls." *Journal of structural Engineering*, 116(3), 619-640.

- Standard, C. S. A. (2014). A23. 3-14, “. Design of concrete structures,” Canadian Standards Association, Mississauga.
- Thomsen IV, J. H., and Wallace, J. W. (2004). “Displacement-based design of slender reinforced concrete structural walls-experimental verification.” *Journal of Structural Engineering*, 130(4), 618-630.
- Tomazevic, M. (1999). “Earthquake-resistant design of masonry buildings.” World Scientific.
- TSC (2007), "Turkish Seismic Design Code for Building" Ministry of Public Works and Resettlement, Ankara, Turkey
- Vaughan, T. P. (2010). “Evaluation of Masonry Wall Performance Under Cyclic Loading” Master of Science Thesis, Washington University, 2010. Washington University Press: Washington 2010.
- Voon, K. C., and Ingham, J. M. (2006). “Experimental in-plane shear strength investigation of reinforced concrete masonry walls.” *Journal of structural engineering*, 132(3), 400-408.
- Wallace, J. W., and Moehle, J. P. (1992). “Ductility and detailing requirements of bearing wall buildings.” *Journal of Structural Engineering*, 118(6), 1625-1644.

Table 2.1: Characteristics of experimental wall database

Wall ID	$L_w$ mm	$t_w$ mm	$H_w$ mm	$H_w/L_w$	$\rho_v$ %	$d_b$ mm	$\rho_{sh}$ %	$f_v$ MPa	$f_u$ MPa	$f'_m$ MPa	$P$ kN	$\Delta_u/H_w$ %	Ref.
1	1830	143	1830	1.00	0.38	15.9	0.24	441	710	20.0	361.1	0.820	Shing et al. 1989
2	1830	143	1830	1.00	0.38	15.9	0.24	441	710	20.0	487.5	0.693	
3	1830	143	1830	1.00	0.38	15.9	0.14	441	710	17.9	0.0	0.958	
4	1830	143	1830	1.00	0.38	15.9	0.24	441	710	20.7	0.0	1.319	
5	1830	143	1830	1.00	0.38	15.9	0.14	441	710	22.1	180.5	1.109	
6	1830	143	1830	1.00	0.38	15.9	0.24	441	710	22.1	180.5	0.858	
7	1830	143	1830	1.00	0.54	19.1	0.24	448	738	22.8	180.5	1.109	
8	1830	137	1830	1.00	0.40	15.9	0.26	441	710	26.2	484.3	0.913	
9	1830	137	1830	1.00	0.40	15.9	0.26	441	710	26.2	484.3	0.967	
10	1830	137	1830	1.00	0.40	15.9	0.26	441	710	26.2	484.3	1.021	
11	1830	137	1830	1.00	0.40	15.9	0.26	441	710	26.2	484.3	1.077	
12	1800	140	1800	1.00	0.62	20.0	0.05	318	366	17.6	0.0	0.556	Voon 2006
13	1800	140	1800	1.00	0.62	20.0	0.14	318	366	17.0	0.0	0.444	
14	1800	190	3600	2.00	0.29	16.0	0.08	502	577	18.5	0.0	0.889	Shedid et al. 2008
15	1800	190	3600	2.00	0.78	20.0	0.13	502	577	18.5	0.0	0.917	
16	1800	190	3600	2.00	0.73	25.0	0.13	502	577	18.5	0.0	0.778	
17	1800	190	3600	2.00	1.31	25.0	0.26	502	577	18.5	0.0	0.833	
18	1800	190	3600	2.00	1.31	25.0	0.26	502	577	18.5	260.0	0.694	
19	1800	190	3600	2.00	1.31	25.0	0.26	624	718	18.5	520.0	0.833	
20	1016	190	2032	2.00	0.33	12.7	0.31	450	518	21.0	0.0	1.450	Kapoi 2012
21	1016	190	2032	2.00	0.33	12.7	0.31	455	523	21.0	270.3	1.750	
22	1016	190	2032	2.00	0.59	22.2	0.31	455	523	15.7	202.7	1.088	
23	1829	190	1422	0.78	0.55	22.2	0.62	455	523	15.7	364.9	0.625	
24	1829	190	1829	1.00	0.55	22.2	0.62	455	523	15.7	264.9	1.083	
25	1422	190	2845	2.00	0.72	19.1	0.16	465	535	15.7	0.0	1.848	
26	1422	190	2845	2.00	0.87	19.1	0.34	465	535	15.7	0.0	2.089	
27	1422	190	2845	2.00	0.87	19.1	0.34	465	535	15.7	283.8	1.929	
28	1007	190	2013	2.00	0.69	19.1	0.31	454	522	19.1	244.3	1.110	Sherman 2011
29	1007	190	2013	2.00	0.69	19.1	0.31	446	513	19.1	244.3	1.274	
30	1007	190	2013	2.00	0.31	12.7	0.31	454	522	21.0	536.2	0.896	
31	1007	190	2013	2.00	0.31	12.7	0.31	450	518	21.0	536.2	0.795	
32	1819	190	1819	1.00	0.31	12.7	0.10	450	518	21.0	0.0	0.698	
33	1819	190	1819	1.00	0.31	12.7	0.31	450	518	21.0	484.6	0.656	
34	1819	190	1413	0.78	0.31	12.7	0.31	450	518	21.0	0.0	1.114	
35	1819	190	1413	0.78	0.31	12.7	0.62	450	518	21.0	484.6	0.719	

Table 2.1 (continued): Characteristics of experimental wall database

Wall ID	$L_w$ mm	$t_w$ mm	$H_w$ mm	$H_w/L_w$	$\rho_v$ %	$d_b$ mm	$\rho_{sh}$ %	$f_y$ MPa	$f_u$ MPa	$f'_m$ MPa	$P/A_g$ kN	$\Delta_u/H_w$ %	Ref.
36	1020	190	2030	1.99	0.69	19.1	0.31	456	725	19.0	245.9	1.110	Ahmadi et al. 2014
37	1020	190	2030	1.99	0.69	19.1	0.31	446	725	21.0	271.8	1.490	
38	1020	190	2030	1.99	0.31	12.7	0.31	456	693	19.0	49.2	0.800	
39	1020	190	2030	1.99	0.31	12.7	0.31	450	693	21.0	54.4	0.910	
40	1830	190	1830	1.00	0.31	12.7	0.10	450	693	21.0	0.0	0.690	
41	1830	190	1830	1.00	0.31	12.7	0.31	450	693	21.0	487.6	0.710	
42	1830	190	1830	1.00	0.31	12.7	0.31	450	693	21.0	0.0	0.900	
43	1830	190	1830	1.00	0.31	12.7	0.31	450	693	21.0	487.6	0.700	
44	1220	190	3660	3.00	0.69	19.1	0.16	421	725	31.0	383.9	1.560	
45	1220	190	3660	3.00	0.31	12.7	0.16	448	693	23.0	569.6	1.930	
46	1220	190	3660	3.00	0.69	19.1	0.16	421	725	23.0	569.6	1.170	
47	1220	190	3660	3.00	0.31	12.7	0.16	448	693	23.0	854.4	1.270	
48	810	190	3660	4.52	0.69	19.1	0.31	421	725	29.0	238.4	3.000	
49	810	190	3660	4.52	0.31	12.7	0.31	448	693	29.0	476.8	2.610	
50	810	190	3660	4.52	0.69	19.1	0.16	421	725	23.0	378.2	2.790	
51	810	190	3660	4.52	0.31	12.7	0.16	448	693	23.0	567.3	1.650	
52	1020	190	2030	1.99	0.31	12.7	0.31	450	693	21.0	0.0	2.200	
53	1020	190	2030	1.99	0.31	12.7	0.31	455	693	21.0	271.8	2.110	
54	1020	190	2030	1.99	0.47	22.2	0.31	455	702	16.0	207.1	1.120	
55	1830	190	1420	0.78	0.47	22.2	0.63	455	702	16.0	371.5	0.930	
56	1830	190	1830	1.00	0.47	22.2	0.63	455	702	16.0	371.5	1.100	
57	1420	190	2840	2.00	0.69	19.1	0.16	465	725	16.0	0.0	1.890	
58	1420	190	2840	2.00	0.59	19.1	0.34	465	725	16.0	0.0	2.100	
59	1420	190	2840	2.00	0.59	19.1	0.34	465	725	16.0	288.3	2.020	
60	2440	190	2440	1.00	0.31	12.7	0.31	423	693	31.0	0.0	0.840	
61	2440	190	2440	1.00	0.16	12.7	0.16	423	693	29.0	0.0	1.760	
62	2440	190	2440	1.00	0.16	12.7	0.16	423	693	28.0	0.0	1.780	
63	2440	190	2440	1.00	0.31	12.7	0.31	423	693	31.0	1535.5	0.760	
64	2440	190	2440	1.00	0.16	12.7	0.16	423	693	29.0	1436.4	0.540	
65	2440	190	2440	1.00	0.16	12.7	0.16	423	693	28.0	1386.9	0.520	

Table 2.1 (continued): Characteristics of experimental wall database

Wall ID	$L_w$	$t_w$	$H_w$	$H_w/L_w$	$\rho_v$	$d_b$	$\rho_{sh}$	$f_y$	$f_u$	$f'_m$	$P/A_g$	$\Delta_u/H_w$ %	Ref.
	mm	mm	mm		%	mm	%	MPa	MPa	MPa	kN		
66	1410	190	1320	0.94	0.51	16.0	0.25	437	503	12.0	66.1	0.758	Vaughan 2010
67	1410	190	2135	1.51	0.51	16.0	0.16	437	503	12.0	66.1	0.835	
68	1410	190	1320	0.94	0.29	16.0	0.16	455	524	12.0	52.5	0.662	
69	1410	190	2135	1.51	0.29	16.0	0.16	455	524	12.0	52.5	0.830	
70	1410	190	1320	0.94	0.51	16.0	0.16	455	524	12.0	52.5	0.663	
71	1410	190	2135	1.51	0.51	16.0	0.16	455	524	12.0	52.5	0.829	
72	1000	190	2135	2.14	0.51	16.0	0.16	455	524	12.0	37.2	1.045	
73	1820	190	1320	0.73	0.28	16.0	0.16	455	524	12.0	67.8	0.588	
74	1220	143	1440	1.18	0.44	22.2	0.39	390	450	15.1	303.1	0.480	
75	1220	143	1440	1.18	0.44	22.2	0.20	390	450	15.1	120.3	0.614	
76	2440	195	2440	1.00	0.33	12.7	0.33	423	681	29.0	0.0	1.301	Hernandez 2012
77	2440	195	2440	1.00	0.16	12.7	0.16	423	681	29.0	0.0	1.822	
78	2440	195	2441	1.00	0.33	12.7	0.33	423	681	29.0	47.6	1.036	
79	2440	195	2442	1.00	0.16	12.7	0.16	423	681	29.0	47.6	1.140	
80	2440	195	2443	1.00	0.33	12.7	0.16	423	681	24.3	0.0	1.871	
81	2440	195	2444	1.00	0.16	12.7	0.16	423	681	24.3	47.6	1.023	

Table 2.2: Yield, ultimate curvatures, and drift capacities of wall database

Wall ID	$\phi_y$	$\phi_u$	$\Delta_m/H_w$ %								Ref.
	$1/10^{-6}$ $mm^{-1}$	$1/10^{-6}$ $mm^{-1}$	Model I <sup>(1)</sup>	Model II <sup>(2)</sup>	Model III <sup>(3)</sup>	Model IV <sup>(4)</sup>	Model V <sup>(5)</sup>	Model VI <sup>(6)</sup>	Model VII <sup>(7)</sup>	Model VIII <sup>(8)</sup>	
1	1.76	9.38	0.406	0.323	0.329	0.489	0.474	0.385	0.400	0.608	Shing et al. 1989
2	1.83	8.12	0.358	0.289	0.294	0.427	0.419	0.333	0.348	0.550	
3	1.57	16.94	0.698	0.530	0.542	0.876	0.800	0.711	0.734	1.071	
4	1.55	19.04	0.780	0.589	0.602	0.968	0.889	0.795	0.810	1.309	
5	1.65	13.53	0.566	0.436	0.445	0.689	0.653	0.557	0.583	0.839	
6	1.65	13.53	0.566	0.436	0.445	0.689	0.653	0.557	0.575	0.839	
7	1.70	11.17	0.475	0.424	0.395	0.594	0.577	0.468	0.482	0.784	
8	1.76	9.73	0.420	0.332	0.339	0.495	0.489	0.396	0.414	0.617	
9	1.76	9.73	0.420	0.332	0.339	0.495	0.489	0.396	0.414	0.617	
10	1.76	9.73	0.420	0.332	0.339	0.495	0.489	0.396	0.414	0.617	
11	1.76	9.73	0.420	0.332	0.339	0.495	0.489	0.396	0.414	0.617	
12	1.22	15.72	0.632	0.452	0.478	0.785	0.597	0.644	0.678	0.940	Voon 2006
13	1.22	15.31	0.617	0.442	0.467	0.768	0.583	0.628	0.652	0.917	
14	1.79	18.64	1.025	0.947	1.063	1.721	1.084	1.056	1.210	1.569	Shedid et al. 2008
15	1.97	8.22	0.537	0.532	0.566	0.817	0.647	0.548	0.601	0.903	
16	1.94	9.63	0.603	0.633	0.661	0.982	0.752	0.617	0.682	1.053	
17	2.07	6.50	0.462	0.479	0.495	0.680	0.582	0.470	0.499	0.826	
18	2.16	5.83	0.435	0.450	0.463	0.616	0.542	0.432	0.458	0.765	
19	2.24	5.29	0.415	0.458	0.449	0.581	0.612	0.403	0.425	0.708	
20	2.99	33.20	1.023	1.011	1.103	1.772	1.124	1.054	1.168	1.739	Kapoi 2012
21	3.42	17.12	0.604	0.600	0.641	0.945	0.687	0.584	0.644	1.008	
22	3.59	13.87	0.522	0.650	0.602	0.875	0.677	0.508	0.546	1.068	
23	1.87	7.63	0.298	0.305	0.249	0.365	0.341	0.285	0.260	0.562	
24	1.83	8.31	0.365	0.364	0.322	0.481	0.420	0.355	0.335	0.658	
25	2.37	10.52	0.535	0.544	0.573	0.848	0.645	0.546	0.597	0.938	
26	2.41	11.96	0.591	0.602	0.637	0.959	0.700	0.605	0.641	0.966	
27	2.60	9.09	0.494	0.501	0.524	0.743	0.580	0.481	0.511	0.791	

(1) Paulay and Priestley (1993)

(2) Priestley and Calvi (1996)

(3) Panagiotakos and Fardis (2001)

(4) Euro Code 8 (2005)

(5) Priestley et al. (2007)

(6) Bohl and Adebar (2011)

(7) Kazaz (2013)

(8) Shedid and El-Dakhkhni (2013)

Table 2.2(Cont): Yield, ultimate curvatures and drift capacities of wall database

Wall ID	$\phi_y$	$\phi_u$	$\Delta_m/H_w$ %								Ref.
	$1/10^6$ $mm^{-1}$	$1/10^6$ $mm^{-1}$	Model I <sup>(1)</sup>	Model II <sup>(2)</sup>	Model III <sup>(3)</sup>	Model IV <sup>(4)</sup>	Model V <sup>(5)</sup>	Model VI <sup>(6)</sup>	Model VII <sup>(7)</sup>	Model VIII <sup>(8)</sup>	
28	3.65	12.59	0.485	0.554	0.540	0.755	0.605	0.473	0.510	0.935	Sherman 2011
29	3.59	12.69	0.486	0.550	0.540	0.758	0.602	0.473	0.511	0.932	
30	3.79	11.86	0.471	0.470	0.494	0.671	0.534	0.440	0.480	0.768	
31	3.76	11.88	0.471	0.469	0.493	0.671	0.532	0.440	0.480	0.767	
32	1.57	18.46	0.754	0.520	0.558	0.898	0.709	0.768	0.799	1.082	
33	1.79	9.73	0.418	0.308	0.326	0.486	0.417	0.399	0.409	0.598	
34	1.57	18.58	0.689	0.464	0.461	0.737	0.644	0.699	0.669	0.997	
35	1.79	9.76	0.373	0.267	0.266	0.395	0.367	0.354	0.332	0.541	
36	3.60	12.50	0.486	0.552	0.539	0.755	0.678	0.473	0.510	0.814	Ahmadi et al. 2014
37	3.50	13.11	0.498	0.564	0.554	0.780	0.697	0.485	0.527	0.829	
38	3.12	26.35	0.843	0.836	0.905	1.431	1.140	0.856	0.940	1.195	
39	3.06	28.38	0.896	0.885	0.961	1.521	1.206	0.910	1.008	1.259	
40	1.56	18.48	0.758	0.521	0.561	0.902	0.832	0.772	0.804	1.007	
41	1.78	9.70	0.419	0.308	0.326	0.487	0.473	0.400	0.410	0.558	
42	1.56	18.48	0.758	0.521	0.561	0.902	0.832	0.772	0.777	1.007	
43	1.78	9.70	0.419	0.308	0.326	0.487	0.473	0.400	0.410	0.559	
44	2.60	13.96	0.752	0.817	0.897	1.309	1.060	0.742	0.849	1.161	
45	2.91	11.43	0.681	0.691	0.766	1.081	0.897	0.649	0.731	0.862	
46	2.85	9.58	0.605	0.643	0.691	0.947	0.808	0.579	0.644	0.871	
47	3.11	8.77	0.596	0.602	0.652	0.861	0.754	0.558	0.616	0.709	
48	4.18	20.25	1.006	1.216	1.330	1.919	1.485	1.000	1.105	1.598	
49	4.61	17.88	0.972	1.085	1.202	1.680	1.326	0.936	1.028	1.241	
50	4.56	14.40	0.860	0.989	1.058	1.433	1.167	0.833	0.908	1.244	
51	4.96	13.19	0.860	0.930	1.002	1.307	1.091	0.818	0.884	1.027	
52	3.00	33.00	1.019	1.006	1.096	1.760	1.372	1.050	1.163	1.687	
53	3.41	17.11	0.603	0.599	0.640	0.943	0.802	0.584	0.644	0.892	
54	3.31	20.24	0.685	0.895	0.814	1.261	1.043	0.661	0.724	1.257	
55	1.87	7.68	0.300	0.307	0.250	0.367	0.370	0.287	0.262	0.541	
56	1.87	7.66	0.341	0.340	0.303	0.444	0.431	0.327	0.312	0.578	
57	2.36	10.76	0.542	0.552	0.582	0.864	0.753	0.554	0.606	0.925	
58	2.36	10.68	0.540	0.549	0.579	0.858	0.749	0.552	0.583	0.921	
59	2.57	8.28	0.460	0.467	0.487	0.678	0.616	0.449	0.476	0.725	
60	1.05	20.38	1.096	0.653	0.743	1.211	1.102	1.117	1.147	1.436	
61	1.02	36.43	1.934	1.121	1.288	2.153	1.896	1.973	2.061	2.416	
62	1.02	35.45	1.883	1.093	1.255	2.101	1.848	1.921	2.006	2.352	
63	1.30	6.18	0.361	0.249	0.272	0.390	0.389	0.332	0.350	0.433	
64	1.29	6.88	0.397	0.269	0.295	0.432	0.424	0.364	0.390	0.473	
65	1.29	6.85	0.396	0.268	0.294	0.431	0.423	0.363	0.389	0.471	

Table 2.2(Continued): Yield, ultimate curvatures, and drift capacities of wall database

Wall	$\phi_y$	$\phi_u$	$\Delta_m/H_w$ %								Ref.
ID	$1/10^{-6}$ $mm^{-1}$	$1/10^{-6}$ $mm^{-1}$	Model I <sup>(1)</sup>	Model II <sup>(2)</sup>	Model III <sup>(3)</sup>	Model IV <sup>(4)</sup>	Model V <sup>(5)</sup>	Model VI <sup>(6)</sup>	Model VII <sup>(7)</sup>	Model VIII <sup>(8)</sup>	
66	2.29	10.52	0.345	0.323	0.291	0.449	0.383	0.343	0.338	0.582	Vaughan 2010
67	2.30	10.44	0.443	0.407	0.427	0.650	0.499	0.444	0.474	0.709	
68	2.26	16.56	0.523	0.500	0.434	0.712	0.573	0.523	0.525	0.885	
69	2.26	16.33	0.643	0.590	0.622	1.011	0.711	0.648	0.699	1.029	
70	2.37	10.43	0.343	0.330	0.293	0.450	0.388	0.343	0.344	0.590	
71	2.38	10.37	0.443	0.413	0.431	0.652	0.508	0.446	0.475	0.720	
72	3.51	14.66	0.555	0.589	0.615	0.923	0.674	0.560	0.609	0.935	
73	1.71	12.45	0.456	0.376	0.327	0.535	0.466	0.455	0.435	0.719	
74	2.68	13.35	0.422	0.482	0.411	0.624	0.494	0.382	0.400	0.752	
75	2.43	21.17	0.631	0.737	0.612	0.986	0.746	0.612	0.651	1.141	
76	1.06	19.59	1.055	0.630	0.717	1.170	1.064	1.075	1.099	1.381	Hernandez 2012
77	1.02	37.07	1.967	1.141	1.310	2.191	1.929	2.007	2.097	2.444	
78	1.07	18.23	0.984	0.590	0.671	1.090	0.996	0.999	1.022	1.279	
79	1.03	33.08	1.759	1.024	1.175	1.958	1.731	1.787	1.869	2.167	
80	1.03	32.32	1.719	1.002	1.148	1.936	1.693	1.754	1.824	2.140	
81	1.04	28.65	1.528	0.895	1.024	1.719	1.511	1.550	1.615	1.887	

(1) Paulay and Priestley (1993)  
(2) Priestley and Calvi (1996)  
(3) Panagiotakos and Fardis (2001)  
(4) Euro Code 8 (2005)

(5) Priestley et al. (2007)  
(6) Bohl and Adebar (2011)  
(7) Kazaz (2013)  
(8) Shedid and El-Dakhakhni (2013)

Table 2.3: Plastic hinge and displacement capacity models

Model	Reff.
$L_p = 0.2L_w + 0.044H_w$	<b>Paulay and Priestley (1993)</b>
$L_p = 0.08H_w + 0.022d_b f_y$	<b>Priestley and Calvi (1996)</b>
$\theta_u = \frac{\phi_y L_w}{3} + (\phi_u - \phi_y) L_p \left(1 - \frac{L_p}{2L_w}\right)$	<b>Panagiotakos and Fardis (2001)</b>
$L_{p,cy} = 0.12L_w + 0.014a_{sl} d_b f_y$	
$L_p = \frac{L_v}{30} + 0.2L_w + 0.11 \frac{d_b f_y}{\sqrt{f_c}}$	<b>Euro Code 8 (2005)</b>
$L_p = k.H + 0.1L_w + L_{sp}$	<b>Priestley et al. (2007)</b>
$L_p = \left(0.2L_w + 0.05 \frac{M}{V}\right) \left(1 - 1.5 \frac{P}{f_c' A_w}\right)$	<b>Bohl and Adebar (2011)</b>
$L_p = 0.27L_w \left(1 - \frac{P}{A_w f_c'}\right) \left(1 - \frac{f_y \rho_{sh}}{f_c'}\right) \left(\frac{M/V}{L_w}\right)^{0.45}$	<b>Kazaz (2013)</b>
$\Delta_u = \Delta_y + (\phi_u - \phi_y) L_2 \left(H_w - \frac{L_2}{2}\right) + \phi_u L_1 \left(H_w + \frac{L_1}{2}\right) + \frac{1}{4} (\phi_u - \phi_3) L_3 \left(H_w - L_2 - \frac{L_3}{3}\right)$	<b>Shedid and El-Dakhakhni (2013)</b>

Table 2.4: Regression analysis results

Model	$\Delta_m / \Delta_{exp}$
<b>Paulay and Priestley (1993)</b>	0.52
<b>Priestley and Calvi (1996)</b>	0.46
<b>Panagiotakos and Fardis (2001)</b>	0.49
<b>Euro Code 8 (2005)</b>	0.73
<b>Priestley et al. (2007)</b>	0.61
<b>Bohl and Adebar (2011)</b>	0.52
<b>Kazaz (2013)</b>	0.55
<b>Shedid and El-Dakhakhni (2013)</b>	0.78

Table 2.5: Proposed model calibration coefficients and errors

Model	Calibration Coefficient			Errors		
	1	2	3	Max	Min	RMS
<b>Paulay and Priestley (1993)</b>	2.63	25.47	---	1.12	-1.75	0.58
<b>Priestley and Calvi (1996)</b>	0.63	7.64	---	1.11	-1.64	0.61
<b>Panagiotakos and Fardis (2001)</b>	0.42	11.99	---	1.11	-1.64	0.61
<b>Euro Code 8 (2005)</b>	0.84	0.35	6.47	1.06	-1.50	0.60
<b>Priestley et al. (2007)</b>	0.86	0.10	6.58	1.06	-1.60	0.59
<b>Bohl and Adebar (2011)</b>	0.01	0.23	---	1.38	-0.98	0.57
<b>Kazaz (2013)</b>	2.63	---	---	2.18	-5.61	0.82
<b>Shedid and El-Dakhakhni (2013)</b>	0.01	2.71	2.32	0.96	-1.22	0.51

Table 2.6: Characteristics of default wall

Model	Parameter (Units)
$d_b$	16 (mm)
$d_{bsh}$	11.5 (mm)
$S_v$	400 (mm)
$S_{sh}$	400 (mm)
$f'_m$	13.5 (MPa)

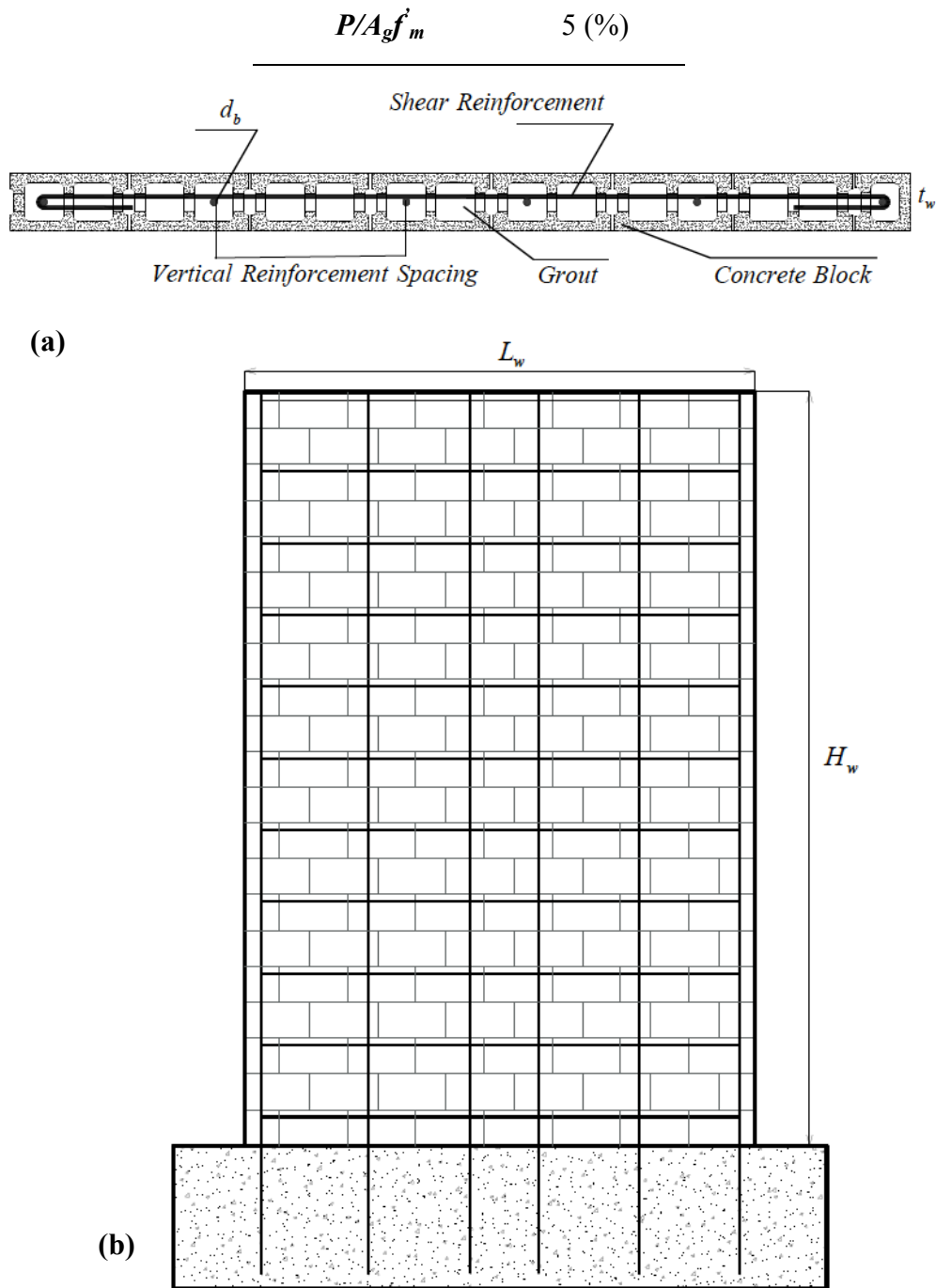


Figure 2.1: Typical Reinforced concrete block shear wall (RCBSW) configuration; a) Rectangular cross section; b) Elevation.

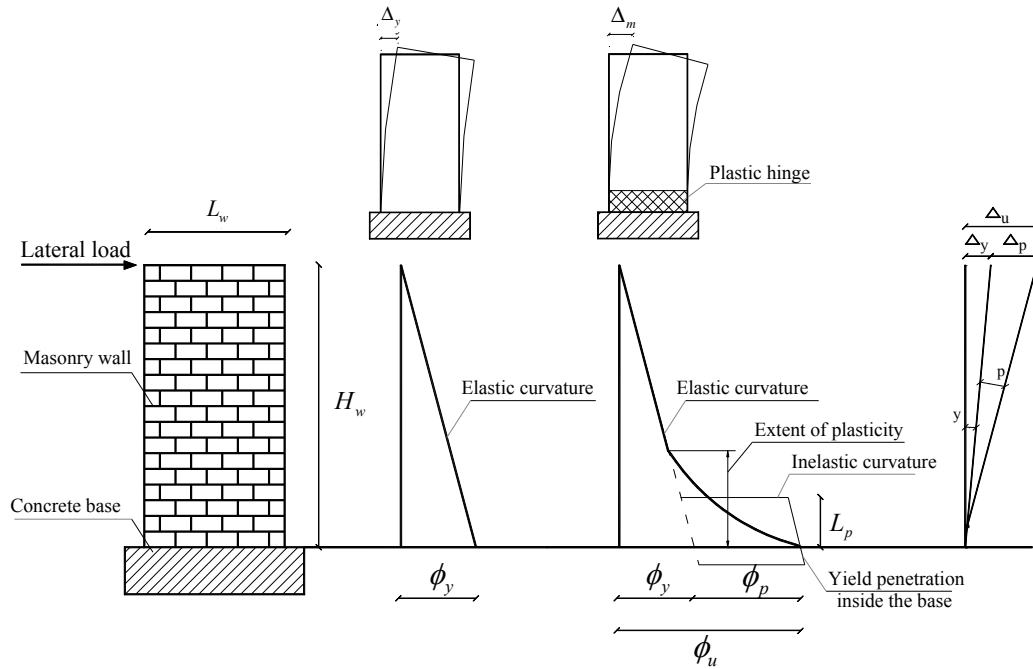


Figure 2.2: Idealized representation of plastic hinge (Paulay and Priestley 1992).

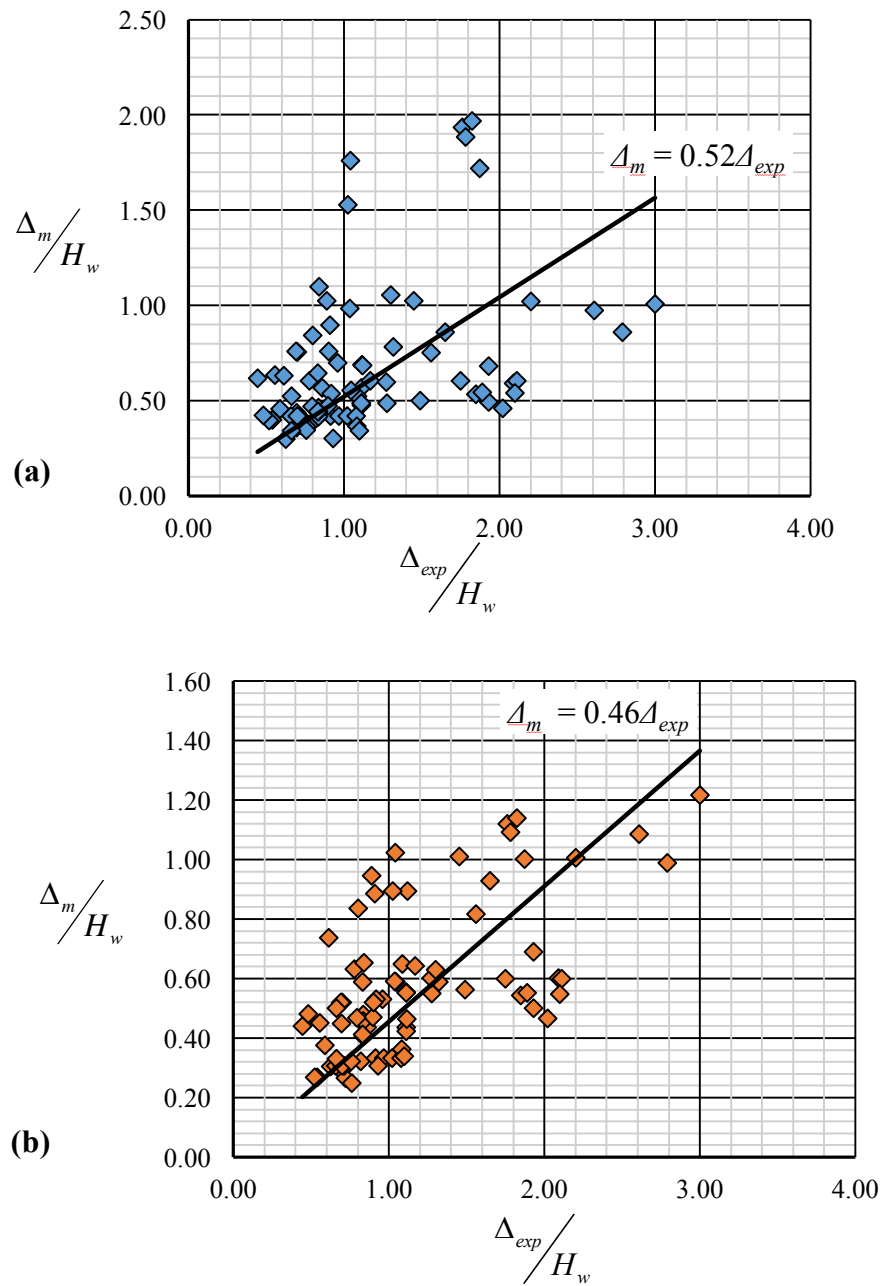


Figure 2.3: Sample linear regression plot of models; a) Paulay and Priestley (1993); b) Priestley and Calvi (1996).

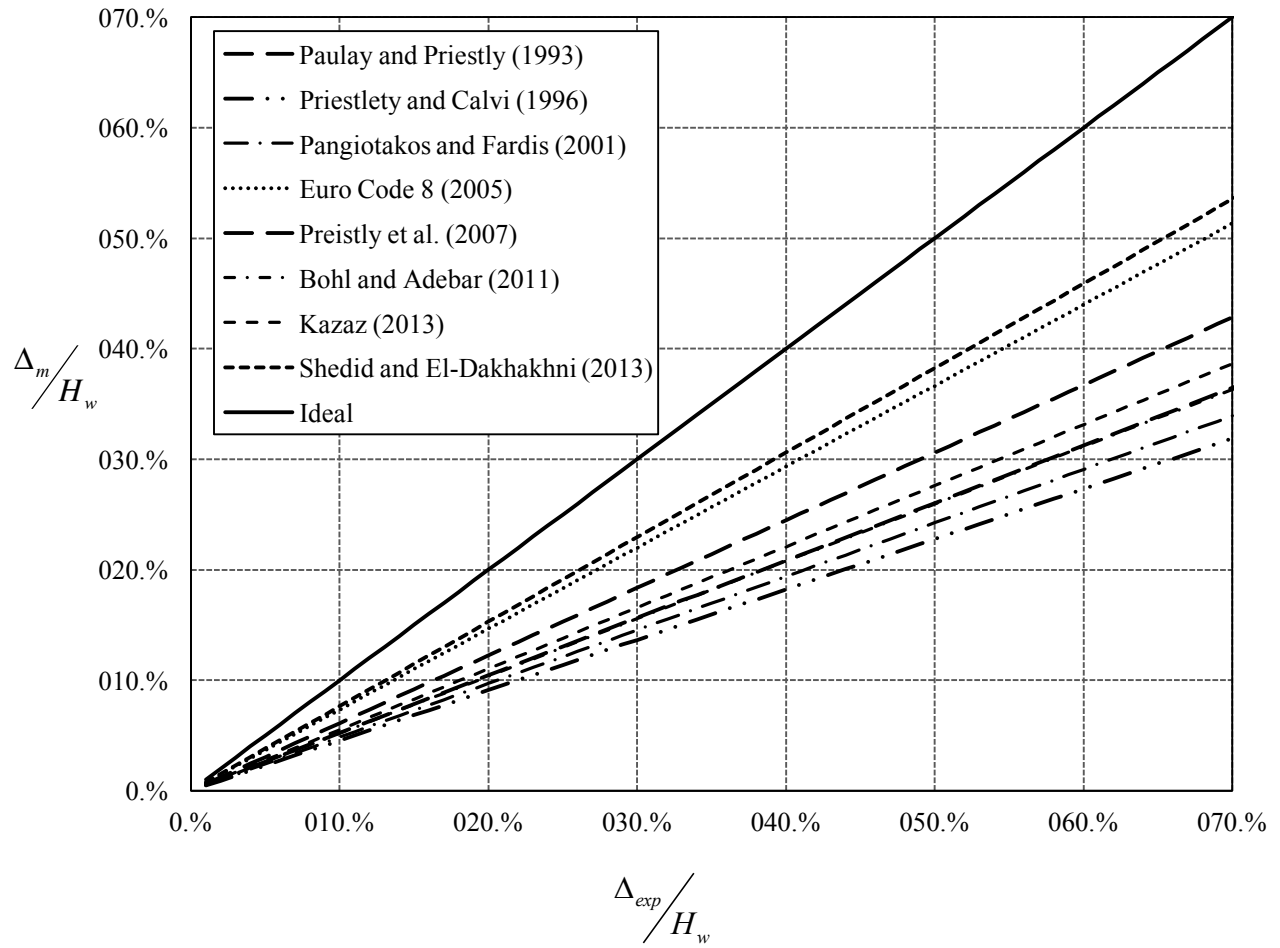


Figure 2.4: Linear regression lines for the eight models.

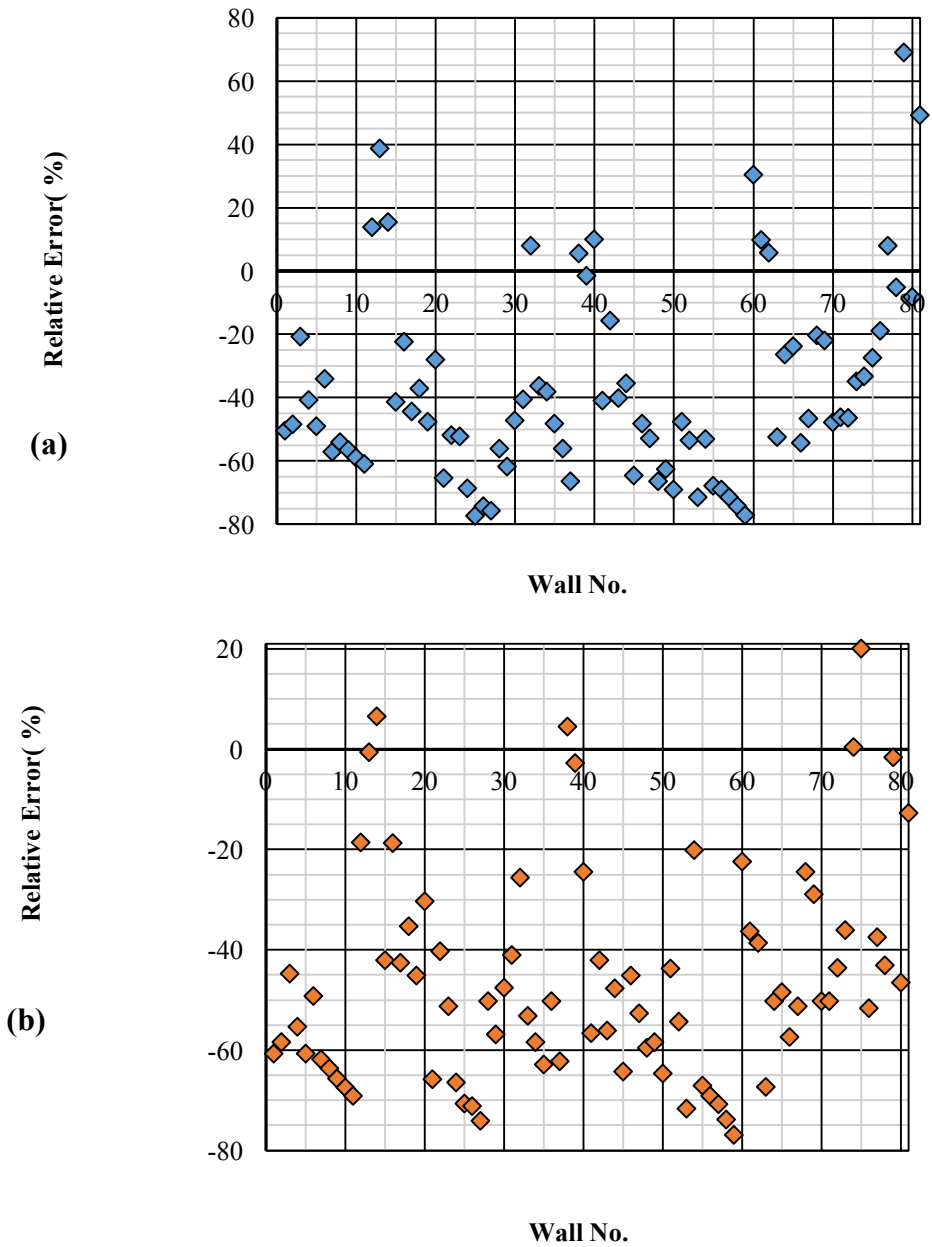


Figure 2.5: Sample residual plot of models; a) Paulay and Priestley (1993) (b) Priestley and Calvi (1996).

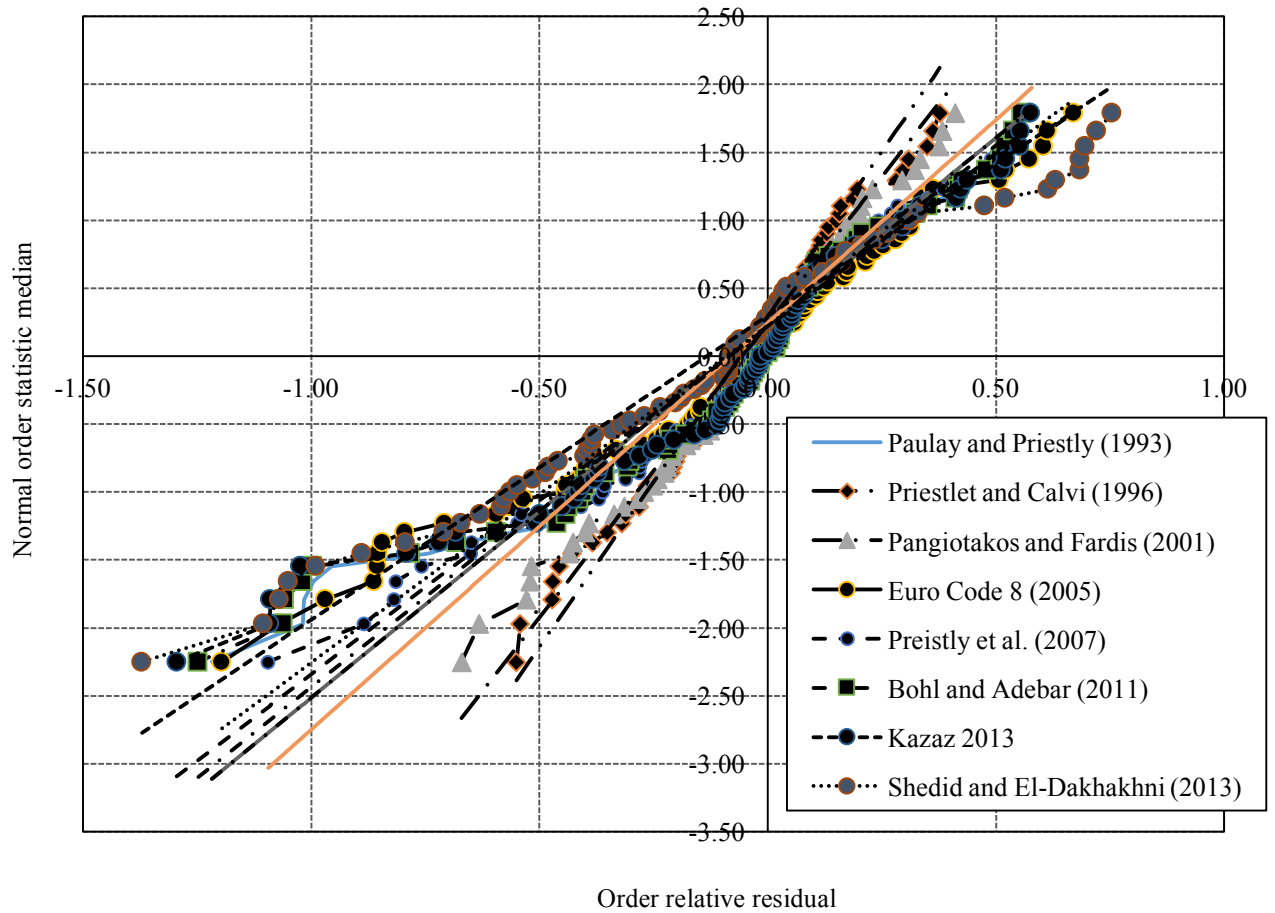


Figure 2.6: Normal probability plot of residuals.

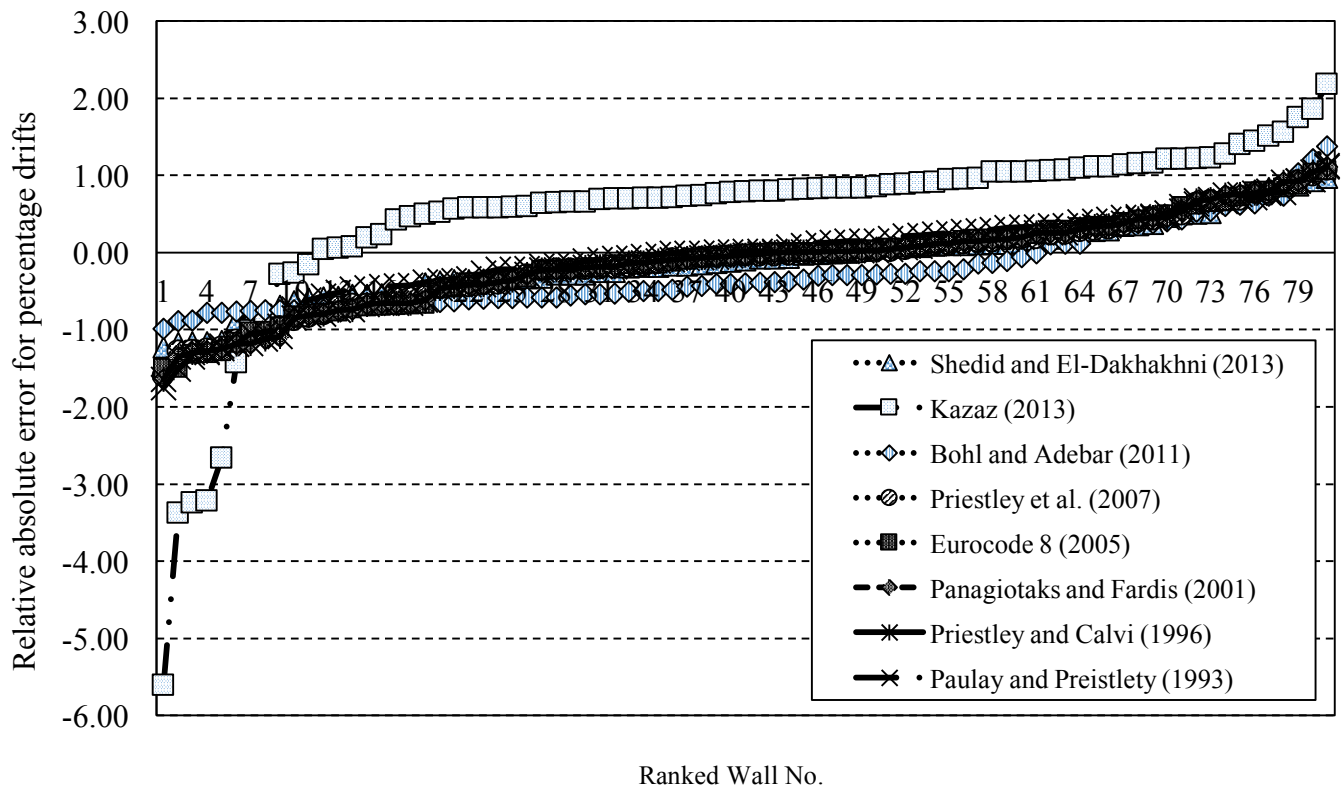


Figure 2.7: Ranked residuals from different calibrated models.

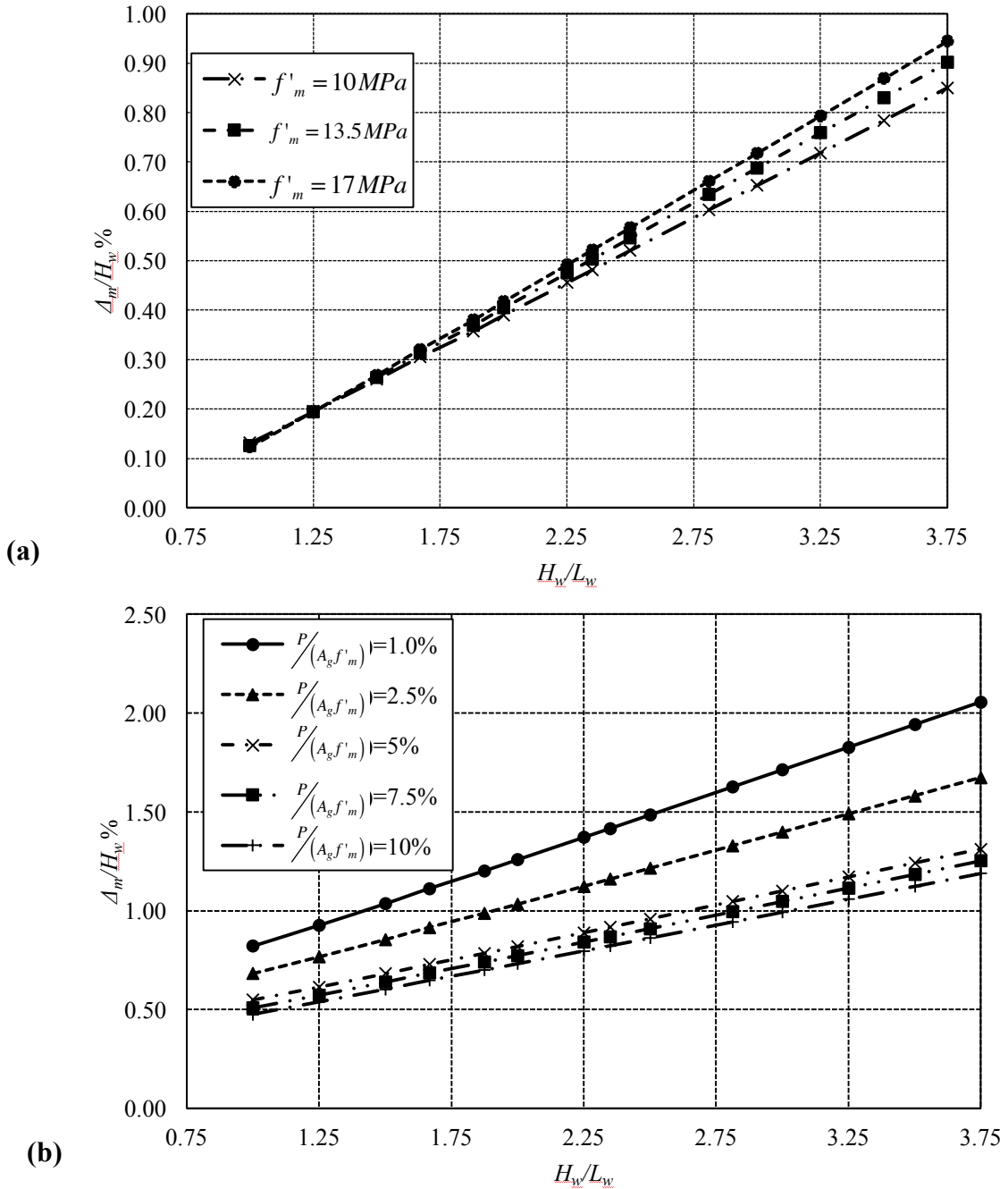


Figure 2.8: Influence of different wall characteristics on the drift capacity using the calibrated model of Shedid and El-Dakhkhni (2013); **a)** The masonry compressive strength; **b)** The axial load ratio.

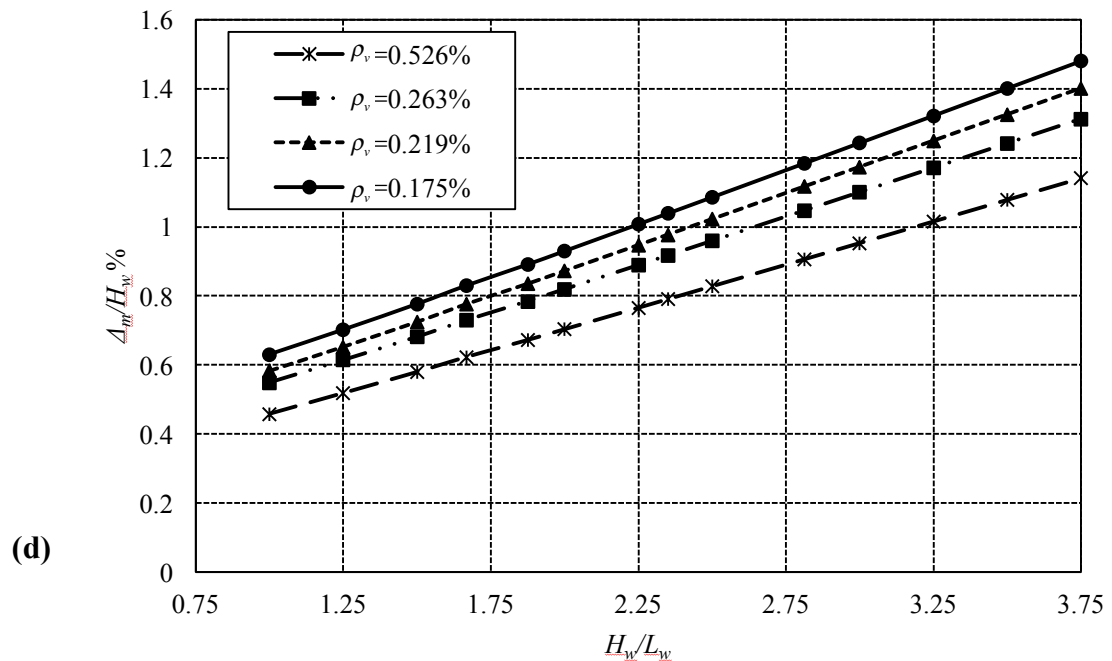
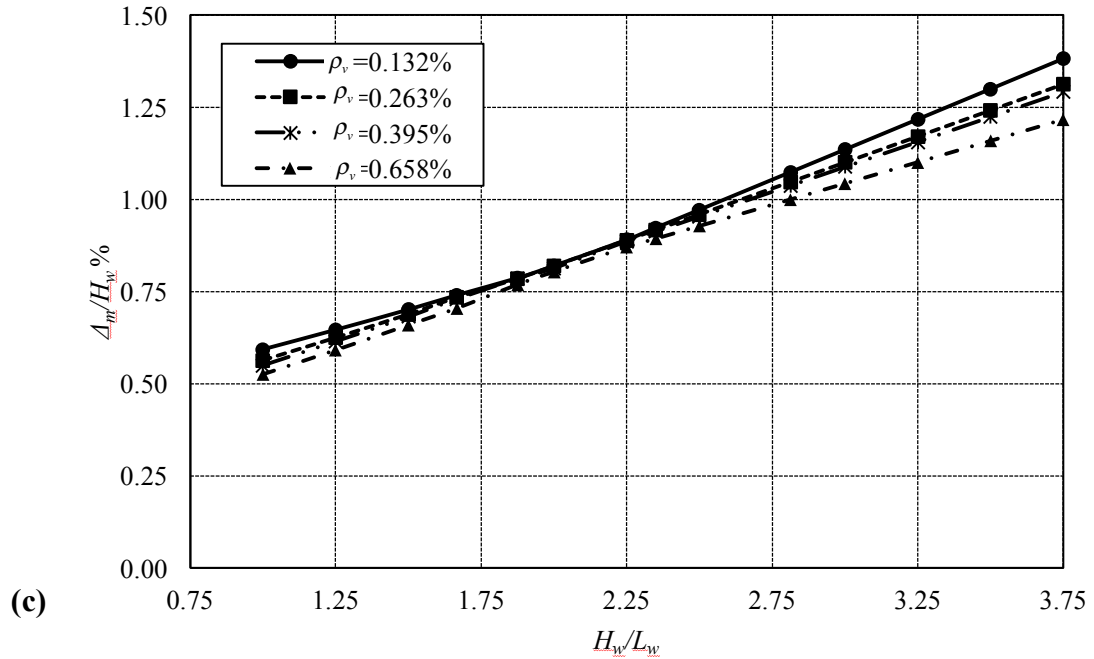


Figure 2.8 (continued): Influence of different wall characteristics on the drift capacity using the calibrated model of Shedid and El-Dakhkhni (2013); c) The vertical reinforcement ratio by changing the bar diameter; (d) The vertical reinforcement ratio by changing the spacing between the vertical bars.

### **CHAPTER 3**

#### **SCORING MODELS FOR REINFORCED MASONRY SHEAR WALL MAXIMUM DISPLACEMENT PREDICTION UNDER SEISMIC LOADS**

##### **3.1 ABSTRACT**

In the past decade, there has been an increased shift towards performance-based Seismic Design (PBSD) approaches to meet the requirements for the next generation of seismic codes worldwide. Displacement-based Seismic Design (DBSD) is key for implementing PBSD approaches as structural performance is typically linked to damage which in turn is associated with component displacements and deformations. Available reinforced masonry shear wall (RMSW) displacement prediction models in the literature are found to be unreliable when compared with published experimental results. This study outlines the use of a statistical multivariate analysis technique and applying it to develop a reliable model for the maximum displacement capacity prediction of RMSW systems. This approach is subsequently used to build scoring models based on an experimental database of 81 flexurally dominated RMSW tested under simulated seismic loads. The models are further utilized to investigate the influence of altering the wall design characteristics on their maximum displacement capacities. The developed models are considered a major step to facilitate DBSD codification of RMSW systems for the next generation of PBSD codes.

### **3.2 INTRODUCTION**

Performance-based seismic design (PBSD) approaches attempt to quantify how components or systems are likely to perform, given a potential seismic hazard that they are likely to experience, considering uncertainties inherent in quantifying both the hazard and the component/system responses. A typical PBSD process starts with the selection of performance objectives [Priestley (2000), FEMA P. 58(2012)]. Each performance objective indicates the acceptable risk of incurring specific damage levels, and the consequent losses as a result of this damage, conditional on a specified level of seismic hazard. Each level of damage, as a performance indicator, is typically predefined by the lateral drifts either at the top floor-level and/or inter-story drifts. Linkage between damage and displacement has been the motivation for the development of displacement-based seismic design methodologies [Moehle (1992), Priestley (1993), and Calvi et al. (2008)].

Masonry systems are among the most common forms of construction in urban areas for low- and mid-rise buildings. In terms of potential seismic hazard, there is a perception that masonry buildings in general possess low level of ductility and are particularly vulnerable under seismic events. This perception is attributed to the observed brittle nature of unreinforced masonry components and systems worldwide during seismic events. However, over the past decades, a large number of experimental studies has demonstrated the seismic performance capabilities enhancements of reinforced masonry shear walls in terms of displacement ductility and energy dissipation capabilities [Klingner et al. (2012), Ahmadi et al (2014)].

Displacement-based seismic design (DBSD) approaches focus on identifying target design displacement as such displacement typically correspond to specific damage/performance level. As such, displacement is the main design input in any DBSD procedure. DBSD also requires quantifying the secant stiffness corresponding to that target displacement as well as hysteretic damping and ductility level. Although outside the scope of the current study, predictive models for such parameters are also needed. Regardless of the procedure adopted for DBSD [Sullivan et al. (2003)], it is necessary to develop and calibrate a displacement capacity model for the structural component and system under consideration. In this respect, several analytical models are proposed to predict the displacement capacity for RMSW with opening, squat wall, or confined masonry governed by shear failure [Yang et al (1992), Mostafaei et al. (2009), Riahi et al. (2009), and Deaton et al. (2009)]. Unlike available models for predicting reinforced *concrete* shear wall (RCSW) displacements, models to predict the displacements of reinforced *masonry* shear walls (RMSW) are scarce in literature. For flexurally-dominated rectangular cantilever RCSW where a plastic region is expected to formed at the interface region between the wall and the foundation, seven different models [Paulay and Priestly (1993), Priestly et al. (1996), Pangiotakos and Fradis (2001), Euro Code 8 (2005), Priestly et al. (2007), Bohl and Adebar (2011), and Kazaz (2012)] have been proposed to predict wall displacement capacities. In addition to the above models, Siam et al. (2015) considered also the model developed for RMSW by Shedid and El-Dakhakhni (2013) and demonstrated that

the maximum displacement predictions of all eight models were unreliable compared to available RMSW experimental database results. It was also found that current models do not account for the shear deformation component for flexurally dominated walls.

Therefore, it was deemed necessary to develop a model that can accurately predict wall displacement capacity taking into account its shear deformations. As such, the focus of the current study is to propose a wall displacement prediction model that accounts for both flexural and shear deformation mechanistic parameters with coefficient calibrated using Multivariate Data Analysis (MVDA) statistical tools. Subsequently, two approaches were used in MVDA: 1) principal component analysis (PCA); and 2) projection to latent structure (PLS) [Eriksson (1999)] using a database of RMSW containing 81 walls from different published studies as will be explained later.

### **3.3 MODEL PARAMETERS**

As the level of seismic demand increases, RMSW experience increased deflections that might force the wall to respond in an inelastic manner. Because of the complex anisotropic nature of RMSW systems, four distinct failure modes or a combination thereof can occur: flexural, rocking, sliding, and diagonal shear. These four failure modes depend on the wall design parameters such as its cross-section configuration, reinforcement details and ratios, material characteristics, and boundary conditions.

Rocking and sliding can be prevented with adequate detailing at the wall-foundation interface zone leaving the flexural and the diagonal shear as the two most common failure mechanisms.

### **3.3.1 Flexural Deformation**

For seismic design, RMSW are typically designed to fail in flexural to ensure a ductile response and effective energy dissipation during seismic events [Thomas and Priestley 1992]. Flexural failure is typically characterized by tensile yielding of the vertical reinforcement, the formation of a plastic hinge zone and crushing of masonry units, grout, and mortar at wall toes [Drusdale et al. 1994]. Crushing is often accompanied by web splitting of the concrete masonry units [Yi and Shrive 2003]. At increased displacements, masonry unit face shell spalling and eventual crushing of grout column also occur in the toe regions followed by a possible buckling of the vertical reinforcement at the toe region [Shedid et al. (2008)]. Flexural wall behavior is typically negatively influenced by high vertical reinforcement ratios which correspond to decreased levels of drifts and ductility and can result in brittle failures [Eikanas 2003]. In addition, flexural strength is enhanced with increased axial forces [Sherman 2011]. Other research studies have also indicated that walls with aspect ratio greater than 1.0 exhibit more flexural-than shear-dominated behavior [Sveinsson et al 1985]. In the event of vertical bar(s) pull-out, additional wall lateral deformation may occur. Modern design codes however, do account for such undesirable effects by providing adequate anchorage

and development length for seismic reinforcement within the foundation. In addition, the effect of reinforcement strain penetration into the foundation [Priestley et al 2007] was shown to have a minimal influence on the overall wall deformation as compared to other contributing factors [Bohl and Adebar (2011), Tomažević et al. (1988)].

Under seismic loading, RMSW are typically assumed to act as cantilevers. In this configuration, top wall displacement corresponding to first yield of the outermost vertical reinforcement is defined as yield displacement which can be calculated by double integration of the curvature profile distribution along the wall height. To simplify the process, and in lieu of the double integration of the wall curvature profile, an equivalent idealized plastic hinge length is typically assumed using Equation (3.1) [Eriksson 1999]. Where curvature is assumed to be constant and equal to ultimate curvature  $\phi_u$  along the equivalent plastic hinge length  $L_p$ .

$$\Delta_{fl} = \Delta_y + \Delta_p = \frac{H_w^2 \phi_y}{3} + (\phi_u - \phi_y) L_p (H_w - 0.5 L_p) \quad (3.1)$$

where  $\Delta_{fl}$  is the flexural displacement (which is equal to the summation of the yield displacement,  $\Delta_y$ , and the plastic displacement,  $\Delta_p$ );  $H_w$  is the wall height; and  $\phi_y$  is the yield curvature.

### 3.3.2 Shear Deformation Parameters

Shear failures are typically undesirable as walls that fail in shear exhibit more brittle behavior and rapid strength degradation after reaching their peak strength. Shear failures are characterized by diagonal tensile cracking. Walls with aspect ratio less than 1.0 are often dominated by shear behavior [Sveinsson et al. 1985]. The shear resistance of RMSW results from the tensile capacity of the shear reinforcement, dowel action of vertical reinforcement, applied axial stress and aggregate interlock [Corley 1966]. Shear behavior can be enhanced by evenly distributing the horizontal reinforcement along the height of the wall which facilitate stress distribution. This can also alter the wall's brittle failure to a more ductile response [Tomažević 1999]. Uniform distribution of vertical reinforcement also reduce the size and amount of cracks which in turn enhances the aggregate interlock mechanism. Finally, increased applied axial load enhances the shear strength by delaying the initiation of cracking and improving the aggregate interlock mechanism [Ibrahim and Suter 1999].

To the best of the authors' knowledge, there is no published analytical model that explicitly predicts shear deformations of RMSW and only a few analytical models are proposed to predict the shear deformations of *reinforced concrete* elements that are flexurally-dominated [Bayer et al. (2011) and Sezen (2008)]. Bayer et al (2011) proposed an empirical equation to estimate RCSW displacement as a *ratio* of their flexural displacements as given Equation (3.2). This model is based on the modified compression field theory [Vecchio and Collins 1986]

assuming that the curvature and the average axial strain are constant over the plastic hinge height.

$$\frac{\Delta_{sh}}{\Delta_{fl}} = 1.5 \frac{\varepsilon_m}{\phi \tan \beta_m} \frac{1}{H_w} \quad (3.2)$$

where  $\Delta_{fl}$  is the flexural displacement;  $\Delta_{sh}$  is the shear displacement;  $\varepsilon_m$  is the average axial strain level at the center of wall section;  $\phi$  is the curvature; and  $\beta_m$  is the cracking angle.

Sezen (2008) proposed a piecewise linear model defining key points in the force-shear deformation relationship of reinforced concrete columns through a parametric study by also implementing the modified compression field theory. The average shear strain or shear displacement at the maximum shear strength have been shown to be influenced by several factors. First, the shear strain is inversely proportional to the square root of the axial stress ratio. In addition, the shear strain varies linearly with the product of vertical steel yield strength  $f_y$  and vertical steel ratio  $\rho_v$ . Based on regression analysis, a linear relationship was proposed to evaluate the shear strain  $\gamma_n$  at the maximum strength, which, when adapted to RCSW, would give:

$$\gamma_n = \frac{f_y \rho_v}{5000 \left( \frac{H_w}{L_w} \right) \sqrt{\frac{P}{A_g f'_c}}} - 0.0004 \quad (3.3)$$

where  $L_w$  is the wall length;  $P$  is the axial load;  $A_g$  is the wall gross cross section area; and  $f'_c$  is the compressive strength of concrete.

Based on the RMSW/RCSW behavior influencing parameters discussed above and the experimental database to be presented next, a model to predict the maximum displacement of RMSW will be developed in this paper. Within the proposed scoring model, the mechanics-based prediction of the yield displacement (corresponding to the first yielding in the vertical steel) is adopted. Subsequently, a combination of different wall design parameters is investigated to quantify their influence on RMSW flexural plastic and shear displacement components along their calibrated factors.

### **3.4 EXPERIMENTAL DATABASE**

In order to develop a reliable model that is capable of predicting displacement capacity, a RMSW seismic performance database is selected with specific criteria. All walls included in the database are: 1) fully grouted; 2) flexural-dominated; 3) contain horizontal (shear) reinforcement; and 4) tested under displacement-controlled quasi-static cycling loading along the wall's in-plane direction. Moreover, the applied axial compressive stress varied from approximately zero (i.e. no external applied axial load but the wall's own weight will be used instead) to 15% of the full wall cross section compressive strength. The vertical and horizontal reinforcement ratios varied from 0.16% to 1.3%, and from 0.05% to 0.63%,

respectively, with a yield strength that ranged between 318 MPa and 624 MPa. The masonry compressive strength fluctuated between 12 MPa and 31 MPa. The experimental database is compiled from the studies reported by Shing et al. 1990 (eleven walls), Voon and Ingham 2005 (two walls), Shedid et al. 2008 (six walls), Vaughan 2010 (ten walls), Sherman 2011 (eight walls), Hernandez 2012 (six walls), Kapoi 2012 (eight walls), and Ahmadi et al. 2014 (30 walls) with a total of 81 walls. The wall characteristics are summarized in Table (3.1) with a typical cross section and elevation is provided in Figure 3.1.

Analysis was conducted on each wall in the database to quantify both its ultimate and yield curvatures ( $\phi_u, \phi_y$ ) using first principles. In the cases where the maximum displacement associated with the peak strength of each wall is not reported explicitly, an induction from the hysteretic loops reported in the original reference is used and reported in Table 3.1. Although the number and amplitude of loading cycles can influence the overall wall-displacement response envelope, it should be noted that there is no general consensus on a universal cyclic loading protocol for RMSW or for any other seismic force resisting component for that matter. As such, while all the 81 walls experienced in-plane cyclic loading until their failure, their loading protocols were not identical. However, until such a universal approach is established, that also may or may not reflect actual seismic loading conditions, and a significant number of RMSW are tested following such protocol, the current study presents a useful calibrated model based on the database of published experimental RMSW test results to date.

### 3.5 MULTI VARIATE DATA ANALYSIS (MVDA) THEORY

Principal Component Analysis (PCA) and Projection to Latent Structure (PLS) are generalized multiple regression methods based on investigating a block of data (in the case of PCA) or relating two blocks of data to each other as input and output (in the case of PLS) [Nelson et al 1996]. These methods are particularly effective in modeling and analyzing variables that are correlated.

#### 3.5.1 Principal Component Analysis (PCA) Background

One of the primary objectives of the PCA as a MVDA method is to get an overview of the dominant patterns and major trends in the data matrix  $X$ . Because the purpose of PCA is to decompose the  $X$ -matrix to detect the hidden phenomena, the concept of variance is key. The direction in the multivariate space with the maximum variation is coupled with a hidden phenomenon [Eriksson 1999]. Therefore, the calculation of latent variables (the principal components) which coincide with these maximum variance directions are an efficient tool to understand and interpret the data. By using PCA, a data matrix  $X$  is modeled as:

$$X = x' + \sum_{k=1} t_k \cdot p_k^T + E \quad (3.4)$$

In Equation 3.4,  $x'$  indicates a standardization of the row data matrix  $X$ . While the second term models the principal component (PC) scores and loading, the third

term,  $E$ , contains the errors [MacGregor et al. 2005]. The PC scores are stored in  $t_k$  and present the coordinate for the observations in the established model hyperplan. The PC loadings are stored in  $p_k^T$  where  $k$  is the number of variables. The loadings define the orientation of the computed PC plane with respect to the original  $X$ -database variables. A graphical representation for a simple case, three variables and two components (see Figure 3.2), shows two PCs forming a plane which represent a window into the multidimensional space. Each observation may be projected onto this plane in order to get new coordinate values (scores) in the new coordinate system.

### 3.5.2 Projection to Latent Structures (PLS) Background

The partial least squares PLS is a regression extension of PCA, which is used when it is of interest to connect the information in two blocks of variables,  $X$  and  $Y$ , to each other. The difference between the PCA and PLS is that the former is a maximum variance projection of  $X$ , whereas the latter is a maximum covariance model of the relationship between  $X$  and  $Y$ . The PLS technique works by selecting factors of input variables in a sequence which successively maximize the explained covariance between input and output variables. Given a matrix of input data,  $X$ , and output data,  $Y$ , a factor of the input data,  $t_k$ , and output data,  $u_k$ , is evaluated such that:

$$X = \sum_{k=1} t_k \bullet p_k^T + E \quad \text{and} \quad Y = \sum_{k=1} u_k \bullet q_k^T + F \quad (3.5)$$

All vectors included in both  $t_k$  vectors and  $u_k$  are mutually orthogonal and selected so the covariance between each pair  $(t_k, u_k)$  is maximized. Linear regression is performed between  $t_k$  and  $u_k$  to produce the inner relationship, such that  $u_k = \beta_k \bullet t_k + \varepsilon_k$  where  $\beta_k$  is a regression coefficient and  $\varepsilon_k$  refers to the prediction error. The PLS method provides the potential for a regularized model through selecting an appropriate number of latent variables  $u_k$  in the model. The benefit of this approach is twofold: first, it has the advantage of examining any change that might occur in the new input variables, including both the measured or controllable variables (explained in the next paragraph), before using the model for prediction by monitoring the input variables using a multivariate chart referred to as DModX (distance to the X-model); second, the PLS method has the ability to show that a relatively small number of low-index latent variables can explain the greater part of the variation in both the input and output variables. A test is applied on the experimental database to examine the relationship between the inputs and the outputs in the latent space. Figure 3.3 reveals a dispersed linear trend between the maximum displacement obtained from experimental database and the predicted maximum displacement which imply the possibility to use the approach for further analysis.

The next sections will address both PCA and PLS model developing towards predicting RMSW displacement capacity starting with plain variables. In this respect, it is important to note that, plain variables can be classified into two sets of variables: controllable and non-controllable. The controllable variables include  $(H_w, L_w, t_w, \rho_v, \rho_{sh}, f'_m, f_y, P)$  where  $t_w, \rho_v, f'_m$  are the wall thickness, the shear reinforcement, and the masonry compressive strength respectively. The non-controllable variables include  $(\alpha, \beta, \phi_y, \phi_p, \phi_u)$  where  $\alpha = \left(1 - \frac{P}{A_g f'_m}\right)$  and  $\beta = \left(1 - \frac{f_y \rho_{sh}}{f'_m}\right)$  represent the axial load effect, the amount of shear reinforcement respectively. Both the controllable and non-controllable variable sets have direct correlations with the wall ultimate displacement,  $\Delta_m$  and in the same time cover most wall design characteristics that could happen to achieve the maximum displacement.

### 3.6 PCA IMPLEMENTATION ON THE EXPERIMENTAL DATABASE

As can be seen from Figure 3.4, a PCA of 14  $(H_w, L_w, t_w, \rho_v, \rho_{sh}, f'_m, f_y, P, \beta, \alpha, \phi_u, \phi_p, \phi_y)$ , and 81 wall (observation) top drifts  $(\Delta_m/H_w)$  yields a model with  $R^2 X : 0.94$ , indicating variation or the goodness of fit for variable  $X$ , and  $Q^2 : 0.53$  that shows the predictive ability or goodness of prediction parameter. The main reason to use the top wall drifts is to normalize the

lateral top displacement within the database. This is because not all the walls have the same scale, as some walls are half-scale and others are full-scale. The PCA-score of the first two components are plotted in Figure 3.4(a), and the corresponding loadings in Figure 3.4(b). The loading plot shows an overview of the relationships among all variables and the response at the same time.

The obtained the score plot, Figure 3.4(a) shows how the 81 wall drift results (observations) relate to each other. Walls close to each other have similar characteristics, whereas wall drift results further away from each other are more dissimilar with respect to the material and geometrical characteristics. Walls 56, 55, 23, and 24 (Table 3.1) are clustered in the lower left-hand corner, thus represent a group of walls that have some similarity in the variables. Walls 38, 68, 14, and 69 (Table 3.1) are close to the origin of the plot, which indicates that they have average characteristics.

The loading plot, Figure 3.4(b), displays the relationship between all variables simultaneously. Variables contributing similar information are grouped together and are correlated (e.g.  $f_y, \rho_v$  are grouped and positively correlated). When the value of one variable increases or decreases, the value of the other variable changes correspondingly. On the other hand, when two variables are located on opposite sides of the plot axes and in diagonally opposed quadrants (e.g.  $\beta, \rho_{sh}$ ), the variables are inversely correlated. Furthermore, the distance from the variable to the loading plot origin has an interpretation in the model whereas the variable  $\phi_y$  is

located furthest away from the loading plot origin, indicates a stronger impact on the model.

The four Walls 23, 24, 55, and 56 (Table 3.1) are characterized by having high values of shear reinforcement ratio  $\rho_{sh}$ . The location of Wall 19 (Table 3.1) in the second quadrant is due to the fact that it contains the highest level of both vertical reinforcement ratio  $\rho_v$  and yield strength  $f_y$ . The model interpretation also reveals that Walls 48, 49, 50, and 51 are clustered and are heavily influenced by displacements and inversely proportioned with wall lengths  $L_w$ , as this group considered the shortest in the wall length.

### 3.7 PROPOSED SCORING MODEL

The maximum drift ratios  $\Delta_m/H_w$ , as a response  $Y$ , along with the 14 geometrical and mechanical characteristics  $(H_w, L_w, t_w, \rho_v, \rho_{sh}, f'_m, f_y, P, \beta, \alpha, \phi_u, \phi_p, \phi_y)$ , as variables  $X$ , are modeled simultaneously with PLS. It should be noted that all wall geometrical and material characteristics are not identical, however, all walls within the selected experimental database experienced the same flexural failure mode, regardless of the wall characteristics.

The first PLS component, accounting for almost 50% of the response variation, captures a strong correlation between  $X$ -factors and  $Y$ -response. The second component, which explains another 2% of the  $Y$ -variation, uncovers a weak

deviating feature for the next component. Therefore, two PLS components are obtained with:  $R^2X : 0.25$ ,  $R^2Y : 0.62$  and  $Q^2 : 0.52$ . In order to interpret the PLS model, scoring and loading plots, Figure 3.5(a) and 3.5(b) respectively, will be considered. The loading plot depicts that the maximum drift is positively influenced by  $H_w, t_w, f'_m, \phi_u, \phi_p$ , and  $\phi_y$  and negatively influenced by  $L_w$  and  $P$ , which is consistent with basic mechanics. Moreover, the loading plot also suggests that the variables  $H_w, \phi_y, \phi_u, L_w$  are the most important to the maximum drift. The three variables  $\rho_v, f_y, \alpha$  are of comparatively low importance as shown in the Variable Importance for Projection (VIP), Figure 3.6.

An attempt is made to remove individual material and geometrical wall characteristics from the previous model and replace them by dimensionless parameters to be used with any consistent system of units. This dimensionless parameters will also follow the principles of mechanics starting from equating the total displacement to the summation of its flexural and shear components as shown in Equation 3.6.

$$\Delta_m = \Delta_{fl} + \Delta_{sh} \quad (3.6)$$

The flexural displacement beyond the elastic range is the summation of yield and plastic displacement as shown in Equation 3.7.

$$\Delta_{fl} = \Delta_y + \Delta_p \quad (3.7)$$

While the calculation of yield displacement is based on deflection at the elastic range as shown in Equation 3.8, the plastic displacement, Equation 3.9, is a function of parameters defined in Equation 3.1. The plastic hinge in this study is defined as a function of  $\alpha, \beta, H_w$ , and  $L_w$  as shown in Equation 3.10.

$$\Delta_y = \frac{\phi_y H^2}{3} \quad (3.8)$$

$$\Delta_p = f\left((\phi_u - \phi_y)L_p(H_w - 0.5L_p)\right) \quad (3.9)$$

$$L_p = g\left(\alpha\beta(H_w + L_w)\right) \quad (3.10)$$

Therefore, the plastic displacement can be a function of individual wall material and geometrical characteristics as given by Equation 3.11.

$$\Delta_p = f\left(\phi_p\left[\alpha\beta(H_w + L_w)\right]\left(H_w - 0.5\left[\alpha\beta(H_w + L_w)\right]\right)\right) \quad (3.11)$$

Equation 3.11 can be used to improve the model drift predictions by introducing calibration coefficients  $a_1, a_2, a_3, a_4, a_5$  and  $a_6$  as follows:

$$\frac{\Delta_p}{H_w} = \phi_p \alpha \beta \left[ a_1 H_w + a_2 L_w - a_3 \alpha \beta H_w - a_4 \alpha \beta \frac{L_w^2}{H_w} - a_5 \alpha \beta L_w \right] \quad (3.12)$$

$$\Delta_{sh} = a_6 \alpha \frac{V_L}{t_w L_w} \frac{1}{f_y} \frac{\rho_v}{\rho_{sh}} H_w \quad (3.13)$$

In this model (Equations 3.12 and 3.13), the  $X$  data matrix is established with five non-dimensional variables and the  $Y$  data matrix contains the maximum drift

without the yield drift  $(\Delta_m - \Delta_y)/H_w$  as the yield drift can be determined from basic mechanics.

Out of the 81 tests results observations, a training set of 71 observations were selected to develop the PLS regression model. The validation would then take place using the remaining ten observations. The PLS model was built on a training dataset by cross-validation, obtaining four components, with  $R^2X : 0.97$ ,  $R^2Y : 0.50$ , and  $Q^2 : 0.45$ . Figure 3.7 illustrate a scatter plot of the two score and loading vectors of the trained PLS model.

The prediction capabilities of the developed PLS model was evaluated using on a test set of the remaining ten observations. The PLS score values ( $t_1$  and  $t_2$ ) for these test observations are indicated by solid circles Figure 3.7(a). From the figure, it can be concluded that the PLS model succeeds in predicting the new observations data. The model analysis yields the coefficients, given in Table 3.2, for an equation that have the capability to evaluate the drift by isolating the flexural and shear contributions from the overall maximum drift for RMSW. The actual and the predicted maximum drifts  $\Delta_m/H_w$ , presented by Figure 3.8, shows a good approximation of  $\Delta_m/H_w$  with the available data. The model gives an average ratio of predicted to actual  $\Delta_m/H_w$  values of 88% with model prediction ability  $Q^2 : 0.53$  with accuracy of approximately 90%. However, considering the different source of aleatory and epistemic uncertainty in any experimental program, it is expected that

the proposed model might not be able to accurately predict each and every experimental data point. Similarly, it should be noted that, because of the complex and anisotropic nature of RMSW, no single simplified mechanics-based model can also be capable of predicting the entire range of the experimental dataset that were compiled from different sources. This fact is not only attributed to different source of uncertainty but also to typical errors in measuring and/or collecting the experimental results. In addition, it should be noted that the proposed model does quantify (separately) the shear and flexural contributions to the overall wall displacements. However, the test results reported within the available experimental database also do not present these two components separately. As such, no comparison between the models prediction of the separate deformation contributions and the corresponding experimental response can be made.

With the final set of model parameters (listed in Equations 3.12 and 3.13), the established developed model code takes less than 90 s to generate the proper calibration factors for the parameters based on entire 81 walls test results. Any further variation in the parameters will require additional 90 s per run.

### **3.8 MODEL PERFORMANCE CHARTS**

After achieving the main objective of the study to develop a reliable model that is capable of predicting the displacement of RMSW corresponding to their peak strength, the model performance charts will be generated to investigate the

influence of both geometrical and material wall characteristics on the corresponding drift ratios. As such, a *default scenario* wall (last column in Table 3.3) is introduced within the maximum and the minimum range of different wall characteristics given in Table 3.1.

The lowest vertical and horizontal spacing of reinforcement is 200 mm (every cell and every course). The yield strength will be kept constant for both vertical and horizontal reinforcement, and is equal to 400 MPa. The compressive strength of masonry varies between 10.0 MPa and 17.0 MPa with S type mortar. For the performance chart development, the wall length is considered constant and is equal to 3,200 mm and the wall thickness is equal to 190 mm. A summary of the selected wall characteristics and the default scenario are given in Table 3.3. After defining the range of wall characteristics, basic mechanics was used for each wall scenario to evaluate its yield and ultimate curvatures, as well as its yield and ultimate moment capacities. The next sections highlight the influence of each characteristic on the wall maximum displacement capacities (presented as maximum drift ratio) for the different wall scenario listed in Table 3.3.

### **3.8.1 Influence of Masonry Compressive Strength**

The developed model (Equations 3.12 and 3.13 and Table 3.2) was first used to capture the influence of altering the wall aspect ratio and the masonry strength on the maximum drift ratio of the walls. At lower wall aspect ratios, the differences between the maximum drifts are smaller compared to the high aspect ratio walls, as

shown in Figure 3.9. At an aspect ratio of 1.00, the maximum drifts are 0.55%, 0.63%, and 0.69% for 10.0, 13.5, and 17.0 MPa masonry strength, respectively. While at aspect ratio of 3.75, the maximum drifts are 1.94%, 2.25%, and 2.51% for 10.0, 13.5, and 17.0 MPa, respectively. The overall maximum drift differences within the range of compressive strength values are 0.14%, 0.31%, 0.46%, and 0.57% for wall with aspect ratios of 1.00, 2.00, 3.00, and 3.75, respectively. For a masonry compressive strength of 10.0 MPa, the maximum displacement ranges between 0.55% and 1.94% for aspect ratios of 1.00 and 3.75, respectively. On the other hand, for a masonry strength of 13.5 MPa, the maximum drifts range between from 0.63% and 2.25% for aspect ratios 1.00 and 3.75, respectively; and for a 17.0 MPa masonry strength, the maximum drifts are between 0.69% and 2.51% for aspect ratios 1.00 and 3.75, respectively.

At low aspect ratio, the difference between the maximum drifts for the various masonry strength is minimal compared to that at high aspect ratio walls. This is attributed to the influence of the shear displacement that reaches 18.6% of aspect ratio 1.00 and decreased to 1.4% when the aspect ratio reaches 3.75. On the other hand, both the yield and plastic flexural deformations increase with the increase of both the masonry compressive strength and the wall aspect ratio.

At higher masonry compressive strengths, their influence on the wall maximum drifts is minimal especially at low aspect ratios. The results also show that increasing the masonry compressive strength to enhance the ability of the walls to sustain higher axial load will slightly affect the maximum displacement for the

low aspect ratio walls (up to 2.00). For higher aspect ratio walls, increasing the compressive strength of masonry results in increased wall maximum displacement. This conforms to basic mechanics predictions as increasing the masonry strength leads to a reduction in the compression block depth within the wall cross section. As such, the neutral axis shifts toward the compression fibers will results in increasing the ultimate curvature which in turn would increase wall maximum displacement.

### 3.8.2 Influence of Axial Load

As can be seen in Figure 3.10, the model is consistent with mechanics regarding the influence of axial load being inversely proportioned with both the flexural and shear displacement capacity of RMSW. At aspect ratio equals to 1.00, the maximum drifts are 0.79%, 0.72%, 0.63%, 0.57%, and 0.53% at the 1.0%, 2.5%, 5.0%, 7.0%, and 10.0% axial load ratio, respectively. While at aspect ratio equals to 3.75, the maximum drifts are 3.23%, 2.81%, 2.25%, 1.87%, and 1.61% at the 1.0%, 2.5%, 5.0%, 7.5%, and 10.0% axial load ratio, respectively. The overall maximum difference between changing the level of applied axial load are 0.25%, 0.83%, 1.31%, and 1.66% for walls aspect ratio equal to 1.00, 2.00, 3.00, 3.75, respectively. For approximately no axial load (axial load of 1% of  $f'_m A_g$ ), the maximum drifts range from 0.79% to 3.27% for aspect ratios 1.00 and 3.75, respectively. Whereas at an axial load ratio of 5% of  $f'_m A_g$  (default scenario), the

maximum drifts ranges from 0.63% to 2.25%. For 10% axial load ratio, the maximum drifts range between 0.53% and 1.61%.

For approximately no axial load (axial load of 1% of  $f'_m A_g$ ), if the aspect ratio is 1.00, the flexural and shear contributions are 89% and 11%, respectively. Increasing the axial load ratio to 10% for wall with 1.00 aspect ratio has an impact on the flexural and shear contributions to the maximum drifts of 73% and 27%, respectively. This depicts the influence of changing the axial load to both the flexural and shear deformation contributions.

For the same wall aspect ratio of 3.75, the maximum drift value varies from 3.27% to 1.61% as the axial stress ratio altered between 1% and 10%. However, within this range, the flexural and shear contributions to the maximum drift remain approximately the same as 98% and 2% respectively. It can thus be concluded that shear deformation has a significant contribution toward RMSW drifts that increases with increasing the axial load ratio, especially for low aspect ratio walls.

### **3.8.3 Influence of Shear Reinforcement**

The shear reinforcement ratio can be changed by either the bar diameter, Figure 3.11(a), or the bar spacing, Figure 3.11(b). Within the selected range of shear reinforcement diameter, the influence on maximum drift within wall different aspect ratio is negligible. Therefore, treating the shear reinforcement bar diameter as an influencing parameter of RMSW drifts is not warranted when compared to

the shear reinforcement spacing. At low aspect ratio, the differences in the maximum drifts as high as 0.26%. This difference is reduced to reach 0.14% and 0.11% for wall aspect ratios of 2.00 and 3.00, respectively and remains almost constant afterward.

Increasing the shear reinforcement spacing from 200 mm to 1,200 mm decreases the shear deformation contribution to the maximum wall drifts from 41% to 10% for walls aspect ratio equals to 1.00. For walls with aspect ratio of 2.00, the shear contribution varies between 13% and 2%. For higher aspect ratio walls the increase in shear reinforcement spacing inversely affects the shear contribution to maximum displacement. The 1.5% drift limit can be reached by using 1,200 mm shear spacing with 2.25 wall aspect ratio, or 800 mm spacing with 2.35 wall aspect ratio, or 200 mm spacing with 2.50 wall aspect ratio. It can be concluded that, for walls with low aspect ratios, the shear reinforcement spacing governs the maximum drifts whereas, for high aspect ratio walls, the influence of shear spacing on maximum drifts diminishes.

#### **3.8.4 Influence of Vertical Reinforcement**

The vertical reinforcement is a key parameter that is known to control the behavior of RMSW. The vertical reinforcement influence can be quantified using two separate attribute. The first attribute is the spacing between bars and the second is the bar diameter. For both attributes, the analysis reveals that their influence on

the maximum drifts is insignificant for low aspect ratio walls compared to that for high aspect ratio walls.

Figure 3.12(a) depicts the influence of altering the vertical reinforcement bar diameter on the maximum wall drifts as a function of the wall aspect ratios. Within the same wall aspect ratio, the difference between the maximum drifts when changing the vertical bar diameter are 0.1%, 0.6%, 1.1%, and 1.43% for walls aspect ratio 1.00, 2.00, 3.00, and 3.75, respectively. All walls with an aspect ratio of 1.00 exhibit approximately the same maximum drifts. However, the contribution of flexural and shear deformation fluctuates with the variation of vertical reinforcement ratios. At a vertical reinforcement ratio of 0.26%, the flexural and shear drifts contributions to the maximum drifts are 81% and 19%, respectively. While the flexural and shear contributions are 68% and 32%, when the vertical reinforcement ratio increases to 0.40%.

Increasing the wall height (and thus wall aspect ratio) for the same wall length and vertical reinforcement does not change the walls' yield and ultimate moment capacities. This, however, changes the moment arm and thus the resulting shear force. Therefore, for example, the flexural drift increases from 68% to 97% and the shear drift contribution decreases from 32% to 3% for 0.40% vertical reinforcement ratio.

Changing the spacing of the vertical reinforcement follows a similar trend of maximum drifts to that of changing bar diameter as shown in Figure 3.12(b). The

change in maximum drifts for low aspect ratio walls are minimal compared to the high aspect ratio walls. For example, keeping all material and geometric characteristics the same for wall aspect ratio of 3.75, the maximum drifts can range between 1.5% and 3.0% by varying the vertical reinforcement ratio between 0.132% and 0.658%, respectively.

### **3.9 DISCUSSION**

The previous sections addressed the quantification of the effect of individual wall geometric material characteristics on the maximum wall drifts. In this section, however, the interaction between these characteristics and the limits of the maximum wall drifts are demonstrated. Figures 9 to 12 are superimposed using the area between outermost lines of each figure to generate Figure 3.13 representing the bounds of maximum drifts for RMSW within the shown aspect ratios.

As can be seen from Figure 3.13, walls with aspect ratios range between 1.00 and approximately 1.25 are significantly influenced by the shear reinforcement. On the other hand, for higher aspect ratio walls, the influence of changing the shear reinforcement on the maximum drift can be neglected. The effect of altering the compressive strength is more pronounced as the effect of changing the shear reinforcement vanishes.

The lower bound of maximum drift is controlled by high percent of axial load, 10% of  $f'_m A_g$ , for wall aspect ratios range from 1.25 to 2.50. When the default wall scenario contains vertical reinforcement equal to 0.66% and the wall aspect ratio is greater than 2.50, the lower bound of maximum drift is achieved and controlled by vertical reinforcement ratio. The upper bound of maximum drift occurs when the default wall scenario experiences approximately no axial load applied (1% of  $f'_m A_g$ ) with wall aspect ratio is greater than 1.25. For an axial load ratio greater than 5% and wall aspect ratio greater than 1.25, the vertical reinforcement ratio governs the limits of the maximum drifts.

Within the default wall scenario and the investigated geometrical and material characteristics introduced in this study, it can be concluded that walls with aspect ratios less than 1.25 are very sensitive to the shear reinforcement ratio. Above this aspect ratio, the RMSW drifts are more sensitive to both axial load and the amount of vertical reinforcement rather than the masonry compressive strength and wall shear reinforcement.

### **3.10 CONCLUSIONS**

Performance-based seismic design approaches are developed to ensure that, at a specific level of seismic hazard, the structural component or system does not experience damaged beyond certain levels. Since inter-story drifts and/or

displacements are the key parameter for damage control, it is rational to examine PBSD procedure wherein displacements are the input of the design process.

In this study, a model is presented for flexurally dominated RMSW to capture the displacement capacity using a multivariate approach based on projections (PCA and PLS). This model predicts the maximum RMSW capacity at peak lateral load using flexural and shear components. The flexural component is represented by yield and plastic deformations, whereas the proposed plastic deformation model can be evaluated using wall length and height and consider the axial load effects. The shear component predictions within the proposed model takes into account several wall geometric and material characteristics including the applied load, the amount of shear reinforcement, and the wall aspect ratio. The advantages of the developed model include the facts that the model: 1) is developed specially for RMSW; 2) quantifies the wall displacement capacity using its geometrical and material characteristics; 3) evaluates the wall flexural and shear deformations separately for flexurally dominated walls; 4) can be used with any consistent set of units (i.e. it is a dimensionless model); 5) is based on database of 81 experimentally tested walls that covers a wide spectrum of RMSW design parameters.

This study further utilizes the presented model to gain an insight into some of the key parameters influencing RMSW displacement capacity. Based on this part of the study, it was shown that shear reinforcement has the most significant influence on wall with aspect ratios between 1.00 and 1.25. For higher aspect ratios, the shear reinforcement influence can be neglected compared to other wall design

parameters. Furthermore, the displacement capacity for walls with aspect ratio ranges between 1.25 and 2.50 is governed by the axial stress ratio (1% for the upper bound and 10% for the lower bound). The analyses also revealed that at high aspect ratios, 2.5-3.75, the displacement capacity of the studied RMSW scenarios is bounded by the 1% axial stress ratio, as an upper bound, and the 0.66% vertical reinforcement ratio, as a lower bound. In addition, for any wall within the high aspect ratio range, the displacement capacity is not as sensitive to the masonry compressive strength and shear reinforcement levels as to the axial stress and the vertical reinforcement ratios. Overall, within the studied RMSW scenarios, the drifts ratios range between approximately 0.50% and 3.25%. Finally, the generated model performance charts can be utilized to select RMSW with different geometrical and mechanical characteristics to meet specific target drift level, thus facilitating adoption of DBSD and PBSB provisions in the next generation of seismic codes.

### 3.11 ACKNOWLEDGMENTS

Financial support is provided through the Natural Science and Engineering Research Council (NSERC) of Canada and the Canada Masonry Design Center (CMDC).

### 3.12 NOTATION

$A_g$  = gross cross sectional area of the wall ( $\text{mm}^2$ )

$a_i$  = proposed model coefficient

$d_b$  = diameter of flexural (vertical) reinforcement (mm)

$E$  = error matrix for  $X$  data

$F$  = error matrix for  $Y$  data

$f'_c$  = concrete compressive strength (MPa)

$f'_m$  = masonry compressive strength (MPa)

$f_u$  = ultimate strength for reinforcement steel bars (MPa)

$f_y$  = yield strength for reinforcement steel bars (MPa)

$H_w$  = wall height (mm)

$k$  = number of variables

$L_p$  = equivalent plastic hinge length (mm)

$L_w$  = wall length (mm)

$P$  = axial compressive load (kN)

$p_k$  = loading value for  $k$  variable associated with  $X$  data

$Q^2$  = predictability/goodness of prediction of parameters

$q_k$  = loading component for  $k$  variable associated with  $Y$  data

$R^2X$  = goodness of fit to  $X$  data

$R^2Y$  = goodness of fit to  $Y$  data

$t_k$  = principal component score for  $k$  variable associated with  $X$  data

$t_w$  = wall thickness (mm)

$V_L$  = ultimate lateral load at top of wall due to ultimate moment (kN)

$X$  = input Data matrix.

$x'$  = standardized data matrix

$u_k$  = principal component score for  $k$  variable associated with  $Y$  data

$Y$  = output data matrix

$\alpha = \left(1 - \frac{P}{A_g f'_m}\right)$  axial load effect parameter

$\beta = \left(1 - \frac{f_y \rho_{sh}}{f'_m}\right)$  shear reinforcement effect parameter

$\beta_m$  = cracking angle outside the plastic hinge zone

$\beta_k$  = regression coefficient.

$\gamma_n$  = shear strain at maximum strength

$\Delta_{fl}$  = flexural displacement (mm)

$\Delta_p$  = plastic displacement (mm)

$\Delta_{sh}$  = shear displacement (mm)

$\Delta_m$  = maximum lateral displacement (mm)

$\Delta_y$  = Yield lateral displacement (mm)

$\varepsilon_k$  = Prediction error.

$\varepsilon_m$  = Average axial strain

$\theta_p$  = plastic rotation of the wall

$\rho_{sh}$  = ratio of horizontal wall reinforcement to  $A_g$

$\rho_v$  = ratio of vertical wall reinforcement to  $A_g$

$\phi$  = curvature of the wall section (1/mm)

$\phi_p$  = plastic curvature of the wall section (1/mm)

$\phi_y$  = yield curvature of the wall section (1/mm)

$\phi_u$  = ultimate curvature of the wall section (1/mm)

### 3.13 REFERENCE

Ahmadi F, Hernandez J, Sherman J, Kapoi C, Klingner RE, McLean DI. Seismic performance of cantilever-reinforced concrete masonry shear walls. *J Struct Eng* 2014;140(9):04014051.

Beyer K, Dazio A, Priestley N. Shear deformations of slender reinforced concrete walls under seismic loading. *ACI Struct J* 2011;108:167–77.

Bohl A, Adebar P. Plastic hinge lengths in high-rise concrete shear walls. *ACI Struct J* 2011;108(2):148–57.

Calvi GM, Priestley MJ, Kowalsky MJ. Displacement-based seismic design of structures. In: 3rd National Conference on Earthquake Engineering and Engineering Seismology; 2008.

Corley William Gene. Rotational capacity of reinforced concrete beams. *Proc ASCE Struct J* 92(ST-4):121-46.

Deaton JB, Sarawit AT, Bolourchi S. Nonlinear force-drift backbone curve for reinforced concrete squat shear walls. In: SMiRT-23 conference, Division V, Paper ID 706.

Drysdale RG, Hamid AA, Baker LR. Masonry structures: behavior and design.

Prentice Hall; 1994.

Eikanas IK. Behavior of concrete masonry shear walls with varying aspect ratio and flexural reinforcement M.S. Thesis, Department of Civil and Environmental Engineering. Pullman, WA: Washington State University; 2003.

Eriksson L. Introduction to multi-and megavariate data analysis using projection methods (PCA & PLS). Umetrics AB; 1999.

Eurocode 8. Design of structures for earthquake resistance-part 3: assessment and retrofitting of buildings. European Committee for Standardization (CEN) 2005.

FEMA P. 58-1. Seismic performance assessment of buildings Volume 1– Methodology; Prepared by Applied Technology Council for the Federal Emergency Management Agency. 2012.

Hernandez, J. F. Quasi-Static Testing of Cantilever Masonry Shear Wall Segments. [dissertation], University of Texas, 2012.

Ibrahim KS, Suter GT. Ductility of concrete masonry shear walls subjected to cyclic loading. In: Proceedings of 8th North American Masonry Conference, Taxes, Austin, USA; 1999.

Kapoi, C. M. Experimental Performance of Concrete Masonry Shear Walls Under In-Plane Loading. [dissertation], Washington State University, 2012.

- Kazaz İ. Analytical study on plastic hinge length of structural walls. *J Struct Eng* 2012;139(11):1938–50.
- Klingner RE, McGinley WM, Shing PB, McLean DI, Jo S, Okail H. Seismic performance of low-rise wood-framed and reinforced masonry buildings with clay masonry veneer. *J Struct Eng* 2012;139(8):1326–39.
- MacGregor JF, Yu H, Muñoz SG, Flores-Cerrillo J. Data-based latent variable methods for process analysis, monitoring and control. *Computer Chemical Eng* 2005;29(6):1217–23.
- Moehle JP. Displacement-based design of RC structures subjected to earthquakes. *Earthquake Spectra* 1992;8(3):403–28.
- Mostafaei H, Vecchio FJ, Kabeyasawa T. Deformation capacity of reinforced concrete columns. *ACI Structural Journal* 2009;106(2).
- Nelson PR, Taylor PA, MacGregor JF. Missing data methods in PCA and PLS: score calculations with incomplete observations. *Chemom Intell Lab Syst* 1996;35(1):45–65.
- Panagiotakos TB, Fardis MN. Deformations of reinforced concrete members at yielding and ultimate. *Structural Journal* 2001;98(2):135–48.
- Paulay T, Priestley MJN. Stability of ductile structural walls. *ACI Structural Journal* 1993;90(4).
- Priestley MN. Myths and fallacies in earthquake engineering—conflicts between design and reality. *Bull New Zealand Natl Soc Earthquake Eng* 1993;26(3):329–41.

- Priestley MN, Seible F, Calvi GM. Seismic design and retrofit of bridges. John Wiley & Sons; 1996.
- Priestley MJ. Performance based seismic design. Bull New Zealand Soc Earthquake Eng 2000;33(3):325–46.
- Priestley MJN, Clavi GM, Kowalsky MJ. Displacement-based seismic design of structures. Pavia, Italy: IUSS Press; 2007.
- Riahi Z, Elwood KJ, Alcocer SM. Backbone model for confined masonry walls for performance-based seismic design. J Struct Eng 2009;135(6):644–54.
- Sezen H. Shear deformation model for reinforced concrete columns. Struct Eng Mech 2008;28(1):39–52.
- Shedid MT, Drysdale RG, El-Dakhakhni WW. Behavior of fully grouted reinforced concrete masonry shear walls failing in flexure: experimental results. J Struct Eng 2008;134(11):1754–67.
- Shedid MT, El-Dakhakhni WW. Plastic hinge model and displacement-based seismic design parameter quantifications for reinforced concrete block structural walls. J Struct Eng 2013;140(4):04013090.
- Sherman JD. Effects of key parameters on the performance of concrete masonry shear walls under in-plane loading Doctoral dissertation. Washington State University; 2011.
- Shing PB, Schuller M, Hoskere VS. In-plane resistance of reinforced masonry shear walls. Journal of structural Engineering. 1990 Mar;116(3):619-40.

- Siam A, Shedid TM, Guo Y, El-Dakhakhani WW. Reliability of plastic hinge models for reinforced concrete and reinforced concrete block structural walls. In: 12th North American Masonry Conference (CD-ROM), Denver Co, USA; 2015.
- Sveinsson BI, McNiven HD, Sucuoglu H. Cyclic loading tests of masonry single Pier-Volume 4: Additional tests with height to width ratio of 1. Earthquake Engineering Research Center, College of Engineering, University of California, Report No. UCB/ERRC-85/15, Berkeley, California; 1985.
- Sullivan TJ, Calvi GM, Priestley MJ, Kowalsky MJ. The limitations and performances of different displacement based design methods. *J Earthquake Eng* 2003;7(spec01):201–41.
- Tomaževic M, Lutman M, Velechovsky T, Zarnic R. Seismic resistance of reinforced masonry walls. In: Proc. 9th World Conference on Earthquake. Eng1988 Aug; vol. 6, p. 97–102.
- Tomaževic M. Earthquake-resistant design of masonry buildings ISBN: 978-1-86094-066-8. World Scientific; 1999.
- Vaughan TP. Evaluation of masonry wall performance under cyclic loading (Doctoral dissertation, Washington State University) 2010.
- Vecchio FJ, Collins MP. The modified compression-field theory for reinforced concrete elements subjected to shear. *ACI J Proc* 1986;83(2).

Voon KC, Ingham JM. Experimental in-plane shear strength investigation of reinforced concrete masonry walls. *Journal of structural engineering*. 2006 Mar;132(3):400-8.

Yang JS, Cheng FY, Sheu MS. Inelastic modelling of backbone curve and hysteresis rules for low-rise RC perforated shear walls. *Earthquake Eng 10th World Conference 1992*:4313.

Yi J, Shrive NG. Behaviour of partially grouted hollow concrete masonry subjected to concentrated loads. *Can J Civ Eng* 2003;30(1):191–202.

Table 3.1: Characteristics of wall database

Wall ID	$L_w$ mm	$t_w$ mm	$H_w$ mm	$H_w/L_w$	$\rho_v$ %	$d_b$ mm	$\rho_{sh}$ %	$f_v$ MPa	$f_u$ MPa	$f'_m$ MPa	$P$ kN	$\Delta_u/H_w$ %	Reff.
1	1830	143	1830	1.00	0.38	15.9	0.24	441	710	20.0	361.1	0.820	Shing et al. 1989
2	1830	143	1830	1.00	0.38	15.9	0.24	441	710	20.0	487.5	0.693	
3	1830	143	1830	1.00	0.38	15.9	0.14	441	710	17.9	0.0	0.958	
4	1830	143	1830	1.00	0.38	15.9	0.24	441	710	20.7	0.0	1.319	
5	1830	143	1830	1.00	0.38	15.9	0.14	441	710	22.1	180.5	1.109	
6	1830	143	1830	1.00	0.38	15.9	0.24	441	710	22.1	180.5	0.858	
7	1830	143	1830	1.00	0.54	19.1	0.24	448	738	22.8	180.5	1.109	
8	1830	137	1830	1.00	0.40	15.9	0.26	441	710	26.2	484.3	0.913	
9	1830	137	1830	1.00	0.40	15.9	0.26	441	710	26.2	484.3	0.967	
10	1830	137	1830	1.00	0.40	15.9	0.26	441	710	26.2	484.3	1.021	
11	1830	137	1830	1.00	0.40	15.9	0.26	441	710	26.2	484.3	1.077	
12	1800	140	1800	1.00	0.62	20.0	0.05	318	366	17.6	0.0	0.556	Voon 2006
13	1800	140	1800	1.00	0.62	20.0	0.14	318	366	17.0	0.0	0.444	
14	1800	190	3600	2.00	0.29	16.0	0.08	502	577	18.5	0.0	0.889	Shedid et al. 2008
15	1800	190	3600	2.00	0.78	20.0	0.13	502	577	18.5	0.0	0.917	
16	1800	190	3600	2.00	0.73	25.0	0.13	502	577	18.5	0.0	0.778	
17	1800	190	3600	2.00	1.31	25.0	0.26	502	577	18.5	0.0	0.833	
18	1800	190	3600	2.00	1.31	25.0	0.26	502	577	18.5	260.0	0.694	
19	1800	190	3600	2.00	1.31	25.0	0.26	624	718	18.5	520.0	0.833	
20	1016	190	2032	2.00	0.33	12.7	0.31	450	518	21.0	0.0	1.450	Kapoi 2012
21	1016	190	2032	2.00	0.33	12.7	0.31	455	523	21.0	270.3	1.750	
22	1016	190	2032	2.00	0.59	22.2	0.31	455	523	15.7	202.7	1.088	
23	1829	190	1422	0.78	0.55	22.2	0.62	455	523	15.7	364.9	0.625	
24	1829	190	1829	1.00	0.55	22.2	0.62	455	523	15.7	264.9	1.083	
25	1422	190	2845	2.00	0.72	19.1	0.16	465	535	15.7	0.0	1.848	
26	1422	190	2845	2.00	0.87	19.1	0.34	465	535	15.7	0.0	2.089	
27	1422	190	2845	2.00	0.87	19.1	0.34	465	535	15.7	283.8	1.929	
28	1007	190	2013	2.00	0.69	19.1	0.31	454	522	19.1	244.3	1.110	Sherman 2011
29	1007	190	2013	2.00	0.69	19.1	0.31	446	513	19.1	244.3	1.274	
30	1007	190	2013	2.00	0.31	12.7	0.31	454	522	21.0	536.2	0.896	
31	1007	190	2013	2.00	0.31	12.7	0.31	450	518	21.0	536.2	0.795	
32	1819	190	1819	1.00	0.31	12.7	0.10	450	518	21.0	0.0	0.698	
33	1819	190	1819	1.00	0.31	12.7	0.31	450	518	21.0	484.6	0.656	
34	1819	190	1413	0.78	0.31	12.7	0.31	450	518	21.0	0.0	1.114	
35	1819	190	1413	0.78	0.31	12.7	0.62	450	518	21.0	484.6	0.719	

Table 3.1 (continued): Characteristics of wall database

Wall ID	$L_w$ mm	$t_w$ mm	$H_w$ mm	$H_w/L_w$	$\rho_v$ %	$d_b$ mm	$\rho_{sh}$ %	$f_y$ MPa	$f_u$ MPa	$f'_m$ MPa	$P/A_g$ kN	$\Delta_u/H_w$ %	Reff.
36	1020	190	2030	1.99	0.69	19.1	0.31	456	725	19.0	245.9	1.110	
37	1020	190	2030	1.99	0.69	19.1	0.31	446	725	21.0	271.8	1.490	
38	1020	190	2030	1.99	0.31	12.7	0.31	456	693	19.0	49.2	0.800	
39	1020	190	2030	1.99	0.31	12.7	0.31	450	693	21.0	54.4	0.910	
40	1830	190	1830	1.00	0.31	12.7	0.10	450	693	21.0	0.0	0.690	
41	1830	190	1830	1.00	0.31	12.7	0.31	450	693	21.0	487.6	0.710	
42	1830	190	1830	1.00	0.31	12.7	0.31	450	693	21.0	0.0	0.900	
43	1830	190	1830	1.00	0.31	12.7	0.31	450	693	21.0	487.6	0.700	
44	1220	190	3660	3.00	0.69	19.1	0.16	421	725	31.0	383.9	1.560	
45	1220	190	3660	3.00	0.31	12.7	0.16	448	693	23.0	569.6	1.930	
46	1220	190	3660	3.00	0.69	19.1	0.16	421	725	23.0	569.6	1.170	
47	1220	190	3660	3.00	0.31	12.7	0.16	448	693	23.0	854.4	1.270	
48	810	190	3660	4.52	0.69	19.1	0.31	421	725	29.0	238.4	3.000	
49	810	190	3660	4.52	0.31	12.7	0.31	448	693	29.0	476.8	2.610	
50	810	190	3660	4.52	0.69	19.1	0.16	421	725	23.0	378.2	2.790	
51	810	190	3660	4.52	0.31	12.7	0.16	448	693	23.0	567.3	1.650	
52	1020	190	2030	1.99	0.31	12.7	0.31	450	693	21.0	0.0	2.200	
53	1020	190	2030	1.99	0.31	12.7	0.31	455	693	21.0	271.8	2.110	
54	1020	190	2030	1.99	0.47	22.2	0.31	455	702	16.0	207.1	1.120	
55	1830	190	1420	0.78	0.47	22.2	0.63	455	702	16.0	371.5	0.930	
56	1830	190	1830	1.00	0.47	22.2	0.63	455	702	16.0	371.5	1.100	
57	1420	190	2840	2.00	0.69	19.1	0.16	465	725	16.0	0.0	1.890	
58	1420	190	2840	2.00	0.59	19.1	0.34	465	725	16.0	0.0	2.100	
59	1420	190	2840	2.00	0.59	19.1	0.34	465	725	16.0	288.3	2.020	
60	2440	190	2440	1.00	0.31	12.7	0.31	423	693	31.0	0.0	0.840	
61	2440	190	2440	1.00	0.16	12.7	0.16	423	693	29.0	0.0	1.760	
62	2440	190	2440	1.00	0.16	12.7	0.16	423	693	28.0	0.0	1.780	
63	2440	190	2440	1.00	0.31	12.7	0.31	423	693	31.0	1535.5	0.760	
64	2440	190	2440	1.00	0.16	12.7	0.16	423	693	29.0	1436.4	0.540	
65	2440	190	2440	1.00	0.16	12.7	0.16	423	693	28.0	1386.9	0.520	

Ahmadi et al. 2014

Table 3.1 (continued): Characteristics of wall database

Wall ID	$L_w$	$t_w$	$H_w$	$H_w/L_w$	$\rho_v$	$d_b$	$\rho_{sh}$	$f_y$	$f_u$	$f'_m$	$P/A_g$	$\Delta_u/H_w$ %	Reff.
	mm	mm	mm		%	mm	%	MPa	MPa	MPa	kN		
66	1410	190	1320	0.94	0.51	16.0	0.25	437	503	12.0	66.1	0.758	Vaughan 2010
67	1410	190	2135	1.51	0.51	16.0	0.16	437	503	12.0	66.1	0.835	
68	1410	190	1320	0.94	0.29	16.0	0.16	455	524	12.0	52.5	0.662	
69	1410	190	2135	1.51	0.29	16.0	0.16	455	524	12.0	52.5	0.830	
70	1410	190	1320	0.94	0.51	16.0	0.16	455	524	12.0	52.5	0.663	
71	1410	190	2135	1.51	0.51	16.0	0.16	455	524	12.0	52.5	0.829	
72	1000	190	2135	2.14	0.51	16.0	0.16	455	524	12.0	37.2	1.045	
73	1820	190	1320	0.73	0.28	16.0	0.16	455	524	12.0	67.8	0.588	
74	1220	143	1440	1.18	0.44	22.2	0.39	390	450	15.1	303.1	0.480	
75	1220	143	1440	1.18	0.44	22.2	0.20	390	450	15.1	120.3	0.614	
76	2440	195	2440	1.00	0.33	12.7	0.33	423	681	29.0	0.0	1.301	Hernandez 2012
77	2440	195	2440	1.00	0.16	12.7	0.16	423	681	29.0	0.0	1.822	
78	2440	195	2441	1.00	0.33	12.7	0.33	423	681	29.0	47.6	1.036	
79	2440	195	2442	1.00	0.16	12.7	0.16	423	681	29.0	47.6	1.140	
80	2440	195	2443	1.00	0.33	12.7	0.16	423	681	24.3	0.0	1.871	
81	2440	195	2444	1.00	0.16	12.7	0.16	423	681	24.3	47.6	1.023	

Table 3.2: Coefficients of the proposed ultimate displacement prediction model

Coefficient	Value
$a_1$	0.47
$a_2$	0.46
$a_3$	0.31
$a_4$	0.30
$a_5$	0.40
$a_6$	0.33

Table 3.3: Range of wall characteristics for the performance chart scenarios and default wall scenario

Parameter	Units	Range					Default
$H_w$	mm	3000	4000	6000	9000	12000	6000
$d_b$	mm	10M (11.5 mm)	15M (16 mm)	20M (19.5 mm)	25M (25.2mm)	---	15M (16 mm)
$d_{b,sh}$	mm	10M	15M	---	---	---	10M (11.5 mm)
$s_v$	mm	200	400	600	800	---	400
$s_{sh}$	mm	200	400	600	800	1200	400
$f'_m$	MPa	10.0	13.5	17.0	---	---	13.5
$P/(A_g f'_m)$	%	0	2.5	5.0	7.5	10	5

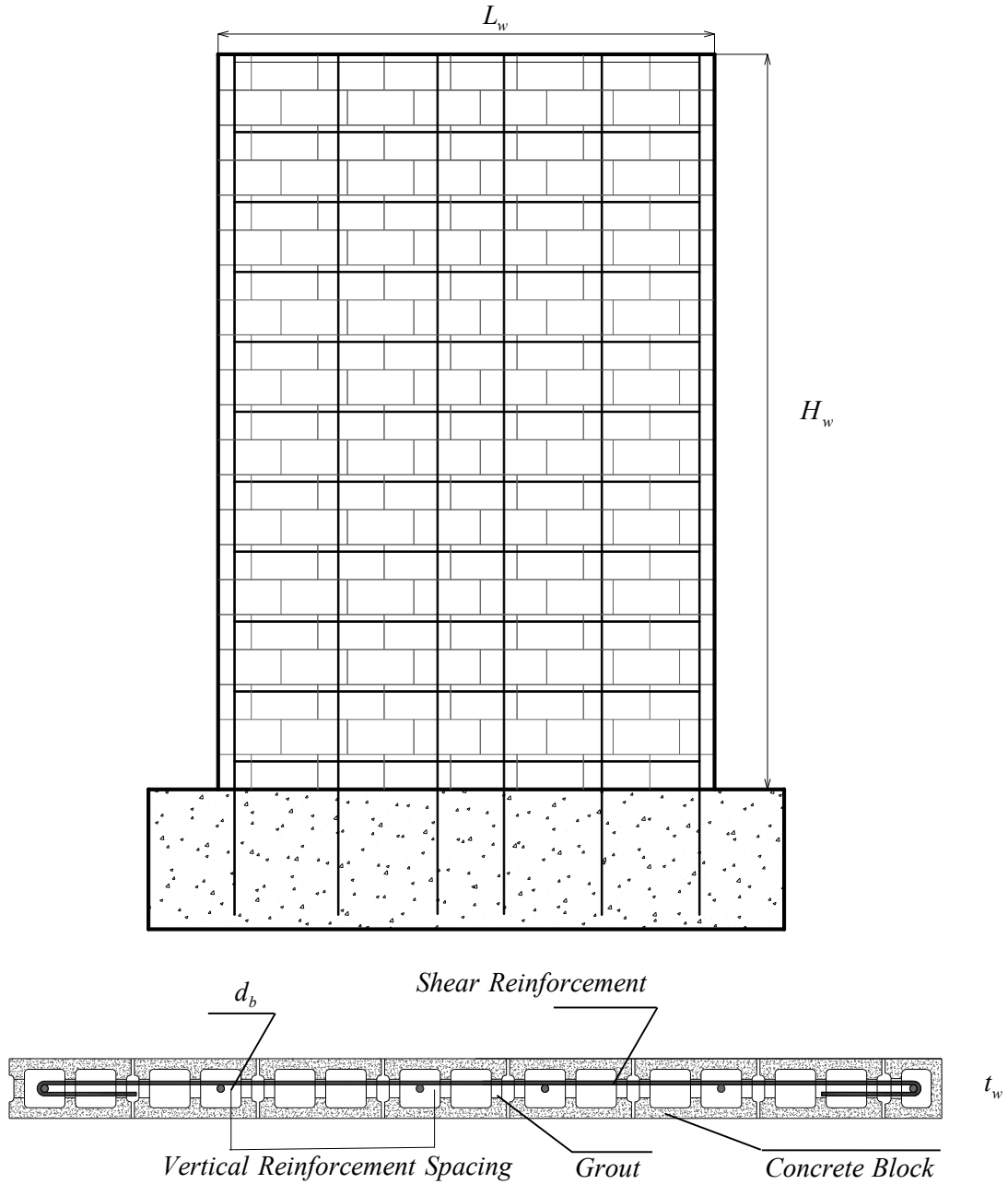


Figure 3.1: Typical RMSW cross section and elevation

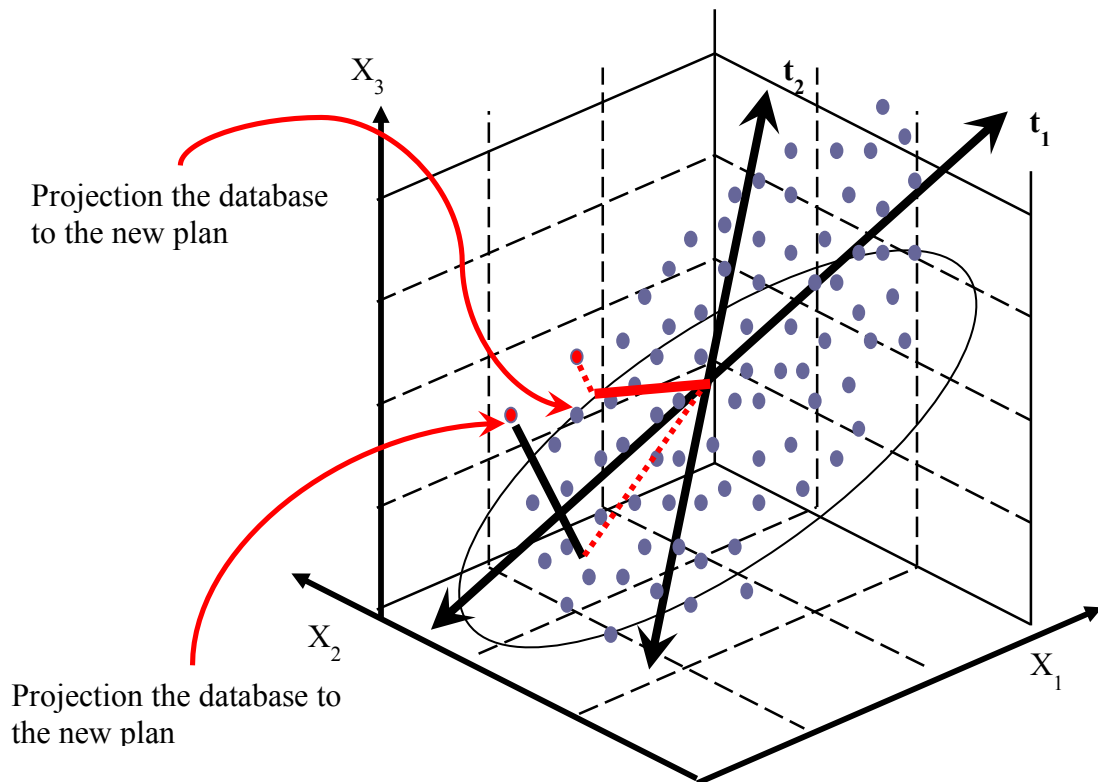


Figure 3.2: Extracting scores and loadings plot data for three variables.

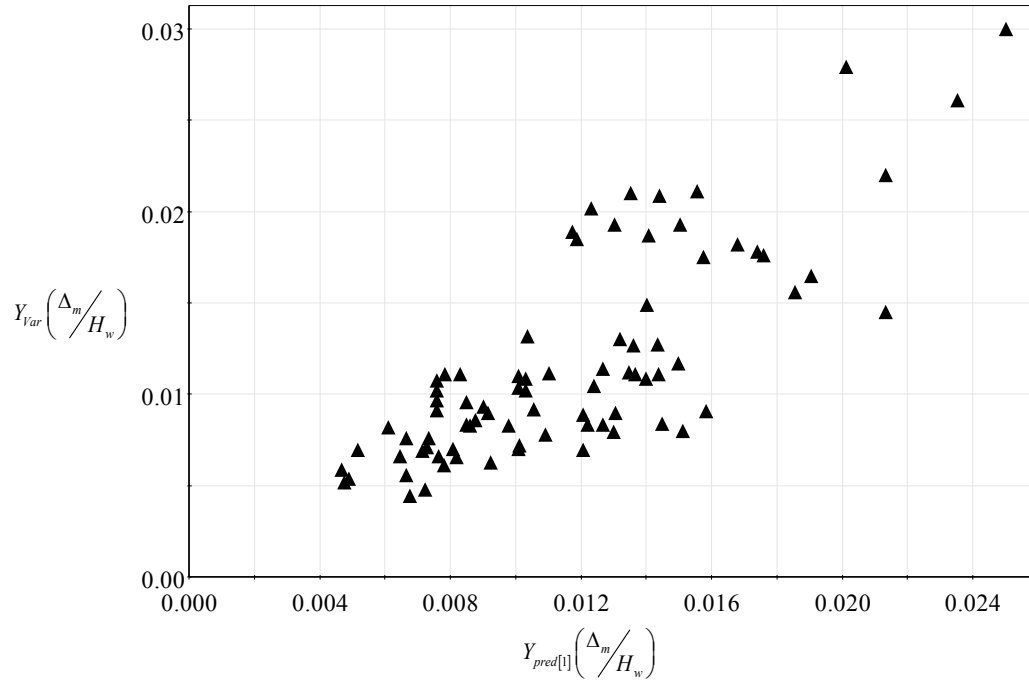
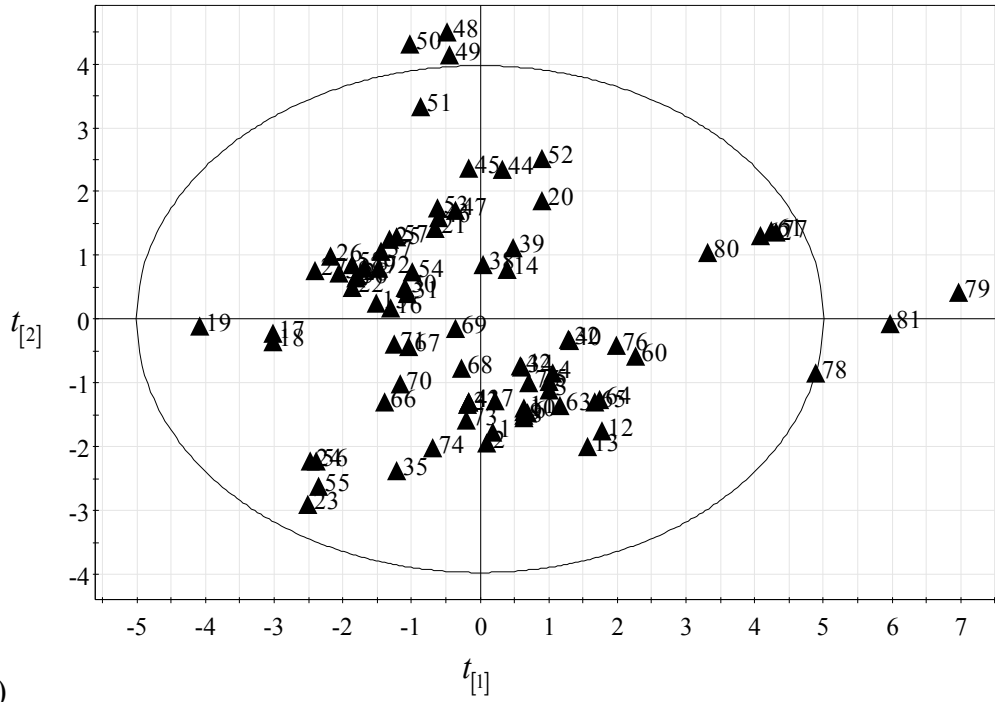
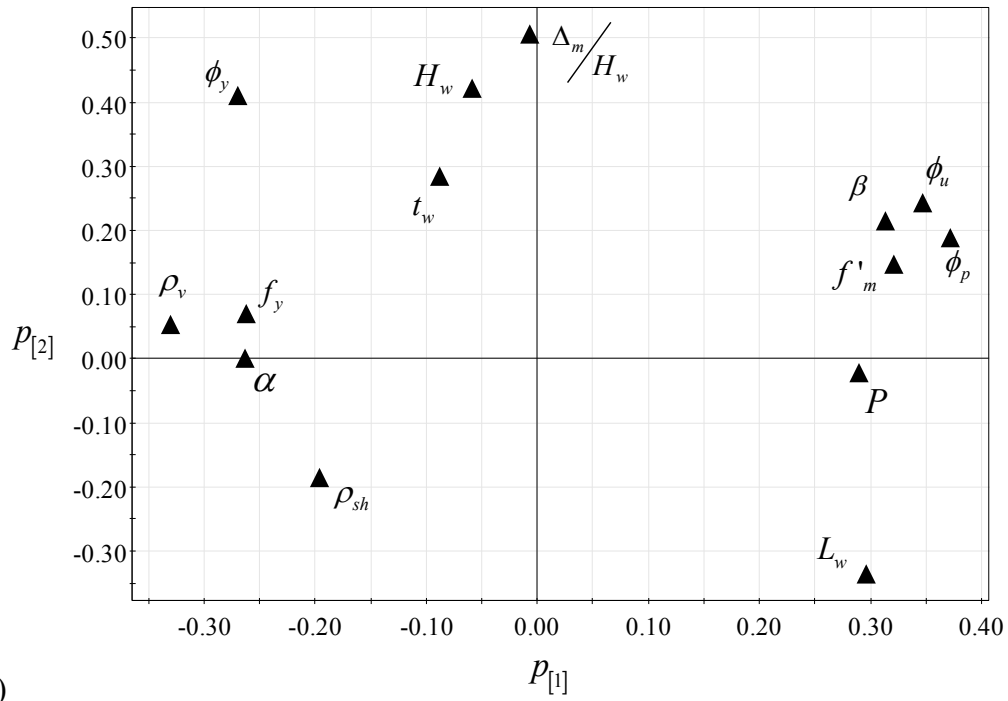


Figure 3.3: Scatter plot to evaluate the applicability of using MVDA

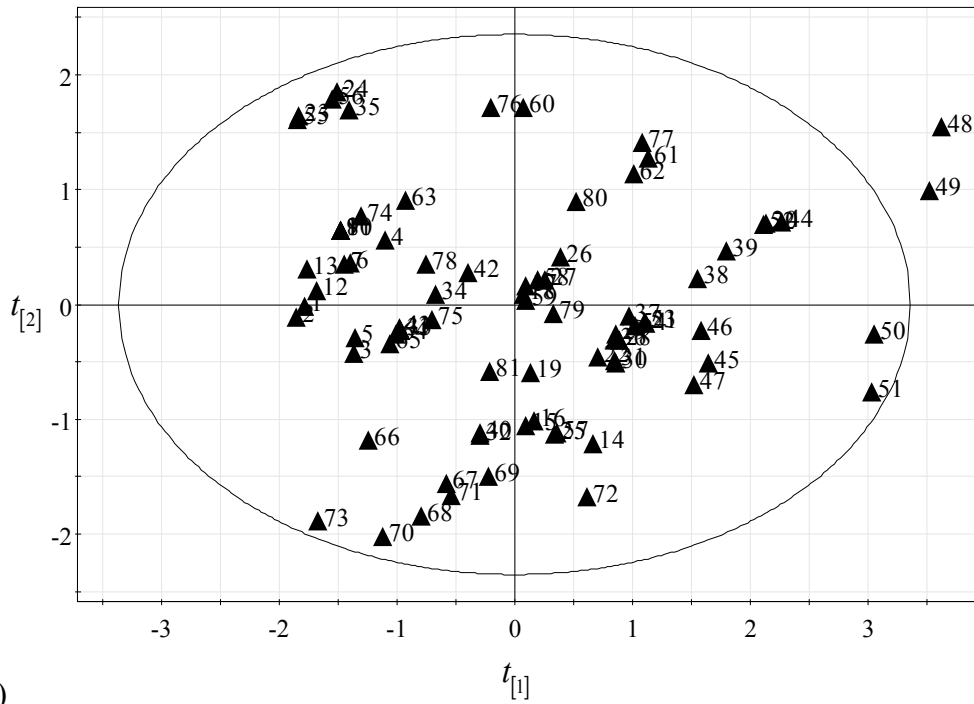


(a)

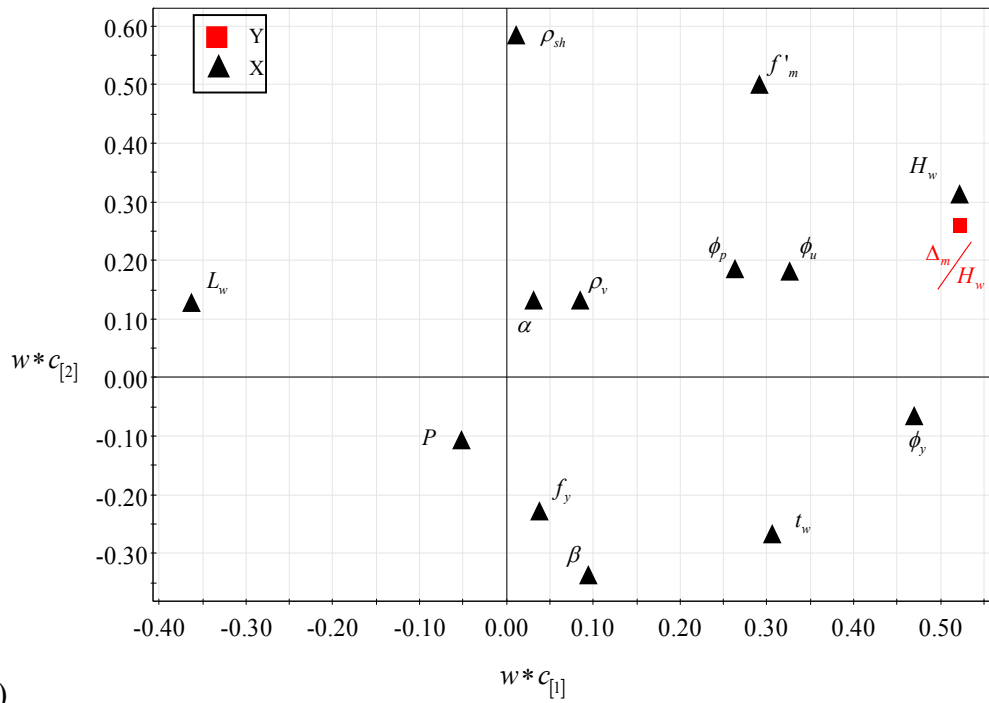


(b)

Figure 3.4: PCA for the RMSW database: (a) Scores plot; and (b) Loadings plot for all variables



(a)



(b)

Figure 3.5: PLS analysis of the RMSW database plain parameter: (a) scores plot; and (b) loadings plot

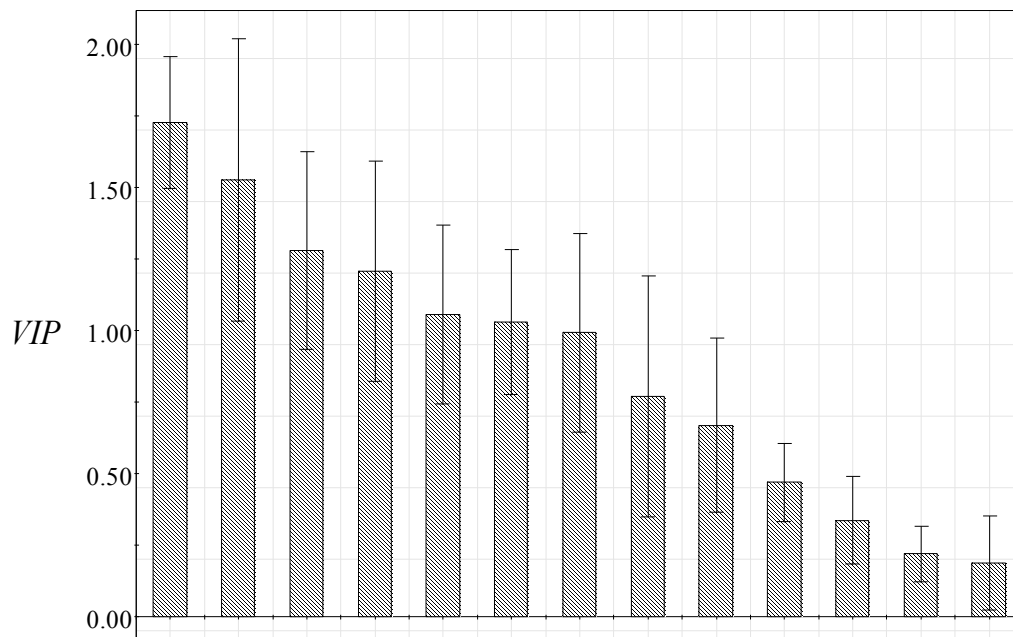


Figure 3.6: Variable important for projection (VIP) plot for PLS of the RMSW database.

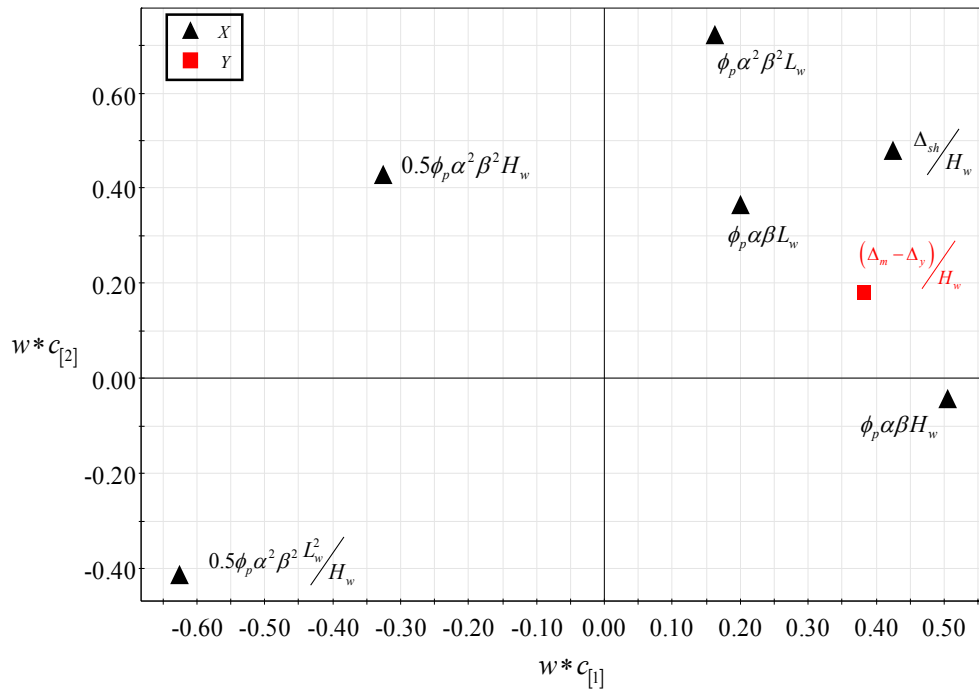
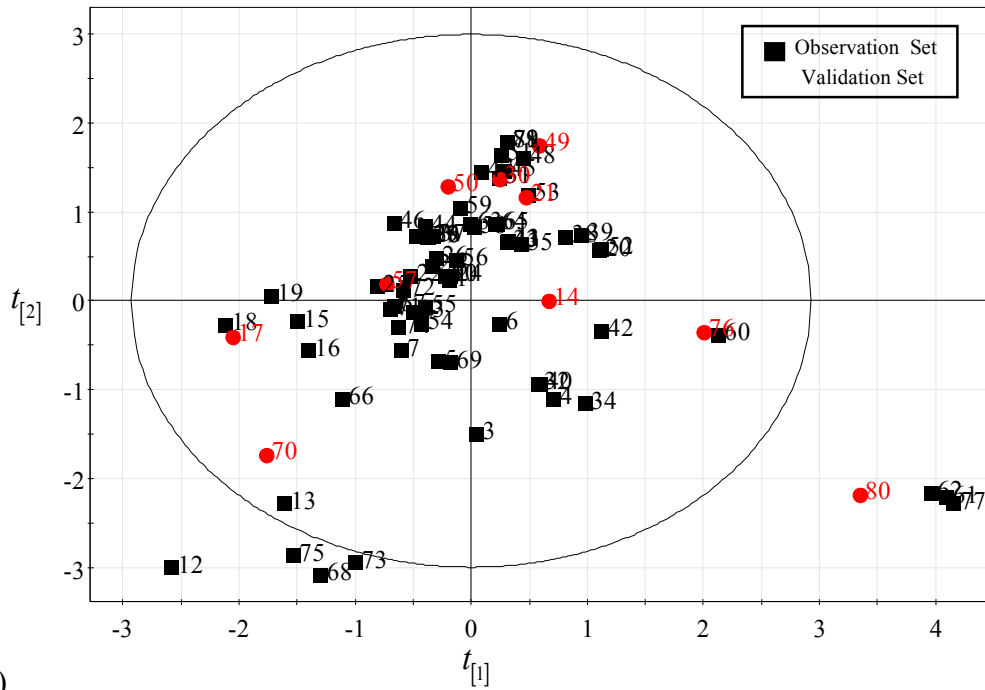


Figure 3.7: PLS analysis of the RMSW database proposed model parameters: (a) Scores plot; and (b) loadings plot

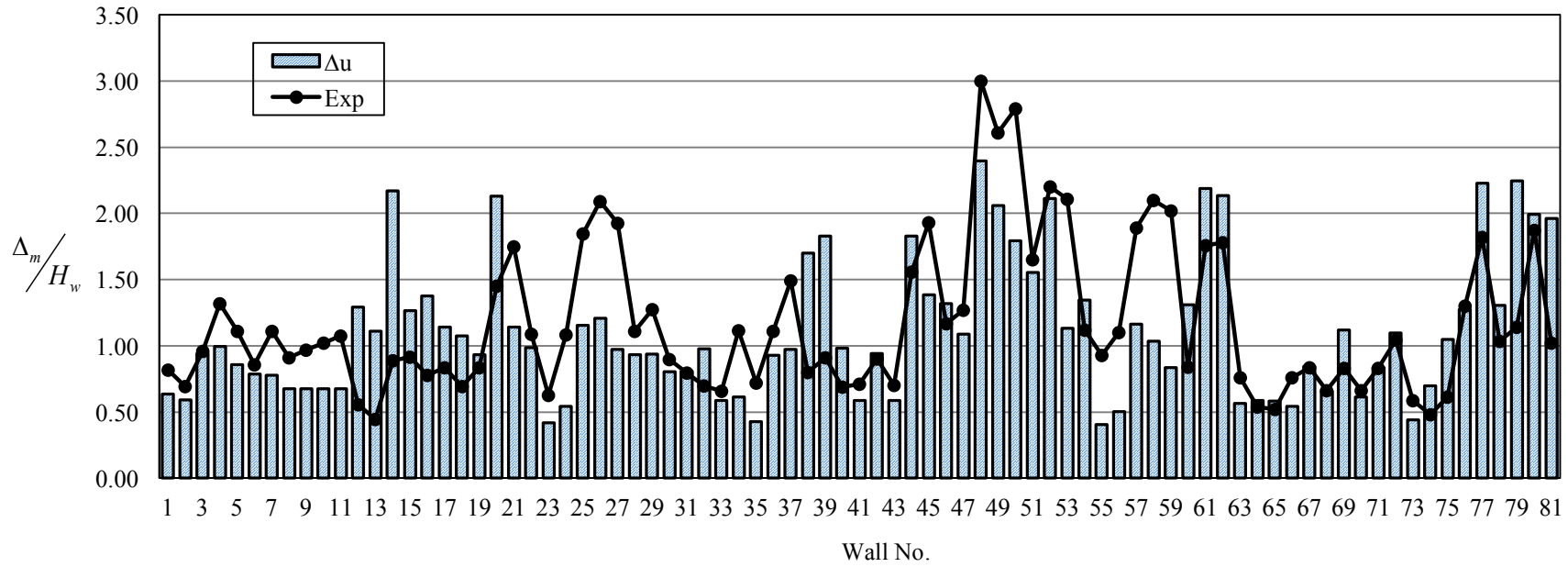


Figure 3.8: Actual to predicted RMSW database drifts.

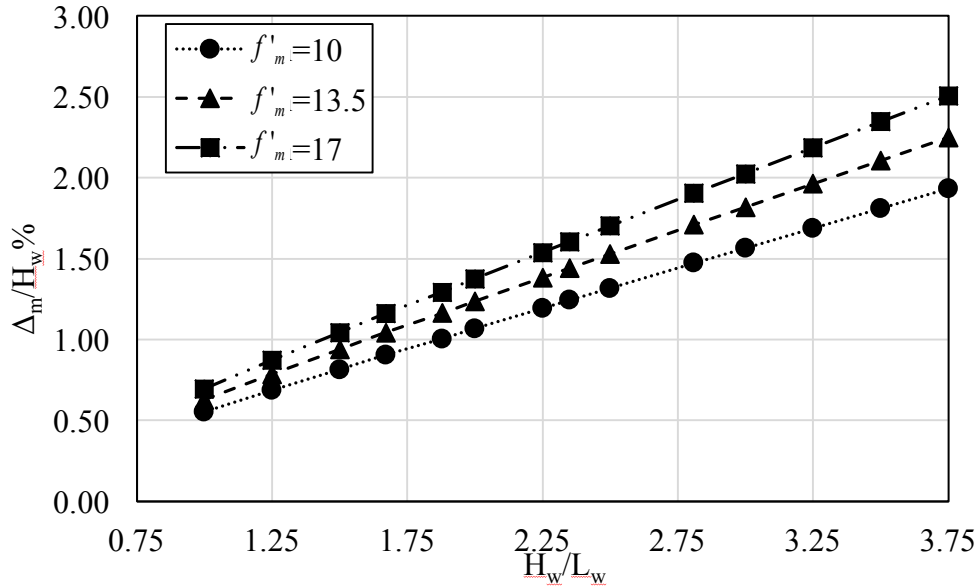


Figure 3.9: Influence of masonry compressive strength on scenario RMSW drift capacities.

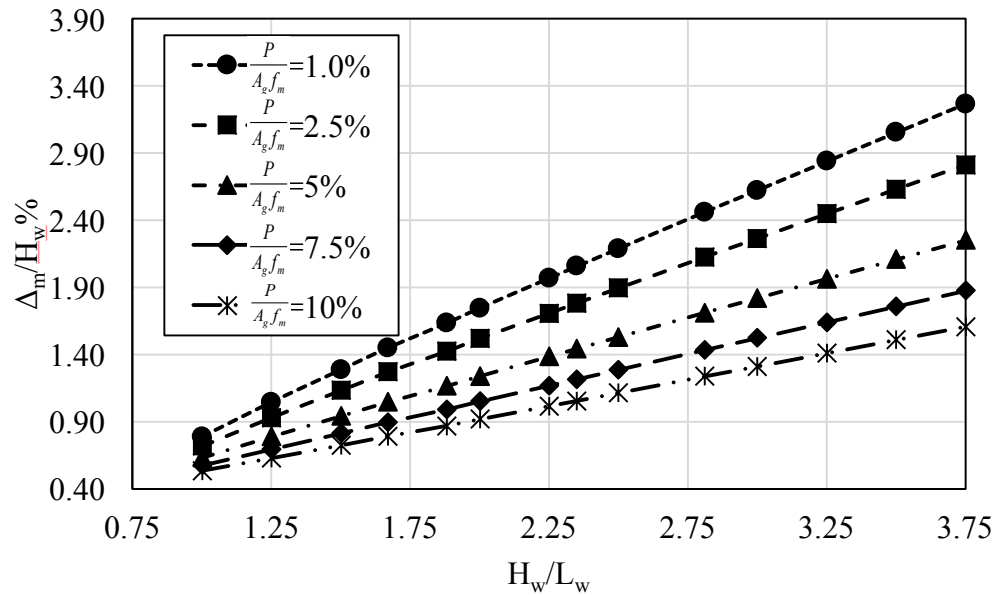


Figure 3.10: Influence of axial load on scenario RMSW drift capacities.

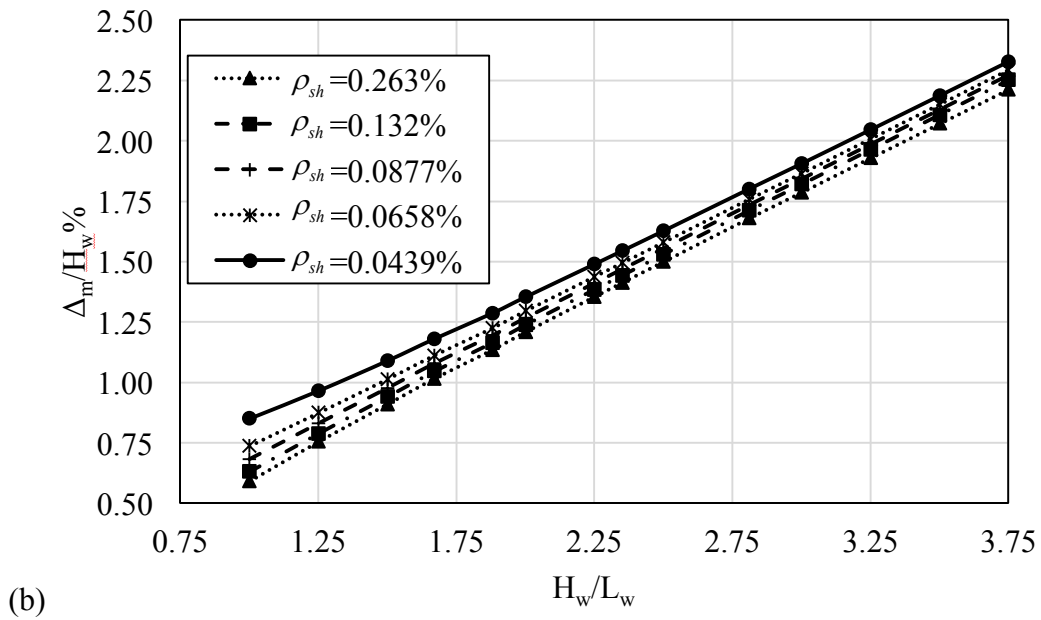
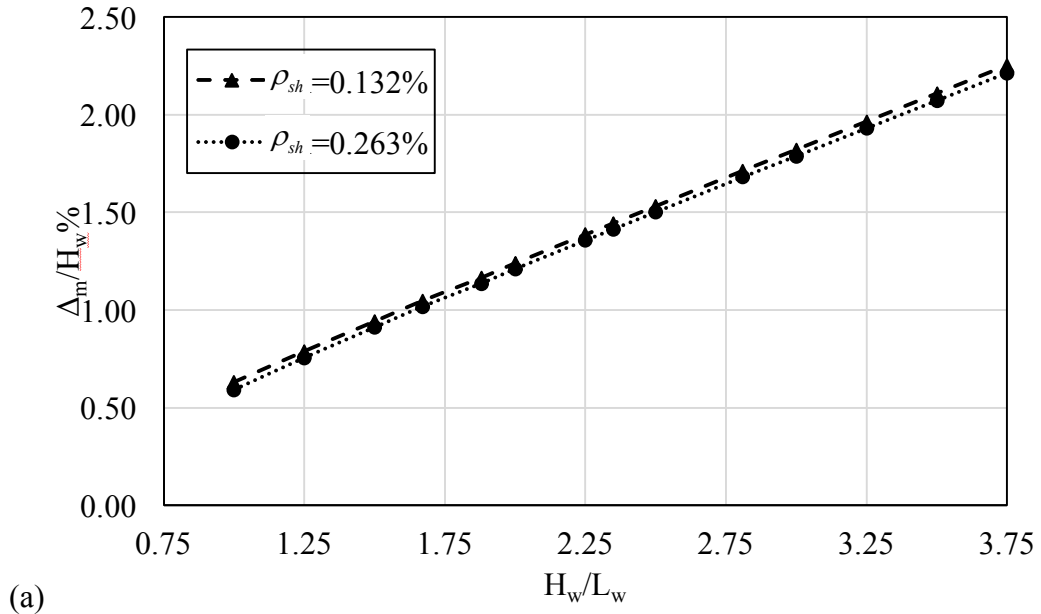


Figure 3.11: Influence of shear reinforcement on scenario RMSW drift capacities: (a) constant spacing with different bar diameters; and (b) constant bar diameter with different spacing

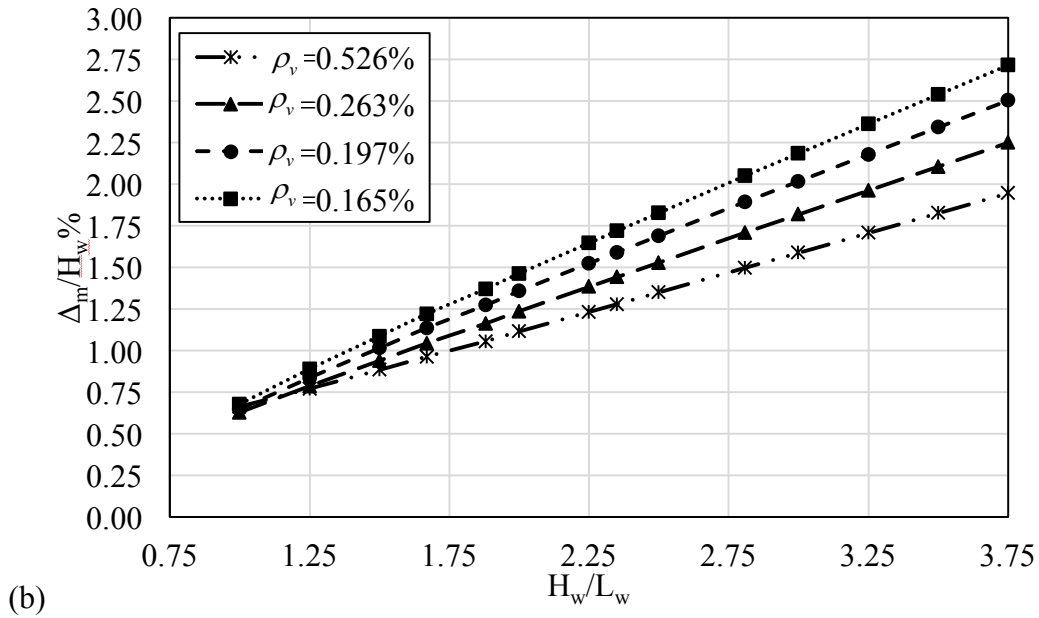
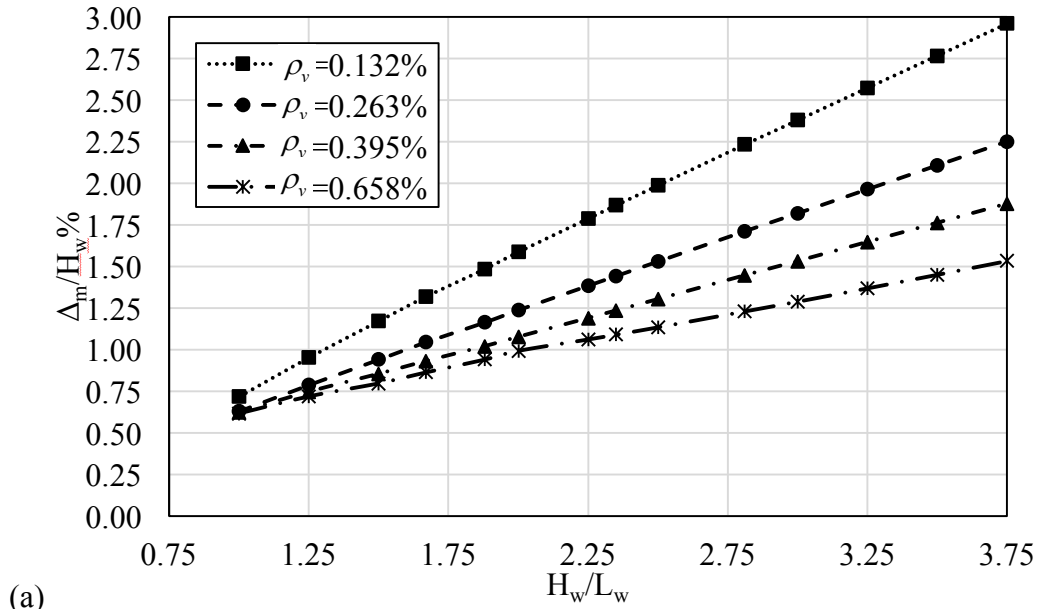


Figure 3.12: Influence of vertical reinforcement on scenario RMSW drift capacities: (a) constant spacing with different bar diameters; and (b) constant bar diameter with different spacing.

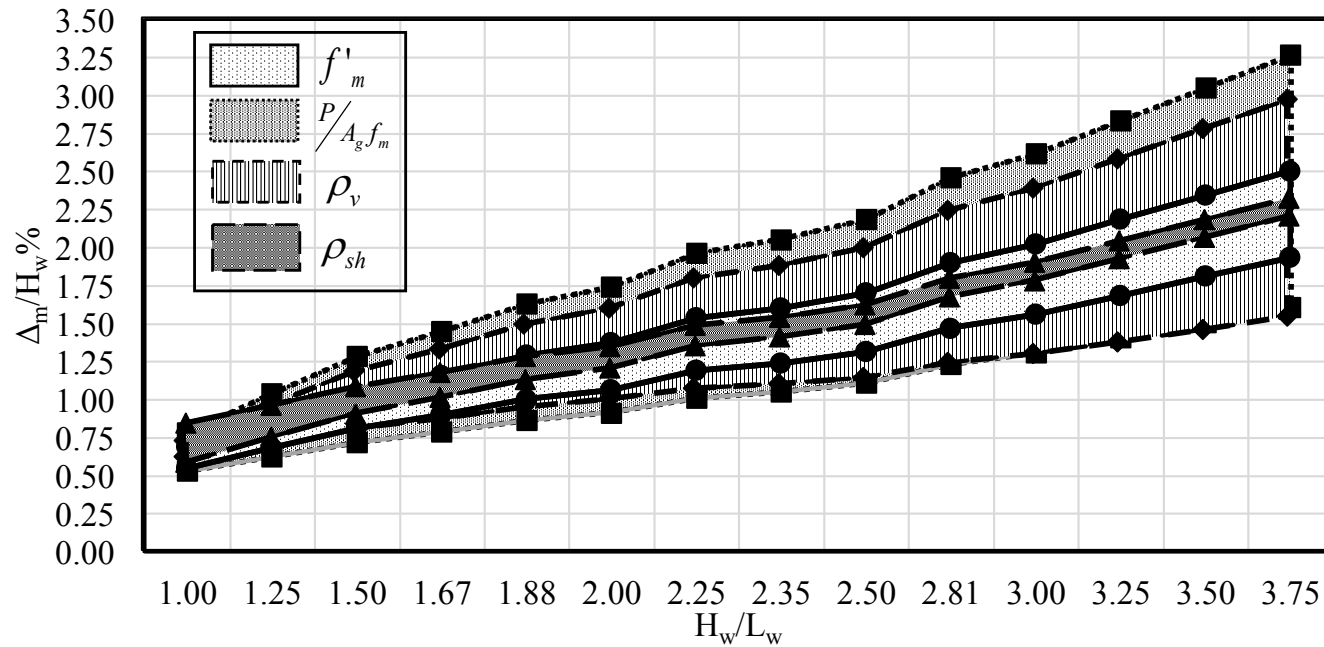


Figure 3.13: Bounds of scenario RMSW drift capacities.

## **CHAPTER 4**

### **SEISMIC RISK ASSESSMENT OF REINFORCED MASONRY STRUCTURAL WALL SYSTEMS USING MULTIVARIATE DATA ANALYSIS**

#### **4.1 ABSTRACT**

In contrast to the single design objective associated with force-based design approaches of different seismic force resisting systems (SFRSs), performance-based seismic design (PBSD) allows the selection of more than one design/performance objective. Each performance objective is linked to a tolerable risk level associated with the considered SFRS experiencing a specific damage at a specified seismic hazard level (presented in the form of fragility curves). Similar to other SFRSs, damage of reinforced masonry shear wall (RMSW) SFRSs can be linked to their lateral displacements/drifts. As such, this study focuses on using a multivariate data analysis technique, to develop a RMSW load-displacement (backbone) curve model. The backbone model is calibrated using a database of RMSW experimental test results, and the model is further utilized to investigate the influence of the wall geometrical and mechanical characteristics on altering the displacement demands of RMSW corresponding to different performance levels. These analysis results are then used to develop RMSW seismic fragility bands to facilitate visualizing the resulting range of displacement (drift) demands, when the different RMSW characteristics are considered. The developed fragility bands are compared to the individual fragility curves currently adopted by the Federal

Emergency Management Agency, FEMA P-58 pre-standards, *Seismic Performance Assessment of Buildings*. This comparison shows that the fragility bands deviate from the individual fragility curves currently adopted by FEMA at each damage state. The developed backbone curve model and fragility-bands are expected to not only facilitate adoption of the RMSW SFRSs in the next generation of PBSB codes but also to equip researchers and designers with a clear understanding of the aspects governing the seismic performance of RMSW systems.

## 4.2 INTRODUCTION

Similar to other seismic force resisting systems (SFRSs), current seismic design provisions for reinforced masonry shear walls (RMSWs) are based on prescriptive detailing requirements which are expected to result in constructed RMSW buildings that are capable of withstanding design-level earthquake without collapse [Park (1997), Wantanabe and Kawashima (2002), Cardone et al. (2008)]. Due to the wide range of uncertainties associated with different seismic hazard levels as well as the uncertainty inherent in SFRSs response (i.e. demand and capacity), multiple performance levels might be sought depending on the magnitude and associated uncertainty of seismic hazard [Cornell (1996), Ghobarah (2001), FEMA 445 (2006), Mackie and Stojadinović (2007)]. This, however, conflicts with the force-based design approaches, currently adopted by most international seismic design

code, where the *life safety/collapse prevention* performance level is, inherently, the only performance objective that buildings are designed to meet. As such, significant effort has been carried out during the past two decades [Bracci et al. (1997), Cornell and Krawinkler (2000), Priestley (2000), ASCE 41-13 (2013)] in order to address the need to develop a holistic performance-based seismic design (PBSD) philosophy [Cornell (1996), Priestley (2000), Bertero and Bertero (2002), Fajfar and Krawinkler (2004)] in lieu of the current force-based seismic design approaches. Moving beyond deterministic analysis, PBSD also considers the uncertainty associated with seismic hazard, response, and damage in an effort to achieve uniform risk building systems [Cornell (1996), Ghojarah (2001)]. Performance levels of RMSWs can be linked to different performance indicators (demand parameters), including the stress/force level and displacement/drift demands [Ghojarah, 2001]. These performance indicators are in turn each linked to a specific level and extent of damage, presented as Damage States (DSs). Although each DS can be influenced by several parameters including the number of cycles and duration of the seismic event, displacement (often normalized as a percentage drift by dividing by the wall height) is regarded as the indicator most directly linked to SFRS performance.

As such, displacement-based seismic design (DBSD) is the stepping stone towards PBSD with the former necessitate knowledge of the SFRS load-displacement behavior (backbone curve) prior to selecting a *target displacement* as the design objective. Once the target displacement is selected, the level of SFRS

strength and stiffness are evaluated and the design/analysis processes continue in an iterative manner until the target displacement is achieved. To facilitate direct linkage to PBSO objectives, a piecewise linear RMSW load-displacement backbone curve will be presented in the current study. The developed backbone curve model is characterized by four RMSW performance levels, namely: the cracking point, the onset of yielding of the outermost tension reinforcement, the displacement associated with the wall maximum strength, and the wall ultimate displacement corresponding to 20% degradation in the wall peak strength.

The above wall performance levels can be linked to DSs and presented in the form of *fragility curves*. In general, fragility curves describe the probability of engineering demand parameter, which is presented as drifts that are linked to different damage states in the current study, to be reached or exceeded [Shinozuka et al. (2000)]. The fragility curves can be categorized based on the method used to develop them [Porter and Kiremidjian (2000)]. The first category is the empirical fragility curves where their development is carried out through curve fitting of experimental results or real life data. The second category is the analytical fragility curves, derived through engineering analyses of SFRS model response. The third category is based on expert opinion or are judgment-based.

This study will start by assessing the capabilities of published backbone curve models, developed for either reinforced concrete shear walls (RCSW) or RMSW, to assess the different model predictions of the RMSW response within an experimental results database compiled from published literature. Realizing the

deficiencies within these models based on this assessment, the study focuses on utilizing principal component analysis (PCA) and partial least square (PLS) technique to develop a new backbone curve model that is calibrated using the experimental RMSW database. Using different RMSW design scenarios, the calibrated backbone model is further utilized to capture the influence of different design parameters on RMSW displacement demands. Finally, the analysis results are used to generate RMSW fragility bands for each DS and to compare the generated bands with the corresponding individual fragility curve adopted by the FEMA P-58 [(FEMA P-58/BD-3.8.10 (2009)] pre-standards.

### **4.3 AVAILABLE BACKBONE PREDICTION MODELS**

There are several models developed to predict the points defining the backbone curve for RCSW. Riahi et al. (2009) and Gérin and Adebar (2004) proposed models to estimate the backbone curve of walls governed by shear failure. For flexurally-dominated shear wall, Wallace (2007) and Habasaki et al (2000) developed backbone curves up to the maximum load only. Several RCSW and RMSW load-displacement relationship prediction models proposed using quad-linear backbone models [e.g. Ashour and El-Dakhkhni (2016), Carrillo and Alcocer (2012), Sánchez (2010), and Hidalgo and Jordan (1996)]. These models evaluate the maximum wall lateral load capacity,  $Q_{max}$ , and subsequently the 80% degraded strength,  $Q_{80\%}$ , using basic mechanics (wall cross section analysis based on enforcing equilibrium and compatibility conditions.), except for Carrillo and

Alcocer's model (2012) where  $Q_{\max}$  is given by Eq. (4.1). For the cracking and yield limits state, basic mechanics analysis is used for all of the models as will be presented next.

Based on the best fit analysis, of the experimental RMSW test results reported by Siyam et al. (2015), Ashour and El-Dakhkhni (2016) proposed set of equations to predict wall drifts using ratios of the yield stiffness,  $K_y$ , as shown in Eqs. (4.1) and (4.2).

$$\Delta_{Q_{\max}} = \frac{Q_{\max}}{K_{\max}}, K_{\max} = 0.6 \times K_y \quad (4.1)$$

$$\Delta_{Q_{80\%}} = \frac{Q_{80\%}}{K_{80\%}}, K_{80\%} = 0.2 \times K_y \quad (4.2)$$

Where  $K_{\max}$  and  $K_{80\%}$  are the secant stiffness at the maximum and ultimate limit states, respectively,  $\Delta_{Q_{\max}}$  and  $\Delta_{Q_{80\%}}$  are the displacements corresponding to  $Q_{\max}$  and  $Q_{80\%}$ , respectively.

Based on trends and nonlinear regression analysis of the experimental results of 39 RCSW tested on shake tables and under quasi-static lateral loading, Carrillo and Alcocer (2012) proposed semi-empirical equations [Eqs. (4.3) to (4.6)] to predict the maximum and ultimate limit states.

$$\frac{\Delta_{Q_{\max}}}{H_w} = \frac{1}{5200} \frac{V_{\max}}{t_w \sqrt{f'_c}} e^{1.30 \left( \frac{M}{VL_w} \right)} \quad (4.3)$$

$$\frac{\Delta_{Q_{80\%}}}{H_w} = \frac{1}{3650} \frac{V_{\max}}{t_w \sqrt{f'_c}} e^{1.35 \left( \frac{M}{VL_w} \right)} \quad (4.4)$$

$$V_{\max} = \left[ \alpha_1 \sqrt{f'_c} + \eta_h \rho_h f_{yh} \right] A_w \leq \alpha_2 A_w \sqrt{f'_c} \quad (4.5)$$

$$\alpha_1 = 0.21 - 0.02 \left( \frac{M}{VL_w} \right) \quad (4.6)$$

where  $\alpha_1$  (given by Eq. 4.6), and  $\alpha_2$  (equal to 0.4), are coefficient defining the relative contribution of the concrete diagonal tension and diagonal compression strength, respectively. This model includes the most important design variables, from Carrillo and Alcocer's point of view, which are: 1) the ratio between the shear span ( $M/V$ ) and the wall length ( $L_w$ ):  $M/VL_w$ , which is essentially the wall's aspect ratio in a single story building; 2) the concrete compressive strength,  $f'_c$  (all the  $\sqrt{f'_c}$  presented in this study are in SI units); 3) the wall gross cross sectional area,  $A_w$ ; 4) the shear reinforcement ratio,  $\rho_{sh}$ ; and 5) the shear reinforcement yield strength,  $f_{y\_sh}$ . This model is limited to: aspect ratios less than or equal to 2.0; concrete strength of up to 25 MPa; and an axial stress that is less than  $0.03f'_c$ .

Sánchez (2010) introduced a load-displacement model calibrated using a large database with a wider range of parameters compared to those utilized by Carrillo and Alcocer (2012). The formulations proposed by Sánchez (2010) takes into account both the flexural and shear deformations in different limits states as given by Eqs. (4.7) and (4.8).

$$\Delta_{Q_{\max}} = \frac{Q_{\max} H_w^3}{3E_c (0.7I_g)} + \frac{Q_{\max} L_w}{300A_w \sqrt{f'_c}} e^{1.33 \left( \frac{M}{VL_w} \right)} \quad (4.7)$$

$$\Delta_{Q_{80\%}} = \left( \Delta_{Q_{\max}} + \frac{9}{\rho_{sh} f_{y_{sh}}} \right) \left( 0.6 \frac{M}{VL_w} + 0.5 \right) \quad (4.8)$$

Hidalgo and Jordan (1996), proposed a simple shear wall backbone curve model that depends on the wall shear span and its aspect ratio (Eqs. 4.9 and 4.10).

$$\Delta_{Q_{\max}} = \left( 0.00185 + 0.0045 \frac{M}{VL_w} \right) H_w \quad (4.9)$$

$$\Delta_{Q_{80\%}} = 0.016 \frac{M}{VL_w} H_w \quad (4.10)$$

It should be noted that the maximum force represented in all these models are not the maximum wall shear capacity. As the aforementioned models focus on the flexurally dominated cantilever wall, the maximum lateral resistance attained by the wall prior to flexural strength degradation is lateral force corresponding to the maximum flexural moment that the wall can sustain based on wall cross section analysis (using basic mechanics) at the wall-foundation interface level. All the aforementioned model predictions will be compared with the corresponding experimental database test results as will be discussed later.

#### 4.4 MODEL PREDICTION ASSESSMENTS

This study utilizes a database of flexurally dominated RMSW tested under cyclic loading to assess the aforementioned models predictability. The experimental results database used in this study is limited to only flexurally-dominated RMSWs tested under cyclic loading. Within the 81 RMSWs originally

reported by Siam et al. (2017), only 65 walls had their hysteretic loops available and, thus, their ultimate displacements were readily available through generating the envelope of the cyclic load-displacement relationship for both push and pull directions. An additional, acceptance criterion was introduced in order to ensure the consistency between the experimentally reported wall strengths and those predicted using basic mechanics: the experimental wall peak strength has to be within +/-20% of the peak lateral load predicted using the basic mechanics. As such, the number of RMSWs in the database considered in the current paper is further reduced to the 48 walls listed in Table 4.1, with their mechanical and geometrical design parameters.

The backbone curves (piecewise linear relationships) for the RMSWs can be defined by four points, each identified by a specific strength level [cracking, yielding, maximum strength, and 80% of the maximum load on the descending branch] and the corresponding displacement. Similar to other studies [e.g. 9,11], the current study links the ultimate wall damage state to the point where 80% of its maximum strength is reached on the descending branch. Herein, wall drifts (lateral displacement divided by the corresponding wall height) will be presented in lieu of the displacement as a normalized form to facilitate comparison. For the comparison with the experimental results, the drifts can be categorized into either those associated with the cracking and yield limit state, where the drifts can be evaluated from basic mechanics; or those corresponding to the walls' maximum strengths and ultimate displacements (corresponding to the 20% reduction of the maximum load

on the descending branch), where the models presented earlier are to be used for such displacement/drift predictions.

#### 4.4.1 Cracking Limit State

The crack limit state is defined by the cracking force,  $Q_{cr}$ , and its associated drifts,

$\Delta_{cr}/H_w$ , calculation is based on Eqs. (4.11) and (4.12).

$$Q_{crack} = \frac{M_{crack}}{H_w} \quad (4.11.a)$$

$$\text{where } M_{crack} = \frac{f_{cr}}{L_w/2} I_g \quad (4.11.b)$$

$$\text{as such, } Q_{crack} = \frac{f_t}{L_w/2} I_g \frac{1}{H_w} = \frac{f_t t_w L_w^3}{0.5 L_w H_w} = \frac{f_t t_w L_w^2}{6 H_w} = \frac{f_t A_w}{6 A_R} \quad (4.11.c)$$

$$\frac{\Delta_{cr}}{H_w} = \frac{\left( \frac{Q_{cr} H^3}{3 E_m I_g} \right) / H_w}{\left( \frac{Q_{cr} H^3}{3 E_m (t_w L_w^3 / 12)} \right) / H_w} = \frac{(12/3) Q_{cr} \left( H_w / L_w \right)^3}{H_w E_m t_w} = \frac{4 Q_{cr} A_R^3}{t_w H_w E_m} \quad (4.12)$$

where  $f_t$  is the masonry tensile strength is taken equal to 0.4 MPa as per Table 8.2.4.2 in the MSJC code (MSJC 2013),  $A_w$  is the cross sectional area,  $A_R$  is the wall aspect ratio,  $H_w$  is the wall height,  $t_w$  is the wall thickness, and  $E_m$  is the masonry Young's modulus evaluated as  $900f'_m$  (MSJC 2013). Since the drifts

corresponding to the cracking stage are very small compared to those at the other three states, they can be considered negligible.

#### 4.4.2 Yield Limit State

The yield limit state is realized at the onset of yield of the outermost vertical bar in the wall cross section. For RMSWs, the lateral drifts beyond the cracking limit result from flexural and shear deformations. However, the lateral displacement values, obtained from the experimental result database, at each limit state are the total displacement values, which include the combined wall flexural and shear deformation components. In addition, this section focuses on assessing backbone models available in the literature using the experimental result database presented in this study. At the yield limit state, the yield displacement can be presented as a combination of flexural,  $\Delta_{y\_flex}$ , and shear component,  $\Delta_{y\_sh}$  [Tang and Su, (2014)]. The yield flexural component can either be estimated using the yield curvature (*first approach*), Eq. (4.13.c), or using the effective inertia of the cross section (*second approach*), Eq. (4.13.d) (Priestley and Hart 1989).

$$\frac{\Delta_y}{H_w} = \frac{\Delta_{y\_flex}}{H_w} + \frac{\Delta_{y\_sh}}{H_w} \quad (4.13.a)$$

$$\frac{\Delta_{y\_sh}}{H_w} = \frac{1.2}{G_m A_e} \quad (4.13.b)$$

$$\frac{\Delta_{y\_flex}}{H_w} = \frac{\phi_y H_w}{3} \quad (4.13.c)$$

$$\text{or, } \frac{\Delta_{y\_flex}}{H_w} = \frac{Q_y H_w^2}{3E_m I_e} \quad (4.13.d)$$

$$\text{where, } I_e = \alpha I_g, A_e = \alpha A_g, \alpha = \left( \frac{100}{f_y} + \frac{P_u}{f'_m A_g} \right) \quad (4.13.e)$$

where,  $\phi_y$  is the yield curvature of the wall section at the interface between the wall and its foundation. The effective moment of inertia,  $I_e$ , and effective wall cross-sectional area,  $A_e$ , are calculated using  $\alpha$  as a reduction factor as from the gross wall section moment of inertia and area respectively [Paulay (1992), and FEMA 306 (1998)], according to Eq. (4.13.b). The masonry shear modulus,  $G_m$ , is taken as 40% of its Young's modulus,  $E_m$  [Paulay and Priestley (1992)].

The data analysis shows that the experimental push and pull direction yield drifts are very similar with an average push/pull displacement ratio equal to 1.03 (Fig. 4.1). However, the first approach [Eq. (4.13.c)] gives, on average, 10% better prediction of the experimental yield displacement than the second approach predictions [(4.13.d)]. The average ratio between the experimental yield drifts and those predicted by Eq. 4.13.c is 0.92 as shown in Table 2. Equation (4.13.c) tends, on average, to underestimate the experimental drifts while Eq. (4.13.d) overestimates the experimental drifts. Although the difference between the two approaches may seem to be insignificant, Eq. (4.13.c) is used for further assessment in this study. This is because Eq. (4.13.c) is based on curvature analysis (basic mechanics) while Eq. (4.13.d) evaluates an effective moment of inertia empirically (Priestley and Hart 1989). The statistical of the experimental yield drifts also shows

that the shear displacement component (ratio) within the yield drifts is, on average, 0.01%, which can be neglected.

#### **4.4.3 Maximum Strength Limit State**

Two drift values (in the push and pull directions) associated with the maximum lateral strength are obtained for each experimentally tested wall. These drifts are sorted in an ascending order with respect to the push direction to compare with their pull direction counterparts as shown in Fig. 4.2. On average, the drifts in the pull cycle at the maximum strength limit state is higher than the push cycle by approximately 11%. The published predictive models, discussed earlier, are compared to experimental drift in the push and pull directions separately. The comparison reveals that three of the models are underestimating, while one is overestimating, the experimental drifts. The overestimated drift ratios between Carrillo and Alcocer's model (Eq. 4.3) and the experimental results at the maximum strength limit state are 1.33 and 1.24 for the push and pull direction, respectively. Also, for walls with aspect ratio greater than 2.5, Carillo and Alcocer's model (Eq. 4.3) over predicts the experimental  $\Delta_{Q_{max}}/H_w$  by two to tenfold. Ashour and El-Dakhakhni's model (Eq. 4.1), Sanchez's model (Eq. 4.7), and Hidalgo and Jordan's model (Eq. 4.9) are, on average, underestimating the  $\Delta_{Q_{max}}/H_w$  with ratios equal to 0.51, 0.55, and 0.55 with respect to push cycle and 0.47, 0.53, and 0.85 for the pull cycle, respectively. As shown in Fig. 4.3, both Ashour and El-Dakhakhni's model

(Eq. 4.1) and Sanchez's model (Eq. 4.7) consistently underestimate the  $\Delta_{Q_{\max}}/H_w$  for all except for five walls. Hidalgo and Jordan's model (Eq. 4.9) is, on average, close to the experimental results in both directions. However, due to the simplicity of the model, it cannot capture the influence of altering mechanical or geometrical parameters other than the wall length and height (e.g. the vertical bar diameter, spacing, and/or yield strength).

For further model analysis, the box plot [Tukey (1977)] is used. Although box plots can be generated in different forms [Frigge et al. (1989)], a common form is shown in Fig. 4.4, which portrays the data from Fig. 4.3 for the three models. The box plot offers a five-number-summary in a schematic form. The ends of a box mark the first and third quartiles, and the median is indicated with a horizontal line positioned within the box. Depending on the model used, the ranges of most or all of the data in the tails of the distribution are marked using the lines extending away from the box, creating "whiskers" [Emerson and Strenio (1983)]. Based on the experimental result database presented in this study and by using the box-whisker plot, both Ashour and El-Dakhakhni's model (Eq. 4.1) and Sanchez's model (Eq. 4.7) consistently underestimate the displacement at the maximum strength limit state. Although, Hidalgo and Jordan's model (Eq. 4.9) is closer to the experimental results in both loading directions, the model is based on the wall length and height only. This over-simplicity of the model formulation limits its capability to capture the effects of altering the mechanical or geometrical wall parameters on the drift predictions. Comparing the different models using the box plot, one can see that in

case of the push direction is used, Fig. 4.4.a, Ashour and El-Dakhakhni's model (Eq. 4.1) prediction for the  $\Delta_{Q_{max}}/H_w$  has outliers that go as far as reaching 2.5 of the experimental results, whereas the Sanchez's model (Eq. 4.7) outliers are closed and centered around 1.5 of the experimental result. Although, the outliers disappear in Hidalgo and Jordan's model (Eq. 4.9) predictions, the median of the model is located close to approximately 0.5 (of the experimental results). In the pull direction (Fig. 4.4.b) the overall model predictions are enhanced, however, Sanchez's model (Eq. 4.7) experienced more outliers spread.

#### 4.4.4 Ultimate Displacement Limit State (at 20% Strength Degradation)

At the ultimate displacement limit state (defined as 20% strength degradation on the descending branch), the experimental push drifts obtained from the database are sorted in an ascending order along with their corresponding pull cycle counterparts and shown in Fig. 4.5. The  $\Delta_{Q_{80\%}}/H_w$  values range between 0.72% and 4.76%. In the database, only two and four walls exceed 3.0% drift in the push and pull directions, respectively. Contrary to the relation between the drifts associated with push and pull direction at the maximum strength limit state where no pattern can be identified, except for five walls, the  $\Delta_{Q_{80\%}}/H_w$  in the pull direction is consistently higher (11% on average) than the  $\Delta_{Q_{80\%}}/H_w$  in the push direction at the ultimate displacement limit state.

Similar to what was observed at the maximum strength limit state, the ratio between Carrillo and Alcocer's model (Eq. 4.4) drift predictions and the

corresponding experimental ultimate displacement results is, on average, equal to 1.32 and 1.28 for both push and pull direction, respectively. Moreover, the same ratio for the Hidalgo and Jordan's model (Eq. 4.10) is even higher than that of the Carrillo and Alcocer's model (Eq. 4.4) and reaches 1.48 and 1.40 in the push and pull direction, respectively. However, the ratios of the drifts (predicted/experimental) by both the Ashour and El-Dakhakhni's (Eq. 4.2) and the Sanchez's (Eq. 4.8) models are less than 1.00 and are equal to 0.69 and 0.32 in the push direction, and 0.67 and 0.31 in the pull direction, respectively. The coefficient of variance for the predicted/experimental drift ratios for the models by Ashour and El-Dakhakhni (Eq. 4.2), Carrillo and Alcocer (Eq. 4.4), Hidalgo and Jordan (Eq. 4.10), and Sanchez (Eq. 4.8) are 0.74, 1.31, 0.34, and 0.65 in the push direction and 0.77, 1.36, 0.38 and 0.66 in the pull direction, respectively. As the Carrillo and Alcocer's model (Eq. 4.4) holds the highest coefficient of variance, this model will not be included in further assessment. Although Hidalgo and Jordan's model (Eq. 4.10) has the lowest coefficient of variation among the four models, the model overestimate 41 walls from the database. Also, as mentioned earlier, Hidalgo and Jordan's model (Eq. 4.10) has a limited ability to capture all the influence of altering the mechanical and geometrical parameters on  $\Delta_{Q_{80\%}}/H_w$  as shown in Fig. 4.6. It is worth noting that, the Sanchez's model consistently underestimates the  $\Delta_{Q_{80\%}}/H_w$  experimental drift values. Likewise, except for five walls, Ashour and El-Dakhakhni's model (Eq. 4.2) has underestimated all the walls within the database. The box plot at the ultimate displacement limit state is almost the same

for both the push and the pull direction as shown in Fig. 4.7. This study is evaluating behavior/general trend of the different model drift predictions compared to the entire database of experimental results rather than to individual walls drift values per se.

#### **4.4.5 Discussion**

Within the experimental database and using the models available in the literature, the RMSW database model predictions of the four limit states are given in Table 4.2. In general, the drifts associated with the cracking limit state is numerically small and comparisons based on simply evaluating the ratio between the mechanics-based predictions and the experimental results would be misleading. At the yield limit state, there are two different approaches to quantify the yield drift, the curvature analysis-based [first approach] being more realistic. Also, within the range of characteristics of the flexurally-dominated walls considered in the current study, the shear deformation contribution to the yield drifts can be neglected. At both the maximum strength and ultimate displacement limit states, all the aforementioned models fail to accurately reflect the influences of all the geometrical and mechanical parameters in predicting the corresponding experimental drift values. Based on the above discussion, it is a clear that a reliable model to predict either  $\Delta_{Q_{\max}}/H_w$  or  $\Delta_{Q_{80\%}}/H_w$  for RMSWs is needed as will be described in the next section.

#### 4.5 MULTIVARIATE-BASED MODEL DEVELOPMENT

As discussed earlier in this study, the drifts associated with the pull direction were consistently higher than the push drifts at the ultimate displacement limit state. Both the PCA and the PLS are multiple regression techniques that are based on mapping the original multidimensional data into a new set of dimensions that is usually of a lower degree (e.g. from three-dimensional space to a new two-dimensional plane). By lowering the problem dimensions in such a way, the variances of the data in the low-dimensional representations are maximized [Wold et al. 1987]. A representation for a simple case (three variables and two PCs) can be found in Siam et al. [2017]. In addition, it is important to note that applying the PCA and PLS techniques to relate the dependent- to independent wall variables was found to underestimate the dependent wall variable, on average [Siam et al. (2017)]. As such, the proposed model for the ultimate displacement prediction will be developed based on the drifts obtained from the pull direction only, as these drifts have been consistently higher than their push direction counterparts (see Fig. 4.5).

In this respect, the drifts associated with the maximum strength limit state for RMSWs proposed using the PCA and PLS analysis (Siam et al. 2017) are as given in Eqs. (4.14) to (4.18).

$$\frac{\Delta_{Q_{\max}}}{H_w} = \frac{(\Delta_{fl} + \Delta_{sh})}{H_w} \quad (4.14)$$

$$\frac{\Delta_{fl}}{H_w} = \frac{(\Delta_y + \Delta_p)}{H_w} \quad (4.15.a)$$

$$\Delta_{sh} = 0.33\alpha \frac{Q_{\max}}{t_w L_w} \frac{1}{f_y} \frac{\rho_v}{\rho_{sh}} H_w \quad (4.15.b)$$

$$\frac{\Delta_y}{H_w} = \frac{\phi_y H}{3} \quad (4.16)$$

$$\frac{\Delta_p}{H_w} = \phi_p \alpha \beta \left[ 0.47H_w + 0.46L_w - 0.31\alpha\beta H_w - 0.3\alpha\beta \frac{L_w^2}{H_w} - 0.4\alpha\beta L_w \right] \quad (4.17)$$

$$\alpha = \left( 1 - \frac{P}{A_g f'_m} \right) \quad (4.18.a)$$

$$\beta = \left( 1 - \frac{f_y \rho_{sh}}{f'_m} \right) \quad (4.18.b)$$

#### 4.5.1 Principal Component Analysis (PCA)

Principal Component Analysis (PCA) is a technique of identifying patterns in data and expressing the data in such a way to evaluate their similarities and differences. Since patterns in data can be hard to identify in datasets that represented in high dimension, where the graphical representation is not possible (more than three dimensions), PCA presents a powerful tool for data analysis (Maitra and Yan 2008).

The PCA analysis is performed on the 48 RMSWs identified within the experimental database, as *observations*, and the 14 wall characteristics, as *variables*. There are 14 parameters used in the PCA analysis, encompassing both wall mechanical and geometrical characteristics, which are the maximum wall cross

section curvature,  $\phi_m$ , wall height,  $H_w$ , wall length,  $L_w$ , wall cross sectional area,  $A_w$ , wall aspect ratio,  $H_w/L_w$ , vertical bar diameter,  $d_b$ , vertical reinforcement ratio,  $\rho_v$ , horizontal bar diameter,  $d_{sh}$ , horizontal reinforcement ratio,  $\rho_{sh}$ , lateral load at ultimate displacement limit state (i.e. 80% of the maximum load),  $Q_{80\%}$ , vertical bar ultimate strength,  $f_u$ , masonry compressive strength,  $f'_m$ , axial compression load,  $P$ , and the top ultimate lateral drift,  $\Delta_{Q_{80\%}}/H_w$ . Principal Components (PCs) are linear combinations of the 14 parameters and are determined so that the first PC has the maximum variance (among all linear combinations) to account for as much variation in the data as possible. The second PC is the linear combination of variables that accounts for as much of the remaining variation as possible, with the constraint that the first and second PC are orthogonal (i.e. the correlation between the first and second PC is zero).

In the present analysis, the first three PCs explain 30%, 24%, and 16%, respectively, of the total variance. The resulting *score plot* (see Fig. 4.8.a) projects the experimental database drifts on the plane made up by the first and the second PCs. Data points with similar values for the parameters explained by the PC appeared close together, and those with large positive or negative scores are extremes in some parameters. The PCA technique identifies (through clustering) groups of walls that share the same characteristics (such as wall length, axial stress amount) which is consistent with the wall characteristics listed in Table 4.1. Therefore, walls with the same characteristics (variables) were found clustered in

groups on the score plot, thus demonstrating the small variations within these clusters. For example, Walls 37, 38, and 39 locations in the score plot form a group which is expected to have more common variables (wall characteristics) than the group of Walls 2, 5, 6, and 7. The position of a wall in the score plot is determined by the values of the measured parameters. The relation between the original variables and the subspace dimension (PCs) are quantified through *loadings*. The loading plot within the PCA framework indicates the correlation among the variables themselves. Variables found in a similar direction from the PC axis are directly correlated, while those found at opposite sides of the PC axis are inversely correlated. For example, the loading plot in Fig. 4.8.b indicates that  $L_w$  is directly correlated with  $A_w$ ; however, inversely correlated with both  $H_w/L_w$  and  $\Delta_u/H_w$  which is consistent with basic mechanics. The loading plot reveals that the similarities observed between Walls 11, 12, and 13 are attributed to their high  $\rho_v$  and to the fact that they possessed the largest  $d_b$  within the database. Also, this group of wall has the lowest values of both  $f'_m$  (14.8 MPa) and  $\phi_m$  among the walls comprising the database. In addition, by observing the information pertaining to Walls 37, 38, and 39 in both Figures 8.a and 8.b simultaneously, one may infer that these walls are clustered together on the score plot (Fig. 8.a) within the same (second) quadrant. In addition, the variables  $H_w/L_w$  and  $\Delta_{80\%}/H_w$  are also located in the same (second) quadrant in the loading plot (Fig. 8.b). This clustering is because these walls commonly have the largest  $H_w/L_w$  values (which is also

proportional to  $\Delta_{80\%}/H_w$ ). Also within the Walls 37, 38, and 39, Wall 37 deviates from Wall 38 and 39 because Wall 37 experienced the largest  $\Delta_{80\%}/H_w$  value within this group of walls. Finally, the walls located close to the origin of the score plot (e.g. Wall 8), generally have average values (compared to the rest of the walls) of the variables considered in the PCA analysis.

#### 4.5.2 Partial Least Square (PLS) Analysis

The Partial Least Square (PLS) (also termed the *projection to latent structure*) method is a statistical analysis technique that generalizes and combines features from PCA and multiple regression analysis. The goal of the PLS technique is to predict and/or analyze a set of dependent variables ( $\Delta_u/H_w$  in this study) using a set of independent variables (wall parameters in this study). This prediction is achieved by extracting from the input variables a set of orthogonal factors (latent variables) which have the ability to predict the dependent variables [Wold (1966)].

In this study, the PLS analysis is conducted to predict the responses of two *dependent variables*,  $\Delta_{Q_{80\%}}/H_w$  and  $Q_{80\%}$ , based on a PCA for 12 geometrical and mechanical parameters (*independent variables*) for the 48 walls. The model obtained from the PLS analysis has a goodness of fit of 83% ( $R^2Y = 0.83$ ) and goodness of prediction of 68% ( $Q^2Y = 0.68$ ). Figure 4.9 presents the PLS analysis for the dataset and both variables and responses with the first two components. Adding another component to the analysis (increasing the latent space dimensions

by one) accounts for only 2% of the prediction variations and is thus not plotted here. The loading plot (Fig. 4.9.b) shows the inverse correlation between the two responses (ultimate drifts and corresponding lateral loads) which is consistent with basic mechanics. Also, the loading plot shows an overview of the relationships among all variables and responses. The loading plot results are consistent with basic mechanics, where  $\Delta_{Q_{80\%}}/H_w$  is directly correlated to  $H_w, f'_m, \phi_m$ , and  $H_w/L_w$  and inversely correlated to  $L_w, A_w, d_b, \rho_v, \rho_{sh}, f_u$ , and  $P$ . On the other hand,  $Q_{80\%}$  is directly proportioned with  $L_w, A_w, \rho_v, \rho_{sh}, f_u$ , and  $P$  with and inversely proportioned with  $H_w, f'_m, \phi_m$ , and  $H_w/L_w$ .

PLS analysis is also carried out considering only the  $\Delta_{Q_{80\%}}/H_w$  with three

combined variables  $((\phi_m H_w), \alpha \left( \frac{\left( \frac{Q_{80\%} H_w}{L_w} \right) S_v}{f_u L_w d_b^2} \right), \text{ and } \alpha \left( \frac{f'_m S_{sh} t_w}{Q_{80\%} d_{sh}} H_w \right))$  to

quantify the calibration factors ( $a_1, a_2$ , and  $a_3$ ) for the proposed model shown in Eq. (19). A dimensional analysis [Harris and Sabnis (1999)] is performed on the geometrical and mechanical parameters for the wall to introduce the different terms in the proposed model. The first term is defined by  $H_w$  and  $\phi_m$  and accounts for the contribution of  $\Delta_{Q_{max}}/H_w$ . The second term represents the parameters responsible for the flexural resistance such as vertical bar spacing,  $S_v$ , vertical bar diameter,  $d_b$ , and the force developed in the wall cross section by the in-plane moment,

$\left( \frac{Q_{80\%} H_w}{L_w} \right)$ . The third term takes into account the parameters related to the shear resistance such as the horizontal bar spacing,  $S_{sh}$ , and the ultimate latera load,  $Q_{80\%}$ .

$$\Delta_u / H_w = a_1 (\phi_m H_w) + a_2 \alpha \left( \frac{\left( \frac{Q_{80\%} H_w}{L_w} \right) S_v}{f_u L_w d_b^2} \right) + a_3 \alpha \left( \frac{f'_m S_{sh} t_w}{Q_{80\%} d_{sh}} H_w \right) \quad (4.19)$$

The scoring and loading plots for the PLS analysis of the first and second components, shown in Fig. 4.10, depict that all the combined parameters have a positive influence on the ultimate drifts. The model calibration factors are show in Table 4.3. To visualize the results, 20% bar is shaded around the average experimental ultimate drifts as shown in Fig. 4.11. On average, the ratio between the predicted  $\Delta_{Q_{80\%}} / H_w$  and the ultimate displacement obtained from the push direction in the experimental database is 86%

#### 4.6 INFLUENCE OF DIFFERENT WALL DESIGN PARAMETERS ON BACKBONE CURVE

At this stage, the backbone for RMSWs can be identified at each limit state. At the yield limit state, curvature analysis will be used to determine both the drift and the corresponding lateral load. Whereas curvature analysis is also used to evaluate the  $Q_{max}$ , the  $\Delta_{Q_{max}} / H_w$  is calculated using Eq. (14). At the ultimate displacement limit state, the lateral load is  $Q_{80\%}$  and  $\Delta_{Q_{80\%}} / H_w$  can be calculated using Eq. (19).

Further analyses are conducted herein to examine the influence of altering both mechanical and geometrical properties for RMSWs on the backbone curve. Three wall lengths, each with a *default scenario*, will be utilized for the analysis in this section as listed in Table 4.4 which also includes a summary of the selected wall characteristics. The three categories have three different wall lengths (2,400 mm, 3,200 mm, and 4,000 mm). Within the analyses presented in this section, the vertical and horizontal reinforcements yield and ultimate strengths, 400 MPa and 540 MPa, respectively, as well as the wall thickness, 190 mm, are all kept constants.

Figure 4. 12 depicts the influence of altering axial stress ratio and the masonry compressive strength to the backbone curve for wall with 3,200 mm length and an aspect ratio of 2.5. As the axial stress ratio increases from 1.0% to 10.0%, the lateral load capacities, at both the maximum strength and ultimate displacement limit states, increase and the corresponding drifts decrease. However, at the yield limit state, the variation in the drifts can be considered minor compared to the variation in the wall yield strength. Increasing the masonry compressive strength (from 10 MPa to 17 MPa, as the practical code-specified range of strength) would increase the maximum curvature and would thus influence the overall wall strength and drift capacity. Nevertheless, the wall response is more influenced by the axial stress ratio than the masonry compressive strength. For the geometrical parameters, Fig. 4.13 shows the change of backbone curve response due to altering the wall aspect ratio using the mechanical parameter for the default wall scenario (see Table 4.4). While, walls with low aspect ratio tends to have high lateral load capacity with limited

ductility capacity, walls with high aspect ratio have low lateral load capacity but with higher ductility capacity. The model is further utilized to generate RMSW fragility bands associated with each damage state using the same wall scenarios presented herein as will be presented in the next section.

#### 4.7 FRAGILITY BAND DEVELOPMENT

The focus of the Federal Emergency Management Agency (FEMA) document on the seismic performance assessment of buildings (FEMA P-58) is to provide a standardized methodology to determine fragility curves associated with predefined damage states (DSs) that a given building system (and its components) would be expected to experience during a given seismic events, as well as the resulting repair costs. These DSs, and the subsequent repair costs, are linked to different demand parameters (drifts in the current study) through fragility curves, which relate the probability of a component(s) surpassing a specific DS at a specific demand level.

For flexurally-dominated RMSWs, the FEMA P-58 defines different limits for DS throughout the background document: FEMA P-58/BD-3.8.10 (2009). This definition relates three DS (I, II, and III) to drift associated with certain level of lateral forces. On the ascending branch of the backbone curve, *slight damage* (DS-I) is defined when the wall reached 80% of its  $Q_{max}$  on the ascending branch. The *moderate* and *sever damage* states, (DS-II and DS-III, respectively) are defined when wall reaches its  $Q_{max}$  and  $Q_{80\%}$ , respectively as shown in Fig. 4.13. The FEMA P-58 provides that gives a single fragility curve (rather than a band as will be

discussed next) for each DS in a background document (FEMA P-58/DB-3.8.10 2012). A fragility curve can be approximated using a two-parameter lognormal distribution function [Ang and Tang 2007]. In this study, the two lognormal distribution parameters (i.e., location and scale) are estimated using the maximum likelihood method, for each DS. To demonstrate the development of the fragility bands, three different wall lengths (2,400; 3,200; and 4,000 mm) are used with the 14 different aspect ratios listed in the first row of Table 4.4 to result in a total of 42 combinations. For each one of these combinations, each of the remaining parameters listed in Table 4.4 were individually altered while keeping all other parameters the same as their default values (the last column of Table 4.4). This results in a total of 968 different *analytically generated walls*. For each analytically generated wall, the backbone curve is obtained and the three DS are defined. In this study, the conditional fragility curve (for a specific set of wall scenario parameters) for each DS is presented in the form of a *fragility band* encompassing all the possible variation of the mechanical parameter for each DS within a subset of the 968 simulations. This is due to the fact that the controlled varying (by means of generating an analytical wall database) of even one of the wall design parameters leads to a range (band) of fragility curves bounded by the limits of that specific wall design parameter. Nonetheless, it is well understood that the availability of only a small set of limited (in terms of not systematically covering the full range of different design parameters) published experimentally tested wall results, may only

provide for a crude fitting of such experimental results in a single fragility curve, rather than providing a fragility band per se.

Figure 4. 14 shows that changing  $f'_m$  from 10 MPa to 17 MPa has a trivial influence on DS-I, rendering the corresponding fragility band to essentially a single curve. However,  $f'_m$  has a more pronounced influence on the drifts corresponding to DS-II and DS-III where the figure shows that the 80% probability of achieving DS-II corresponds to 1.58% to 2.03% drift *range* and that this range is 3.93% to 5.08% for a DS-III. The fragility bands, as influenced by the axial stress ratio, are depicted in Fig. 4.15. The figure shows that the drifts associated with 80% probability of realizing the three DS range between 0.77% to 1.17%, 1.32% to 2.65, and 4.23% to 5.26% for DS-I, DS-II, and DS-III, respectively. As shown in Fig, 16, the effect of varying  $\rho_{sh}$  on DS-I fragility is trivial. Similarly, at 80% probability of achieving DS-II, the drifts vary within a very close range between 1.81% and 1.91%. This range increases to be from 3.75% to 6.12% for DS-III. Finally, Fig. 4.17 shows that altering  $\rho_v$  results in 80% probability of achieving DS-I, DS-II, and DS-III that correspond to drift ranges from 0.51% to 0.89%, 1.59% to 2.21%, and 3.52% to 5.68%, respectively.

The fragility bands can also provide a more meaningful to express the variability (as it relates to the range of wall design parameters) within the *damageability* of the wall under a specific demand (e.g. drift) level. For example, in case of changing the axial stress ratio (Fig. 4.15) and considering the RMSW

experienced 1.5% lateral drift (see vertical line in Fig. 4.15), FEMA P-58/DB-3.8.10 (2012) fragility curves gives 99%, 93%, and 49% probability for DS-I, DS-II and DS-III, respectively. On the other hand, the fragility bands introduced in this study shows that at 1.5% later drift the probability to experience DS-I, DS-II, and DS-III *range* between 93% to 99%, 29% to 89%, and 6% to 8%, respectively. This example demonstrates that the probability of reaching a specific DS (fragility) should not be considered a unique value for a specific drift level. Instead, the probability should be presented by a range (band) of drifts for any DS.

Based on the results shown in Figs. 14-17, it can be inferred that DS-I is influenced by altering both the axial stress ratio and  $\rho_v$ , rather than altering  $f'_m$  and  $\rho_{sh}$ . Within the mechanical parameter varied in this study, DS-II is more sensitive to the axial stress ratio than other mechanical parameters. Also, the fragility bands show that, with all possible scenarios considered (except for walls with 1.0% compressive axial stress ratio) when a wall reaches a 2.25% drift ratio, there is at least 80% that DS-II is realized. The FEMA P-58/BD-3.8.10 single fragility curves are presented in Figs. 14 to 17 for each DS. Except for changing the bands associated with altering the axial stress ratio, FEMA P-58 fragility curve for DS-I is close to the upper bound of the developed DS-I fragility band. However, the DS-II and DS-III FEAM P-58 fragility curves are consistently associate with higher probabilities and lower drift ratios compared with the developed bands. In addition, FEMA P-58 fragility curve development is based on the experimental results of a limited number of walls (only 44 versus the 968 generated in the current

study), with a very narrow range of wall characteristics (e.g. mostly with  $H_w/L_w = 1.0$ ). This limited number of data points and characteristics range resulted in lower drift limits, for the different DS, within the FEMA P-58, compared to those presented herein

#### 4.8 CONCLUSION

Lessons from recent earthquakes have clearly demonstrated that, generally, code-conforming buildings have survived design-basis events, albeit with, often times, significant and irreparable damage. As such, there has been a growing need for a paradigm shift in term of the way we design and detail structures under different levels of seismic hazard. This has led to the development of PBSD approaches that link the structural performance to seismic risk in terms of monetary and possibly intangible losses associated with structural and nonstructural damages. Subsequently, multiple DSs or *design objective* within PBSD have been developed and linked to different levels of performance objectives. Similar to other SFRSs, the link between different RMSW DSs and performance levels is expressed in terms of lateral drifts based on the wall backbone curve. As such, reliable backbone curve for RMSW is the key for accurate estimation and quantification of different DSs. In this respect, four published backbone models were assessed against the experimental results of 48 flexurally-dominated RMSW. This assessment revealed the need to develop an experimentally calibrated reliable backbone curve, that was developed herein using MVDA. The developed backbone model is further utilized

to create an analytical RMSW database (968 walls) based on a wide range of mechanical and geometrical parameters. Overall, the model shows the ability to capture the alteration of both mechanical and geometrical parameters on the backbone curve and DS as outlined in the FEMA P-58 document. However, as the FEMA P-58 document gives a single curve per each DS because of the limited number of RMSW results (44 walls), the 968 analytically generated wall database was used to develop fragility bands that present a more encompassing and clearer DS picture corresponding to the effects of design variability on wall damageability. In addition, the fragility bands show a significant deviation from the FEMA fragility curves, especially for DS-III where it is recommended to update FEMA fragility curves by including a larger number of walls with a wider range of wall characteristics. Subsequently, this study does not only aim at presenting a technique to develop a reliable backbone curve model for RMSW, but also prospering a new way for visualizing corresponding fragility/damageability for RMSW PBSD codification and seismic risk assessment.

#### **4.9 ACKNOWLEDGMENT**

Financial support has been provided through a Post Graduate Industrial Scholarship funded jointly by the Natural Sciences and Engineering Research Council (NSERC) of Canada and the Canada Masonry Design Centre (CMDC). Additional support has been provided through the McMaster University Institute for Multi-Hazard Systemic Risk Studies (INTERFACE).

#### 4.10 NOTATION

- $A_e$  = Effective cross sectional area of the wall ( $\text{mm}^2$ )
- $A_g$  = Gross cross sectional area of the wall ( $\text{mm}^2$ )
- $CV$  = Coefficient of variance
- $d_b$  = Diameter of flexural (vertical) reinforcement (mm)
- $E_m$  = Masonry young's modules
- $f'_m$  = Masonry Compressive strength (MPa)
- $f_u$  = Ultimate strength for reinforcement steel bars (MPa)
- $f_y$  = Yield strength for reinforcement steel bars (MPa)
- $G_m$  = Masonry shear modules
- $H_w$  = Wall height (mm)
- $I_e$  = Effective moment of inertia
- $L_p$  = Equivalent plastic hinge length (mm)
- $L_w$  = Wall length (mm)
- $P$  = Axial compressive load (kN)
- $Q_{crack}$  = Cracking lateral load
- $Q_{max}$  = Maximum lateral load
- $Q_{80\%}$  = Ultimate lateral load (80% of  $Q_{max}$ )
- $Q_y$  = Yield lateral load
- $Q^2$  = Predictive ability or goodness of prediction of parameters
- $R^2X$  = Goodness of fit to X data

$R^2Y$  = Goodness of fit to Y data

$t_w$  = Wall thickness (mm)

$\alpha = \left(1 - \frac{P}{A_g f'_m}\right)$  Axial load effect

$\beta = \left(1 - \frac{f_y \rho_{sh}}{f'_m}\right)$  Amount of shear reinforcement.

$\Delta_{crack}$  = Cracking lateral displacement (mm)

$\Delta_{fl}$  = Flexural displacement (mm)

$\Delta_p$  = Plastic displacement (mm)

$\Delta_{sh}$  = Shear displacement (mm)

$\Delta_{Qmax}$  = Maximum lateral displacement (mm)

$\Delta_{Q80\%}$  = maximum lateral displacement for shear wall (mm)

$\Delta_y$  = Yield lateral displacement for shear wall (mm)

$\Delta_{y\_flex}$  = Flexural component of yield lateral for shear wall (mm)

$\Delta_{y\_sh}$  = Shear component of yield lateral for shear wall (mm)

$\rho_{sh}$  = Horizontal reinforcement ratio

$\rho_v$  = Vertical reinforcement ratio

$\phi_p$  = Plastic curvature of the wall section (1/mm)

$\phi_y$  = Yield curvature of the wall section (1/mm)

$\phi_m$  = Maximum curvature of the wall section (1/mm)

#### **4.11 REFERENCES**

- Ahmadi F, Hernandez J, Sherman J, Kapoi C, Klingner RE, McLean DI. Seismic performance of cantilever-reinforced concrete masonry shear walls. *Journal of Structural Engineering*. 2014 Apr 10;140(9):04014051.
- Tang WH, Ang A. *Probability Concepts in Engineering: Emphasis on Applications to Civil & Environmental Engineering*. Wiley; 2007.
- American Society of Civil Engineers. *Seismic rehabilitation of existing buildings*. ASCE Publications; 2007.
- Ashour A, El-Dakhkhni W. Influence of floor diaphragm–wall coupling on the system-level seismic performance of an asymmetrical reinforced concrete block building. *Journal of Structural Engineering*. 2016 Apr 26;142(10):04016071.
- Bertero RD, Bertero VV. Performance- based seismic engineering: the need for a reliable conceptual comprehensive approach. *Earthquake Engineering & Structural Dynamics*. 2002 Mar 1;31(3):627-52.
- Bracci JM, Kunnath SK, Reinhorn AM. Seismic performance and retrofit evaluation of reinforced concrete structures. *Journal of Structural Engineering*. 1997 Jan;123(1):3-10.
- Cardone D, Dolce M, Palermo G. Force-based vs. direct displacement-based design of buildings with seismic isolation. In *The 14th World Conference on Earthquake Engineering* 2008 Oct.
- Carrillo J, Alcocer SM. Backbone model for performance-based seismic design of RC walls for low-rise housing. *Earthquake Spectra*. 2012 Aug;28(3):943-64.

- Cornell CA. Calculating building seismic performance reliability: a basis for multi-level design norms. In Proceedings of the 11th world conference on earthquake engineering 1996 Jun (Vol. 10, pp. 5707-5712).
- Cornell CA, Krawinkler H. Progress and challenges in seismic performance assessment. PEER Center News. 2000 Apr;3(2):1-3.
- Emerson JD, Strenio J. Boxplots and batch comparison. Understanding robust and exploratory data analysis. 1983;58.
- Fajfar P, Krawinkler H. Performance-based seismic design concepts and implementation. In Proceedings of the International Workshop, Bled, Slovenia 2004 Jun 28 (Vol. 28, pp. 2004-05).
- FEMA 306. Evaluation of Earthquake Damaged Concrete and Masonry Wall Buildings. Applied Technology Council, Washington, DC, 1998.
- FEMA-445, Next-generation performance-based seismic design guidelines-program plan for new and existing building. Applied Technology Council, Washington, DC, 2006.
- FEMA P-58. Seismic Performance Assessment of Buildings. Applied Technology Council, Washington, D.C, 2012.
- FEMA P-58/BD-3.8.10. Damage State and Fragility Curves for Reinforced Masonry Shear Walls. FEMA P-58/BD-3.8.10, Applied Technology Council, Washington, DC, 2009.
- Frigge M, Hoaglin DC, Iglewicz B. Some implementations of the boxplot. The American Statistician. 1989 Feb 1;43(1):50-4.

- Gérin M, Adebar P. Accounting for shear in seismic analysis of concrete structure, 13th World Conf. on Earthquake Eng. Vancouver, CD Rom Paper. 2004(939):15.
- Ghobarah A. Performance-based design in earthquake engineering: state of development. *Engineering structures*. 2001 Aug 31;23(8):878-84.
- Habasaki A, Kitada Y, Nishikawa T, Takiguchi K, Torita H. Multi-Directional Loading Test for R/C Seismic Shear Walls. In CD-ROM Proc. of 12th World Conference on Earthquake Engineering (12WCEE) 2000.
- Harris HG, Sabnis G. *Structural modeling and experimental techniques*. CRC press; 1999 Mar 30.
- Hernandez, J. F. *Quasi-Static Testing of Cantilever Masonry Shear Wall Segments*. [dissertation], University of Texas, 2012.
- Hidalgo PA, Jordan RM. Strength and energy dissipation characteristics of reinforced concrete walls under shear failure. In *Proceedings of the Eleventh World Conference on Earthquake Engineering, Acapulco, Mexico 1996*.
- Kapoi, C. M. *Experimental Performance of Concrete Masonry Shear Walls Under In-Plane Loading*. [dissertation], Washington State University, 2012.
- Mackie KR, Stojadinović B. Performance- based seismic bridge design for damage and loss limit states. *Earthquake Engineering & Structural Dynamics*. 2007 Oct 25;36(13):1953-71.

- Maitra S, Yan J. Principle component analysis and partial least squares: Two-dimension reduction techniques for regression. *Applying Multivariate Statistical Models*. 2008 Jun 15;79.
- Masonry Standards Joint Committee. Building code requirements and specification for masonry structures. ACI 530-13/ASCE 5-13/TMS 402-13, American Concrete Institute, the American Society of Civil Engineers and the Masonry Society Portland, United States: Ringgold Inc. Retrieved from <http://search.proquest.com.ezproxy.library.dal.ca/docview/894457499>; 2013.
- Park R. A static force-based procedure for the seismic assessment of existing reinforced concrete moment resisting frames. *Bulletin of the New Zealand National Society for Earthquake Engineering*. 1997 Sep;30(3):213-26.
- Paulay T., and Priestly, M. *Seismic design of reinforced concrete and masonry buildings*. Wiley, New York 1992.
- Porter KA, Kiremidjian AS. *Assembly-based vulnerability of buildings and its uses in seismic performance evaluation and risk-management decision-making*. SPA Risk LLC; 2000.
- Priestley MJ, Hart GC. *Design recommendations for the period of vibration of masonry wall buildings*. University of California, San Diego and Los Angeles. Calif. Research Report SSRP 89/05; 1989.
- Priestley MJ. Performance based seismic design. *Bulletin of the New Zealand society for earthquake engineering*. 2000 Jan 31;33(3):325-46.

- Riahi Z, Elwood KJ, Alcocer SM. Backbone model for confined masonry walls for performance-based seismic design. *Journal of Structural Engineering*. 2009 Feb 25;135(6):644-54.
- Sánchez, A. Seismic behavior of housing with concrete walls. Technical Report, Institute of Engineering, National University of Mexico, UNAM, 2010.
- Shedid MT, Drysdale RG, El-Dakhakhni WW. Behavior of fully grouted reinforced concrete masonry shear walls failing in flexure: Experimental results. *Journal of structural engineering*. 2008 Nov;134(11):1754-67.
- Sherman, J. D. Effects of Key Parameters on The Performance of Concrete Masonry Shear Walls Under In-Plane Loading. [dissertation], Washington State University. 2011.
- Shing PB, Schuller M, Hoskere VS. In-plane resistance of reinforced masonry shear walls. *Journal of structural Engineering*. 1990 Mar;116(3):619-40.
- Shinozuka M, Feng MQ, Lee J, Naganuma T. Statistical analysis of fragility curves. *Journal of engineering mechanics*. 2000 Dec;126(12):1224-31.
- Siam AS, Hussein WM, El-Dakhakhni WW. Scoring models for reinforced masonry shear wall maximum displacement prediction under seismic loads. *Engineering Structures*. 2017 Apr 1; 136:511-22.
- Siyam MA, El-Dakhakhni WW, Shedid MT, Drysdale RG. Seismic response evaluation of ductile reinforced concrete block structural walls. I: Experimental results and force-based design parameters. *Journal of Performance of Constructed Facilities*. 2015 Jul 29;30(4):04015066.

- Tang TO, Su RK. Shear and flexural stiffnesses of reinforced concrete shear walls subjected to cyclic loading. *The Open Construction & Building Technology Journal*. 2014.
- Tukey JW. *Exploratory data analysis*. Addison-Wesley Series in Behavioral Science: Quantitative Methods, Reading, Mass.: Addison-Wesley, 1977. 1977.
- Wallace JW. Modelling issues for tall reinforced concrete core wall buildings. *The structural design of tall and special buildings*. 2007 Dec 15;16(5):615-32.
- Watanabe G, Kawashima K. An evaluation of the force reduction factor in the force-based seismic design. *NIST special publication SP*. 2002:201-18.
- Wold H. Estimation of principal components and related models by iterative least squares. *Multivariate analysis*. 1966;1:391-420.
- Wold S, Esbensen K, Geladi P. Principal component analysis. *Chemometrics and intelligent laboratory systems*. 1987 Aug 1;2(1-3):37-52.
- Voon KC, Ingham JM. Experimental in-plane shear strength investigation of reinforced concrete masonry walls. *Journal of structural engineering*. 2006 Mar;132(3):400-8.

Table 4.1: The experimental RMSW database

Wall ID	$L_w$ mm	$t_w$ mm	$H_w$ mm	$H_w/L_w$	$\rho_v$ %	$d_b$ mm	$\rho_{sh}$ %	$s_{sh}$ mm	$d_{sh}$ mm	$f_u$ MPa	$f_m$ MPa	$P$ kN	Reference
1	1830	143	1830	1.0	0.38	15.9	0.24	366	12.7	710	19.99	361.1	Shing et al. (1989)
2	1830	143	1830	1.0	0.38	15.9	0.24	366	9.5	710	19.99	487.5	
3	1830	143	1830	1.0	0.38	15.9	0.14	366	9.5	710	22.06	180.5	
4	1830	143	1830	1.0	0.38	15.9	0.24	366	12.7	710	22.06	180.5	
5	1830	143	1830	1.0	0.54	19.1	0.24	366	12.7	738	22.75	180.5	
6	1800	140	1800	1.0	0.62	20.0	0.05	360	6	365.7	17.6	11.3	Voon and Ingham (2006)
7	1800	140	1800	1.0	0.62	20.0	0.14	360	11.3	365.7	17	11.3	
8	1800	190	3600	2.0	0.29	16	0.08	600	9.5	577.3	14.8	30.8	Shedid et al. (2008)
9	1800	190	3600	2.0	0.78	20	0.13	400	9.5	577.3	14.8	30.8	
10	1800	190	3600	2.0	0.73	25	0.13	400	9.5	577.3	14.8	30.8	
11	1800	190	3600	2.0	1.31	25	0.26	200	9.5	577.3	14.8	30.8	
12	1800	190	3600	2.0	1.31	25	0.26	200	9.5	577.3	14.8	260.0	
13	1800	190	3600	2.0	1.31	25	0.26	200	9.5	718	14.8	520.0	
14	1016	190	2032	2.0	0.33	12.7	0.312	200	12.7	517.5	20.95	10.5	Kapoi (2012)
15	1016	190	2032	2.0	0.33	12.7	0.312	200	12.7	523.25	20.95	270.3	
16	1016	190	2032	2.0	0.59	22.2	0.312	200	12.7	523.25	15.71	202.7	
17	1829	190	1422	0.78	0.55	22.2	0.625	200	12.7	523.25	15.71	364.9	
18	1829	190	1829	1.0	0.55	22.2	0.625	200	12.7	523.25	15.71	364.9	
19	1422	190	2845	2.0	0.72	19.1	0.156	400	12.7	534.75	15.71	20.6	
20	1422	190	2845	2.0	0.87	19.1	0.344	200	9.5	534.75	15.71	20.6	
21	1422	190	2845	2.0	0.87	19.1	0.344	200	9.5	535	15.71	283.8	
22	1007	190	2013	2.0	0.69	19.1	0.312	200	12.7	522.05	19.1	244.3	Sherman (2011)
23	1007	190	2013	2.0	0.69	19.1	0.312	200	12.7	513.32	19.1	244.3	
24	1007	190	2013	2.0	0.31	12.7	0.312	200	12.7	522.05	21.0	536.2	
25	1007	190	2013	2.0	0.31	12.7	0.312	200	12.7	518.08	21.0	536.2	
26	1819	190	1819	1.0	0.31	12.7	0.104	600	12.7	518.08	21.0	16.8	
27	1819	190	1819	1.0	0.31	12.7	0.312	200	12.7	518.08	21.0	484.6	
28	1819	190	1413	0.78	0.31	12.7	0.312	200	12.7	518.08	21.0	13.1	
29	1819	190	1413	0.78	0.31	12.7	0.625	200	12.7	518	21.0	484.6	
30	1020	190	2030	2.0	0.69	19.1	0.313	203	12.7	524.4	19	245.9	Ahmadi et al. (2014)
31	1020	190	2030	2.0	0.69	19.1	0.313	203	12.7	512.9	21	271.8	
32	1830	190	1830	1.0	0.31	12.7	0.104	609	12.7	517.5	21	17.0	
33	1830	190	1830	1.0	0.31	12.7	0.313	203	12.7	517.5	21	487.6	
34	1220	190	3660	3.0	0.69	19.1	0.157	406	12.7	484.15	31	383.9	

Table 1 (continued): The experimental RMSW database

Wall ID	$L_w$ mm	$t_w$ mm	$H_w$ mm	$H_w/L_w$	$\rho_v$ %	$d_b$ mm	$\rho_{sh}$ %	$s_{sh}$ mm	$d_{sh}$ mm	$f_u$ MPa	$f_m$ MPa	$P$ kN	Reference	
35	1220	190	3660	3.0	0.31	12.7	0.157	406	12.7	515.2	23	569.6	Ahmadi et al. (2014)	
36	1220	190	3660	3.0	0.69	19.1	0.157	406	12.7	484.15	23	569.6		
37	810	190	3660	4.52	0.69	19.1	0.313	203	12.7	484.15	29	238.4		
38	810	190	3660	4.52	0.69	19.1	0.157	406	12.7	484.15	23	378.2		
39	810	190	3660	4.52	0.31	12.7	0.157	406	12.7	515.2	23	567.3		
40	1020	190	2030	2.0	0.31	12.7	0.313	203	12.7	517.5	21	10.5		
41	1020	190	2030	2.0	0.31	12.7	0.313	203	12.7	523.25	21	271.8		
42	1830	190	1420	0.78	0.47	22.22	0.626	203	12.7	523.25	16	371.5		
43	1830	190	1830	1.0	0.47	22.22	0.626	203	12.7	523.25	16	371.5		
44	1420	190	2840	2.0	0.69	19.1	0.157	406	12.7	534.75	16	20.5		
45	2440	190	2440	1.0	0.31	12.7	0.313	203	12.7	486.45	31	30.2		
46	2440	190	2440	1.0	0.16	12.7	0.157	406	12.7	486.45	28	30.2		
47	2440	190	2440	1.0	0.33	12.7	0.33	200	12.7	680.65	29	4.8		Hernandez (2012)
48	2440	190	2440	1.0	0.33	12.7	0.16	406	12.7	680.65	24.3	4.8		

Table 4.2: Average ratio between model predictions and experimental drifts

	Direction	$\Delta_v/H_w$ (%)		$\Delta_{Omax}/H_w$ (%)		$\Delta_{O80\%}/H_w$ (%)	
		Average	CV (%)	average	CV (%)	average	CV (%)
Basic Mechanics	Push	0.92	56	-	-	-	-
	Pull	0.95	54	-	-	-	-
Ashour and El-Dakhakhni (2016)	Push	-	-	0.51	86	0.69	72
	Pull	-	-	0.47	78	0.67	76
Carrillo and Alcocer (2012)	Push	-	-	1.36	111	1.32	131
	Pull	-	-	1.28	130	1.28	136
Hidalgo and Jordan (2012)	Push	-	-	0.90	44	1.48	34
	Pull	-	-	0.85	43	1.40	38
Sanchez (2010)	Push	-	-	0.55	67	0.32	64
	Pull	-	-	0.53	70	0.31	66

Table 4.3: Proposed model calibration coefficient

Coefficient	Value
$a_1$	0.192
$a_2$	0.020
$a_3$	$2.28 \times 10^{-6}$

Table 4.4: Design parameters and default scenario for the analytical wall database

Parameter	Units	Range	Default
$H_w / L_w$	---	1.00, 1.25, 1.50, 1.675, 1.875, 2.00, 2.25, 2.35, 2.50, 2.8125, 3.00, 3.25, 3.5, and 3.75	2.00
$d_b$	mm	10M (11.5mm), 15M (16mm), 20M (19.5mm), and 25M (25.2mm)	15M
$d_{b_{sh}}$	mm	10M (11.5mm), and 15M (16mm)	10M
$s_v$	mm	200, 400, 600, and 800	400
$s_{sh}$	mm	200, 400, 600, 800, and 1200	400
$f'_m$	MPa	10, 13.5, and 17	13.5
$P / (A_g f'_m)$	%	0, 2.5, 5.0, 7.5, and 10	5

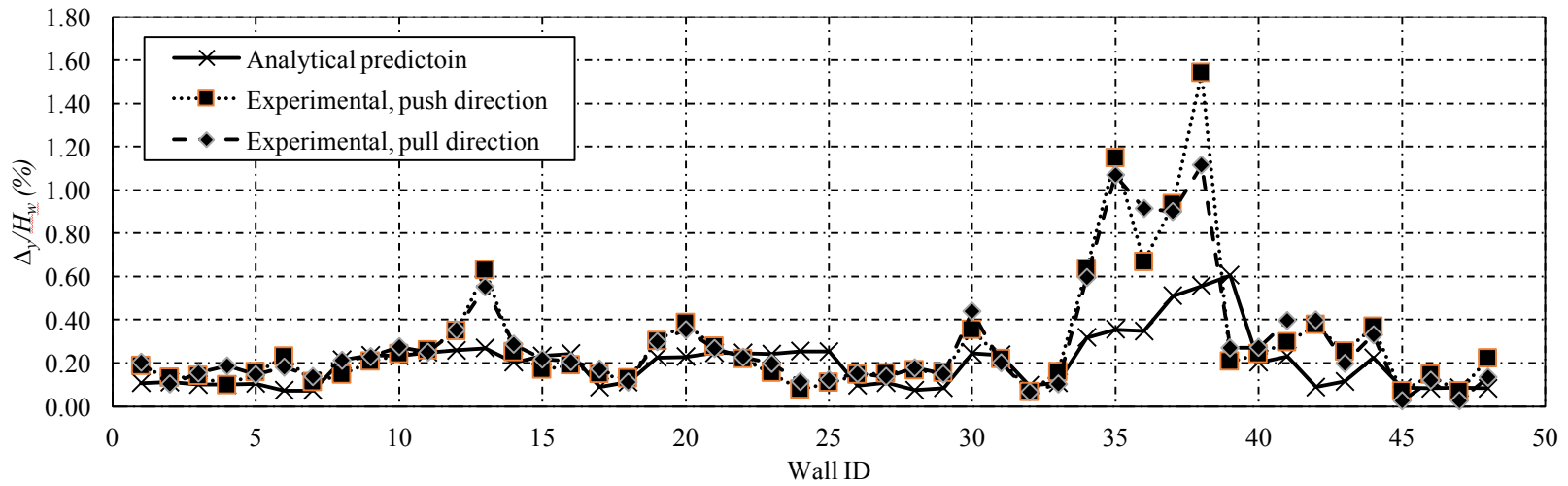


Figure 4.1: Experimental versus analytical predictions of drifts at the yield limit state.

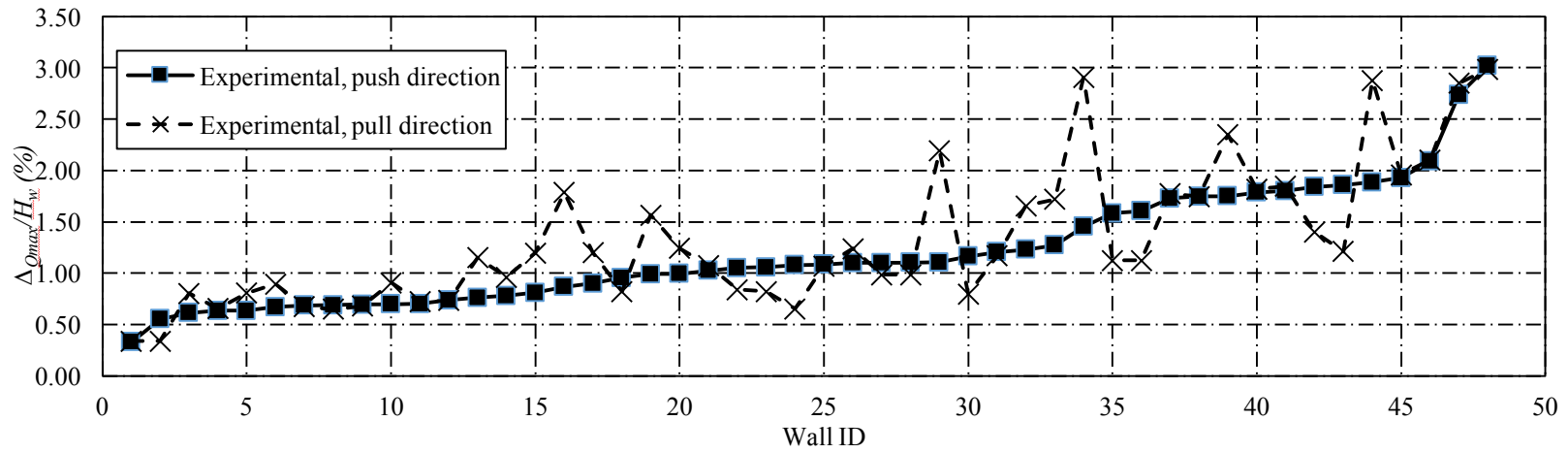


Figure 4.2: Push and pull experimental drifts at the maximum strength limit state.

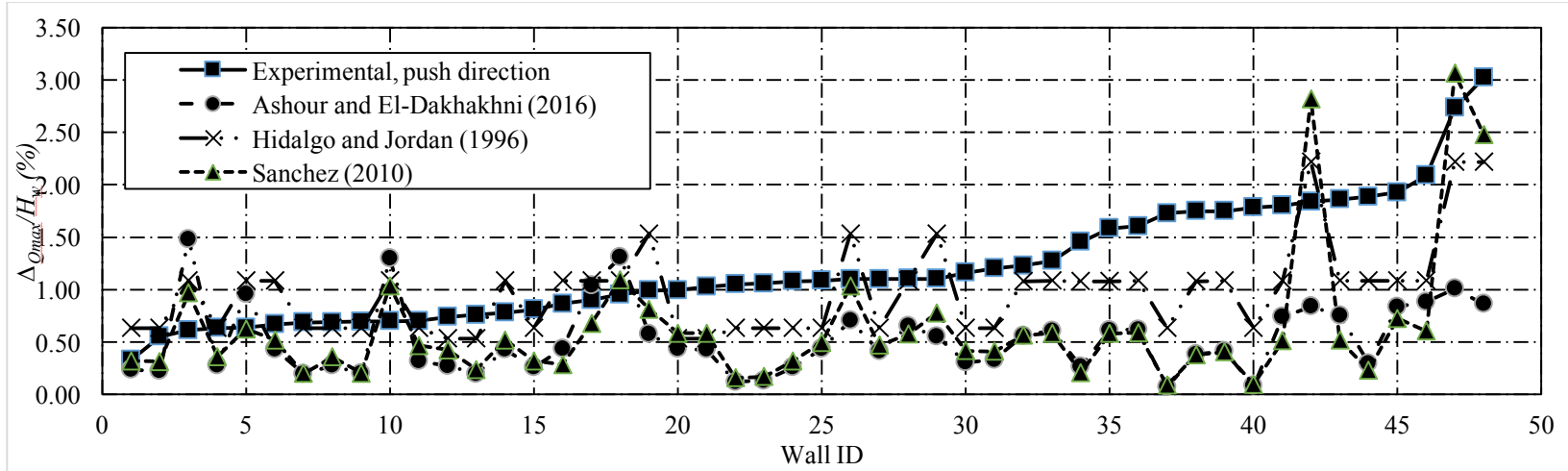


Figure 4.3: Experimental versus analytical predictions of drifts at the maximum strength limit state.

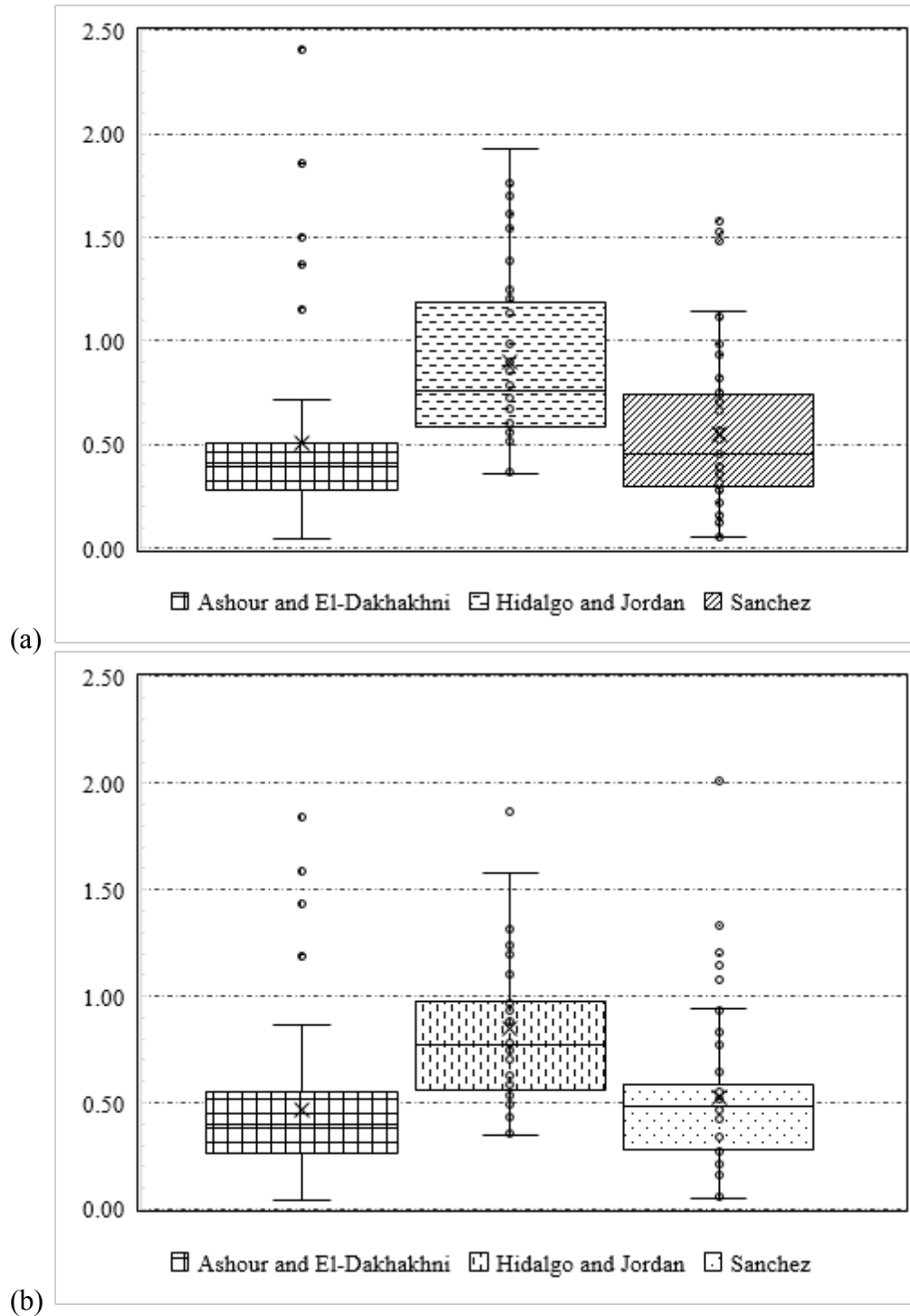


Figure 4.4: Model prediction evaluation at the maximum strength limit state: (a) push direction; and (b) pull direction.

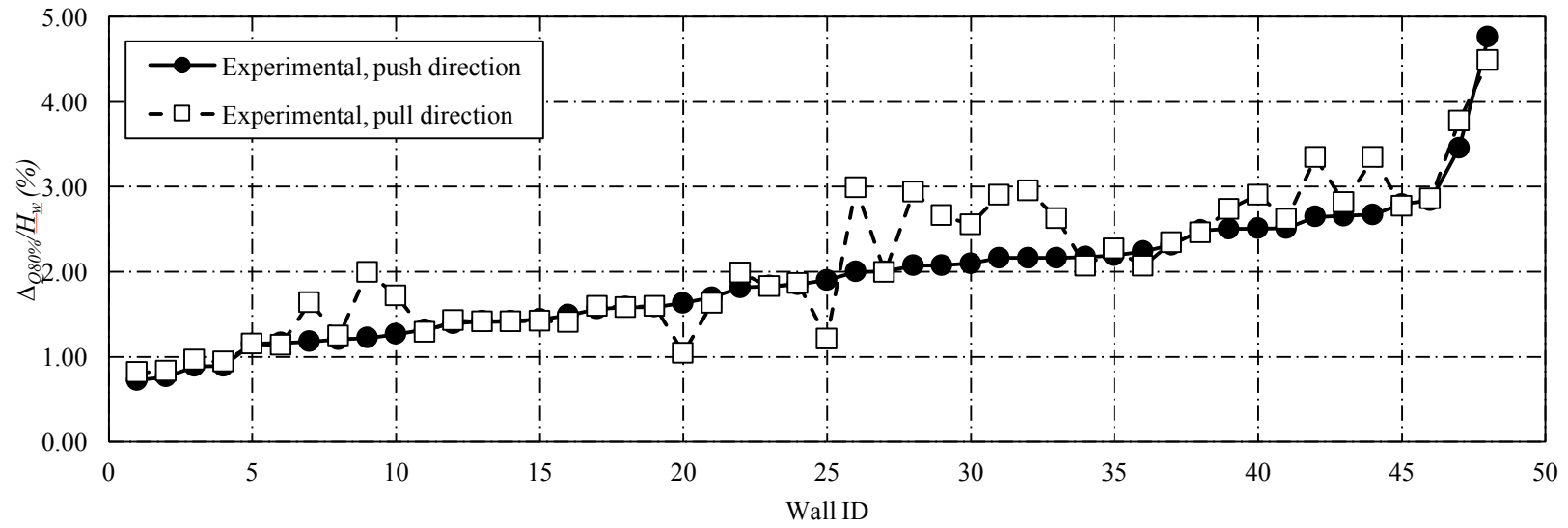


Figure 4.5: Push and pull experimental drifts at the ultimate displacement limit state.

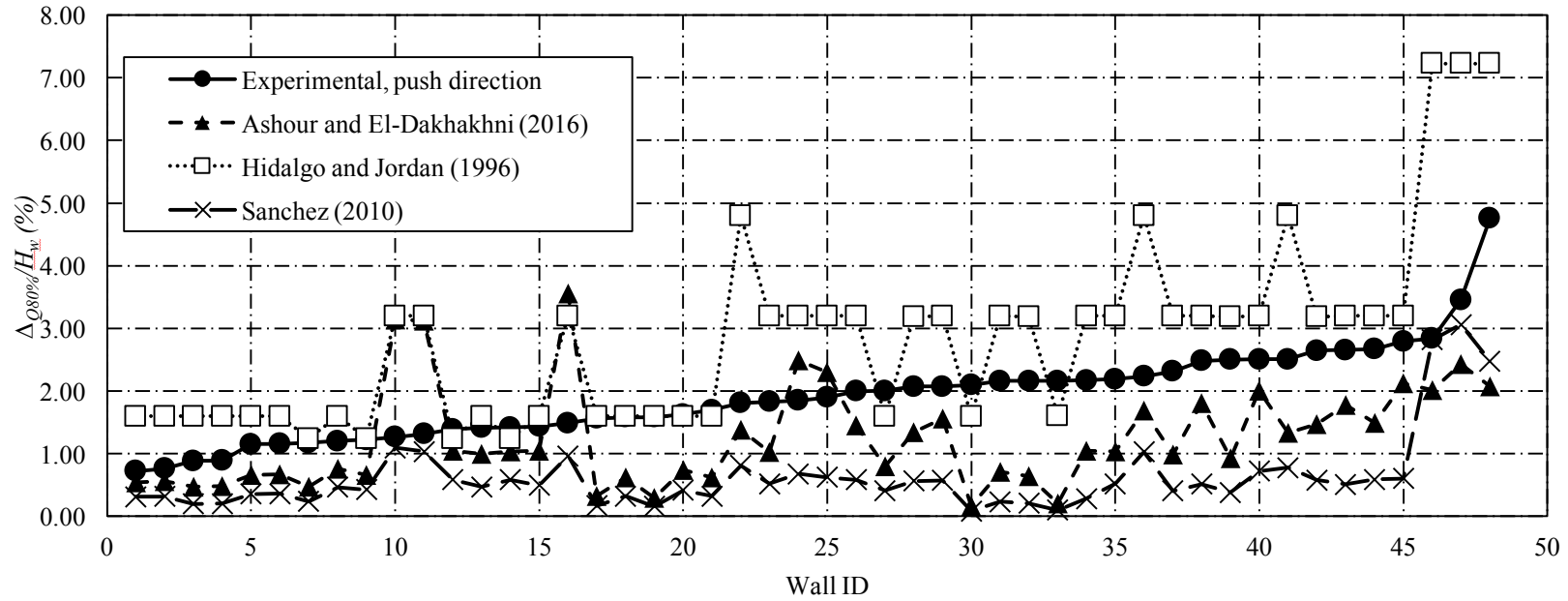
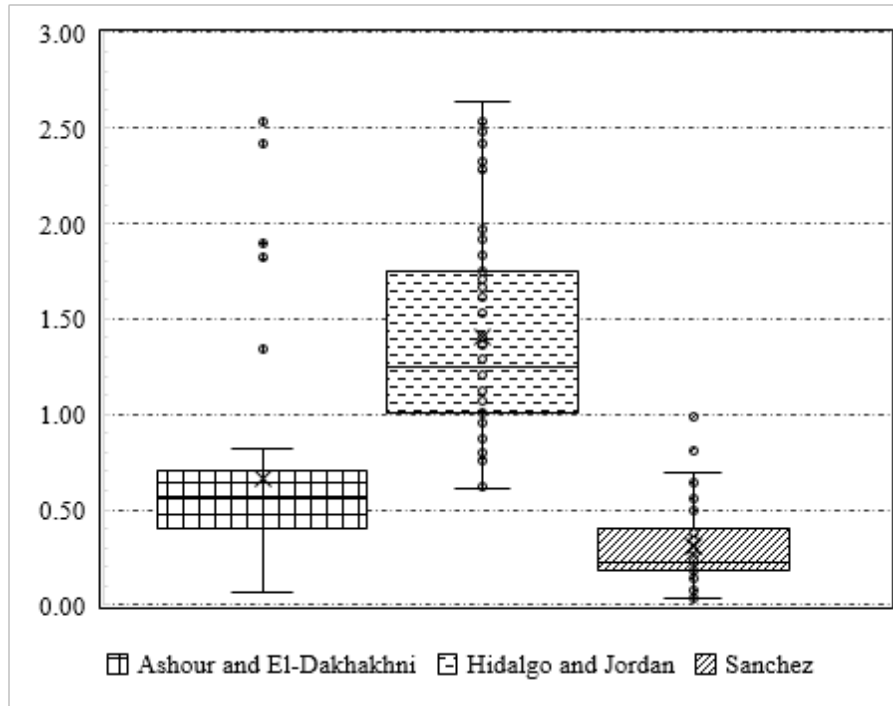
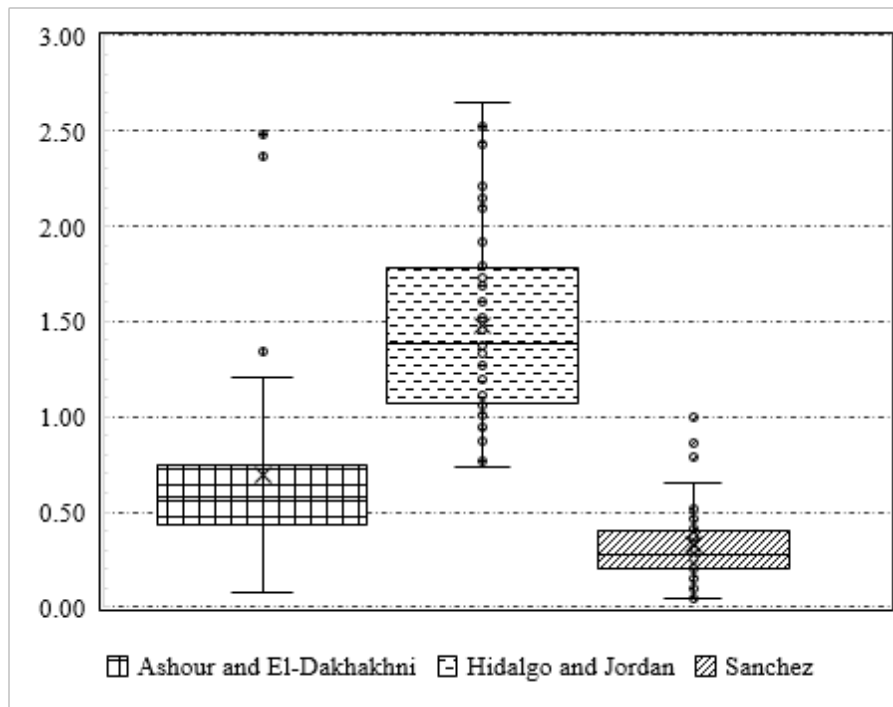


Figure 4.6: Experimental versus analytical predictions of drifts at the ultimate displacement limit state.

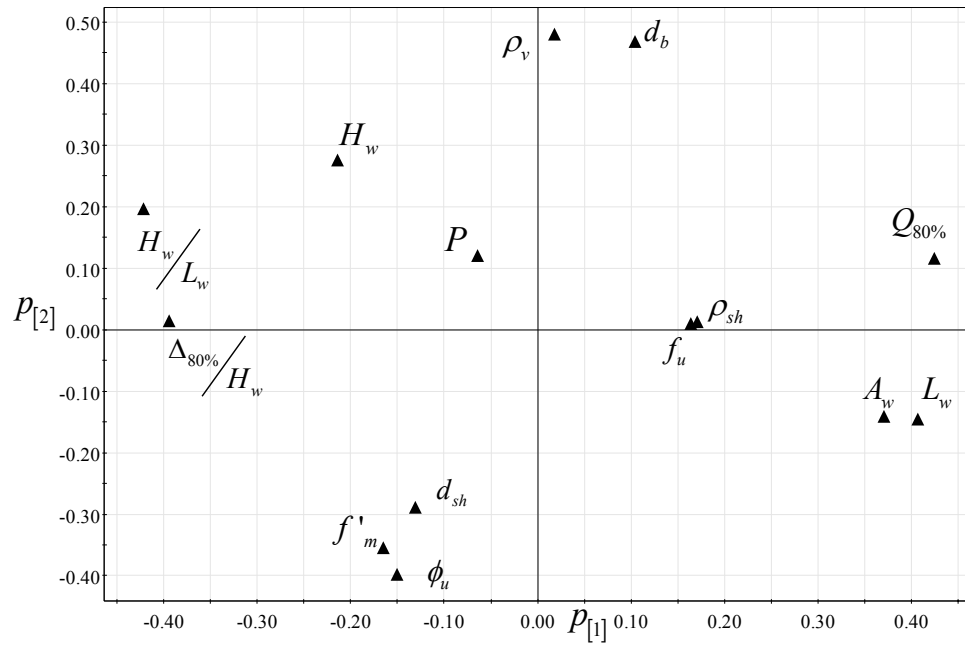


(a)

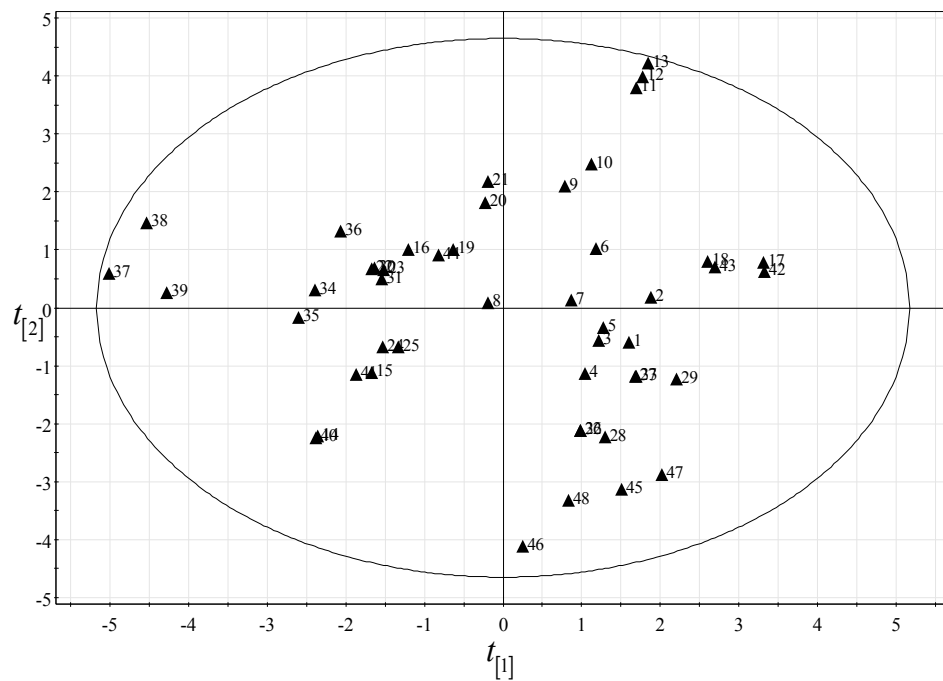


(b)

Figure 4.7: Model prediction evaluation at the ultimate displacement limit state: (a) push direction; and (b) pull direction.



(a)



(b)

Figure 4.8: (a) Score plot for all database (b) Loading plot for all variables

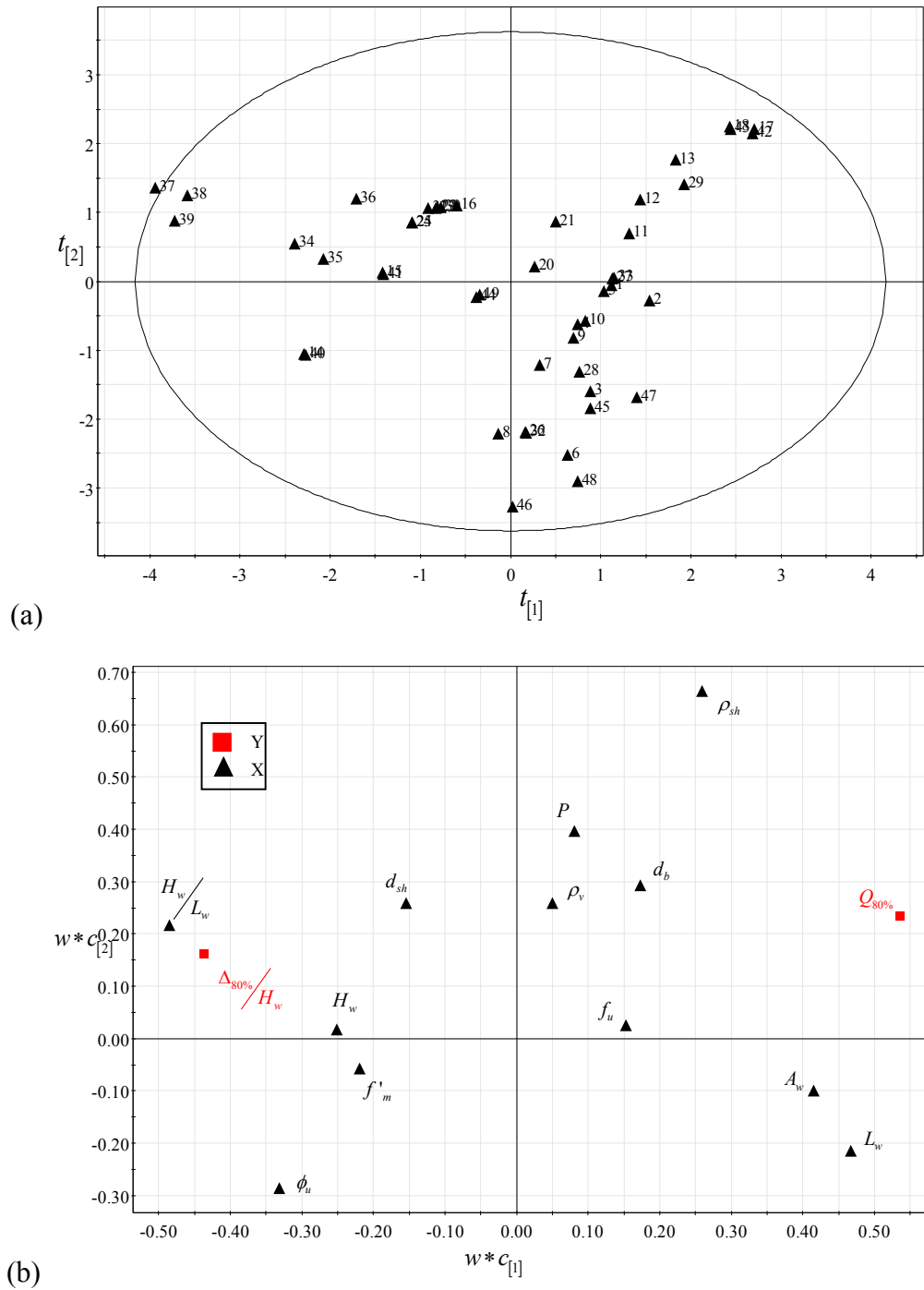


Figure 4.9: PLS, (a)score plot. (b) loading plot

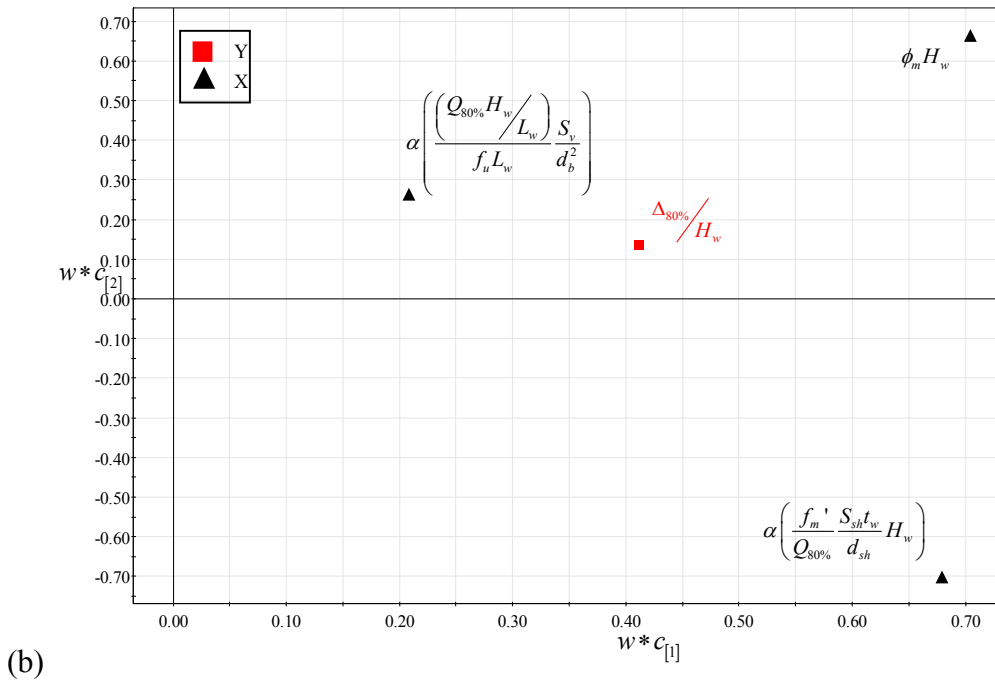
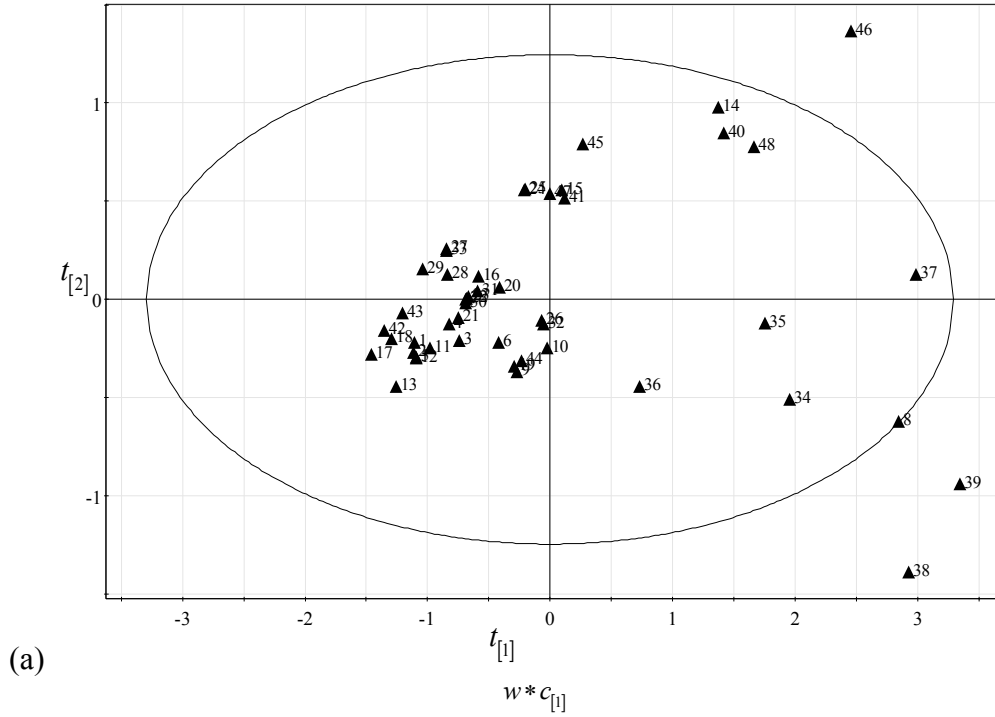


Figure 4.10: (a) Score plot and (b) loading plot for the proposed model.

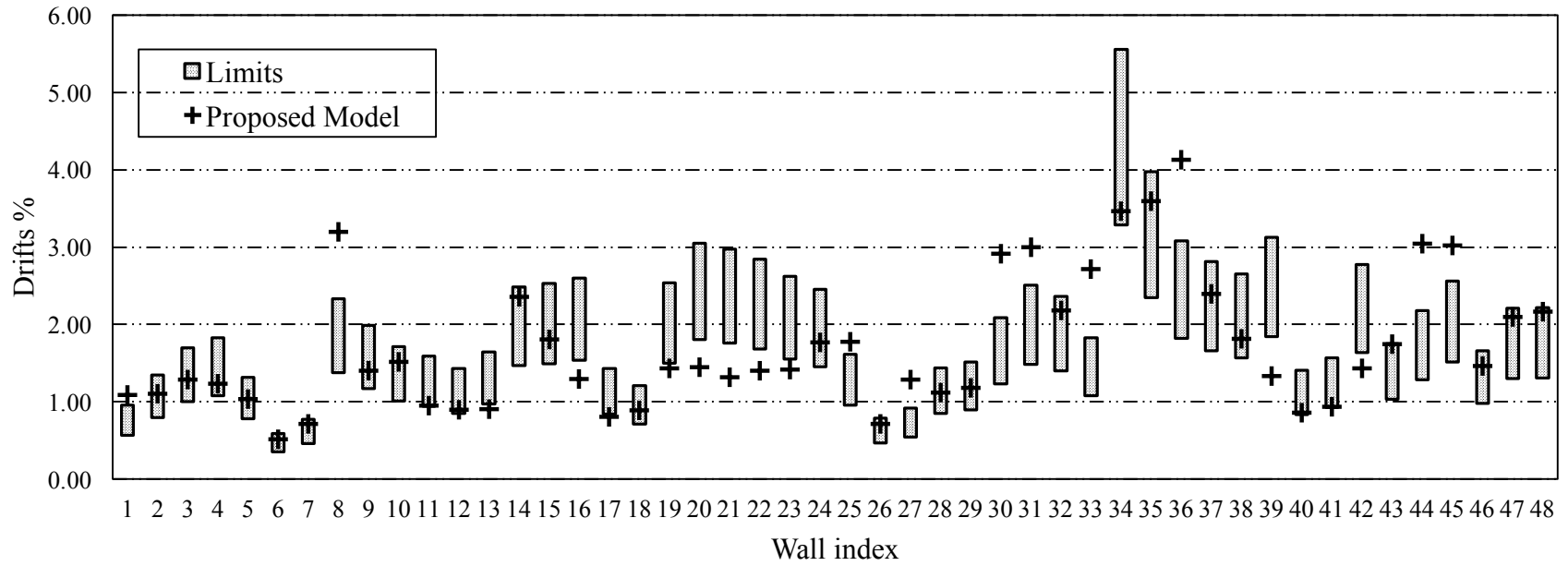


Figure 4.11: Proposed model drifts compare to experimental data limits.

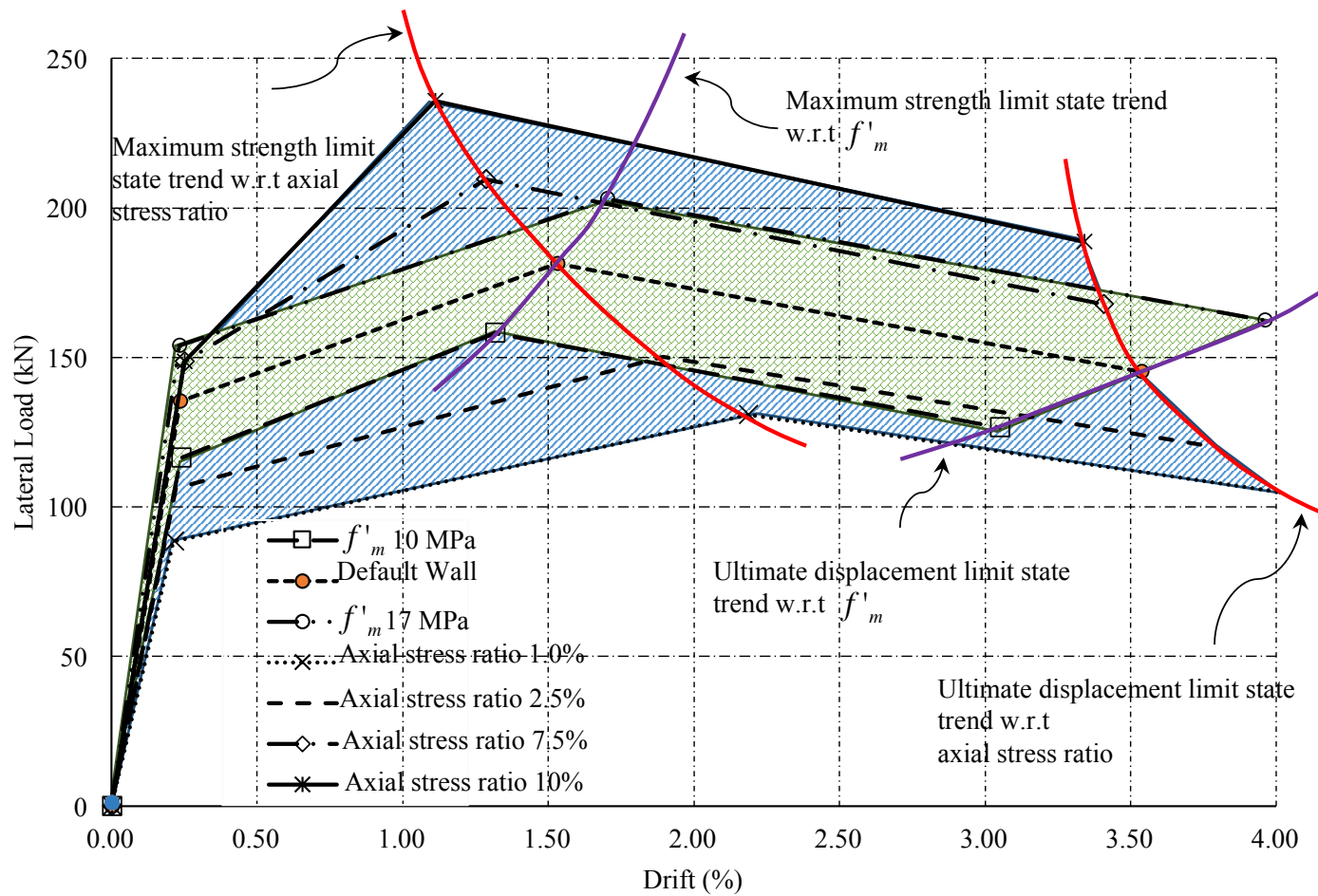


Figure 4.12: Influence of changing the axial stress ratio and masonry compressive strength on wall backbone curves.

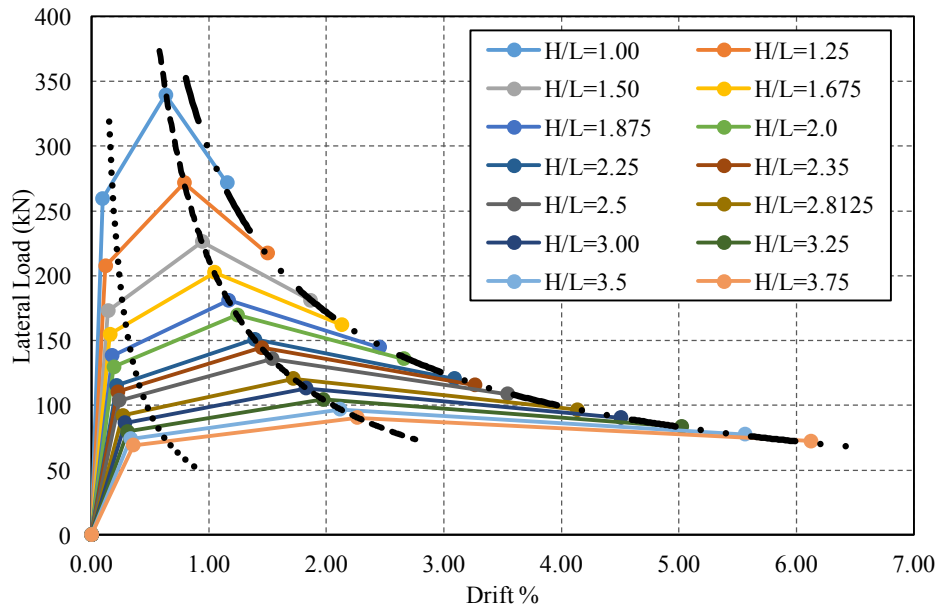


Figure 4.13: Backbone curves and DS variation for different wall aspect ratio.  
(L=2,400 mm, default scenario).

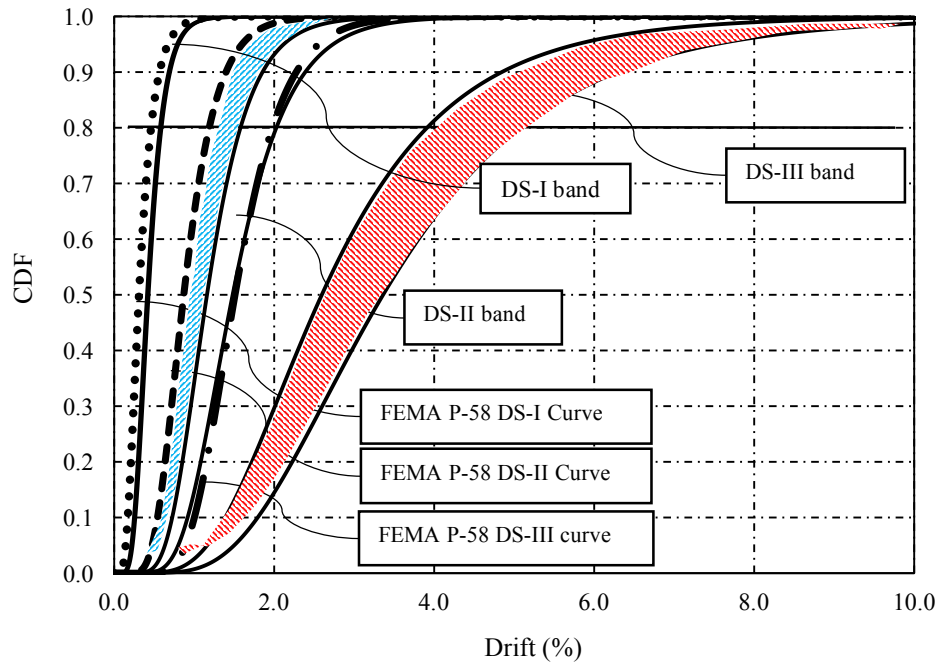


Figure 4.14: Effect of  $f'_m$  variability on the fragility curves.

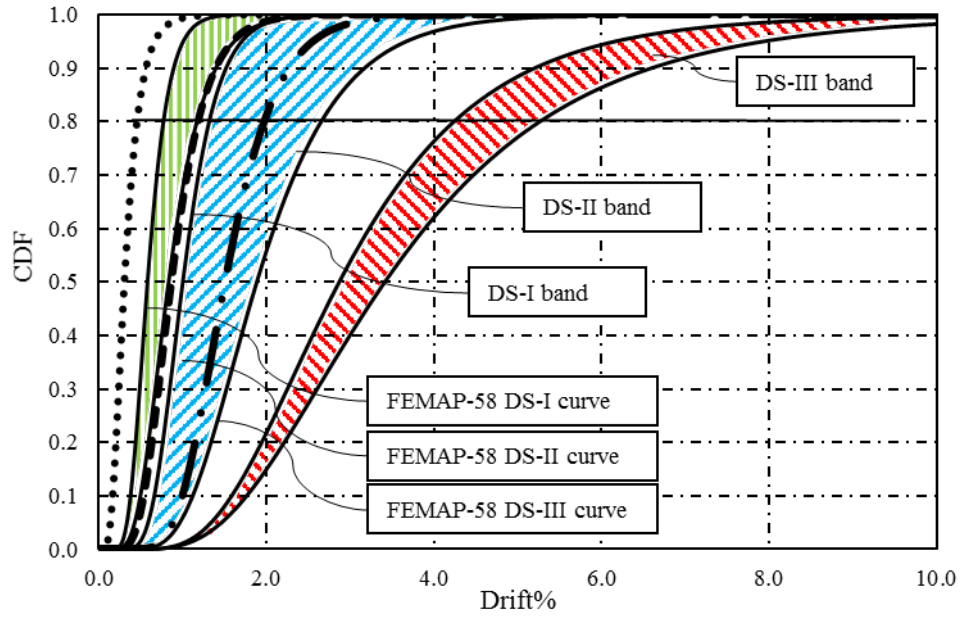


Figure 4.15: Effect of axial stress variability on the fragility curves.

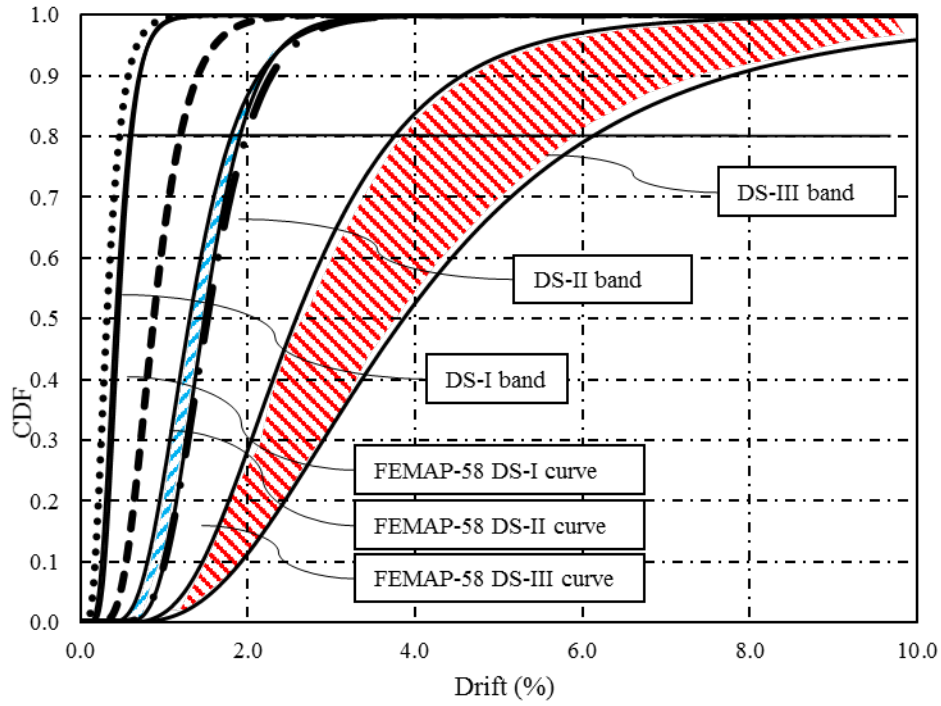


Figure 4.16: Effect of  $\rho_{sh}$  variability on the fragility curves.

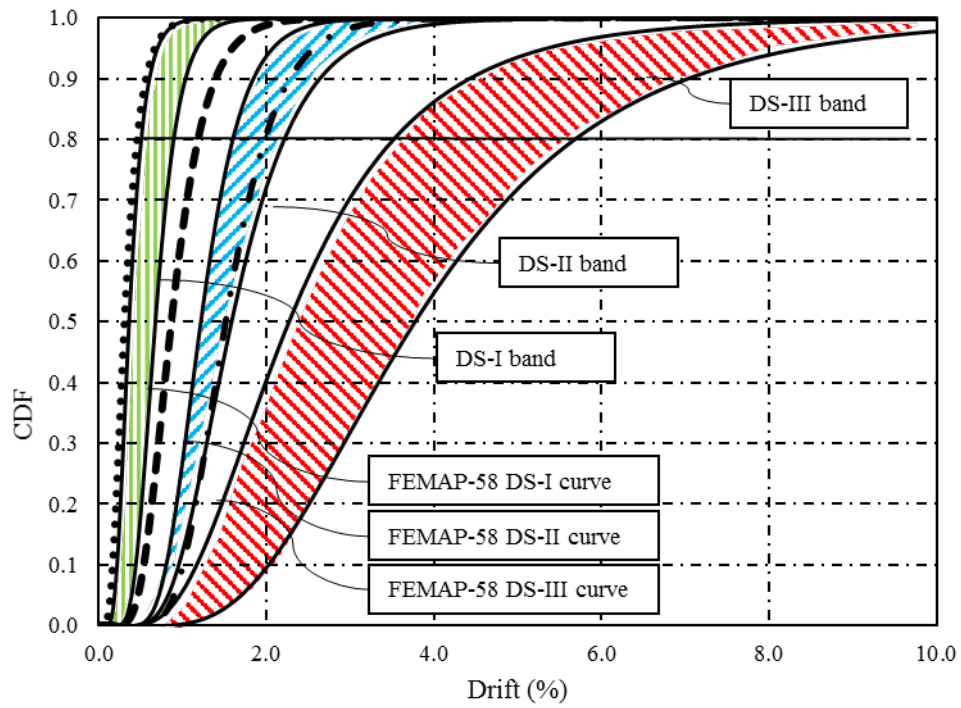


Figure 4.17: Effect of  $\rho_v$  variability on the fragility curves.

## **CHAPTER 5**

### **SUMMARY, CONCLUSIONS, AND RECOMMENDATIONS**

#### **5.1 SUMMARY**

This dissertation focuses on developing reliable parameters that can be adopted for predicting the response of flexurally dominated RMSW within different seismic design frameworks (i.e. FBSD, DBD, and PBSB). More specifically, this dissertation highlights the reliability of different plastic hinge models used to evaluate the ductility behavior of RMSW, when FBSD is used. In addition, this dissertation contributes towards the DBSD through developing an analytical model to quantify RMSW displacement at peak lateral load. This model utilizes MVDA through two different techniques (i.e. PCA and PLS). The results demonstrate the sensitivity of the developed model to different geometrical and mechanical RMSW characteristics. Afterwards, the developed model is extended to identify the ultimate displacement, defined as that associated with degradation to 80% of the strength and the subsequent linkage to different DSs within the PBSB approach. Finally, a comparison is performed to evaluate the differences between the fragility curves presented in FEMA P-58/BD-3.8.10 and the fragility bands introduced in this dissertation. It is hoped that this dissertation would provide a comprehensive body of work toward codification of RMSW seismic response through developing reliable predictive models for the current and next generation of international seismic codes and standards.

## **5.2 CONCLUSIONS**

The utilization of different statistical techniques to analyze and synthesize the experimental results of flexurally dominated RMSW facilitated the development of a reliable complete backbone curve. In addition, the dissertation contributes to the knowledgebase in this area by introducing a more meaningful way of visualizing fragility/damageability of RMSW linked to different DSs. The following presents overview conclusions based on the research reported in the previous chapters.

The assessment of different RMSW response prediction models available in the literature shows the deviation of these model predictions from the corresponding experimental results. This deviation is attributable to either the model formulation simplicity and/or the model development rationale. Simple models generally lack the ability of capturing the influence of altering the geometrical and material characteristics and therefore these models are typically not very accurate in terms of predicting RMSW lateral displacements. Moreover, the majority of current models are based on RCSW experimental results, where concrete characteristics and reinforcement detailing in RCSW differ from their counterparts in RMSW. Nonetheless, all available models are calibrated and their reliability is assessed based on RMSE and residual analysis. Subsequently, the Shedid and El-Dakhakhni (2013) calibrated model is then selected, based on its improved capability of predicting the experimental results, to evaluate the influences of altering RMSW design characteristics on their maximum drift

capacities. Nonetheless, these calibrated models do not explicitly account for the additional shear deformation contribution to the overall wall displacement.

In this dissertation, linear regression analysis is initially performed to assess the reliability of the available plastic hinge models in the literature. Not only because the regression analysis is based on considering the least square error in the y-axis direction between the dependent variable and the model, but because the same analysis is typically used in univariate problems, when only a single independent variable is considered. As such, the MVDA, through the PCA and PLS techniques, overcomes the aforementioned error type calculation and the univariate consideration. These techniques minimize the error orthogonally to the model, not on the y-axis direction, and can thus introduce multiple regressions. While the PCA technique is a projection method that helps visualizing all the information contained within the data set, the PLS technique generalize and combines features from PCA technique and multiple regressions. In this dissertation, the PCA and PLS techniques are performed on the experimental RMSW database and the resulting two main graphical representations (i.e. the scoring and the loading plots) were used to develop different conclusions. The scoring plot shows the projection of the experimental database walls on a new plan defined by the first and the second principal components, whereas walls sharing the same characteristics are grouped (clustered) together. In addition, walls located close to the origin of the score plot indicate their average characteristics among the walls within the experimental database. The loading plot in the PLS techniques shows the relationship

(correlation) between the wall parameters (independent variables) and the wall response in terms of lateral drifts (dependent variable). As the information gained from the loading plots concurred with basic mechanics, subsequent dimensional analysis and model calibration are conducted.

The PCA and PLS analyses are implemented in this dissertation to predict the displacements at both the peak lateral load and the ultimate displacement limit states. The resulting MVDA-based model can predict the backbone curve of walls with different properties (e.g. wall length, height, yield and ultimate curvatures, and the axial stress-level). In addition, the model was used to generate an analytical database to evaluate key parameters affecting RMSW peak lateral load and the ultimate displacement limit states. Based on this evaluation, the horizontal reinforcement ratio,  $\rho_{sh}$ , has the most significant effect on lateral displacements of walls with low aspect ratios. For walls with higher aspect ratios, lateral displacements are bounded by the influence of the (low) axial stress as an upper bound and the influence of the (high) amount of vertical reinforcement ratio,  $\rho_v$ , as lower bound. In addition, the influence of the masonry compressive strength,  $f'_m$ , or  $\rho_{sh}$  on the RMSW displacements at different limit states can be ignored compared to the axial stress-level and  $\rho_v$  for high aspect ratio walls.

With a reliable backbone curve for RMSW being readily available, different DSs (I, II, and III) are developed as per FEMA P-58 definition. The FEMA P-58 gives individual fragility curve for each DS due to the limited number of walls and narrow

parameter range within the experimental results utilized to produce these individual curves. However, the analytically generated RMSW results database showed the variability (as it relates to the range of wall design parameters) within the damageability of the wall under the same demand (drift) levels. In this respect, the concept of fragility bands is introduced in this dissertation as an alternative to fragility curves. Within the mechanical parameter variability, each DS is more sensitive to one or more parameters over the others. The comparison between the FEMA P-58 fragility curves and the proposed fragility bands reveals that at DS-I, FEMA P-58 fragility curves match the upper bound of the developed fragility bands. In addition, at both DS-II and DS-III, the FEAM P-58 fragility curves are consistently associated with higher probabilities of damage at lower drift ratios compared to the developed fragility bands. This inconsistency between the FEMA P-58 fragility curves and the proposed fragility bands is attributable to the fact that FEMA P-58 curves are based on a limited number of walls (only 44 wall) with aspect ratio equals to 1.00 compared to much larger dataset (968 Wall) with wide range of aspect ratio and covers wide range of different mechanical and geometrical parameters. This limited number of walls with their narrow range of characteristics is expected to yield lower drift levels for different DS within the FEMA P-58 curves compared to those of the fragility bands introduced in this dissertation.

### **5.3 RECOMMENDATION FOR FUTURE RESEARCH**

This dissertation presents the application of PCA and PLS techniques, on an experimental results database, in order to develop an analytical model that can predict the response of flexurally dominated RMSW at different limit states. In addition, the dissertation evaluates the influence of altering both the mechanical and geometrical wall parameters on the RMSW behavior through a large analytically generated database. Nonetheless, several issues remain unresolved and might require further investigation. The following points highlight some of the possible areas to extend the use of PCA and PLS techniques to contribute to the knowledgebase pertaining to the development of RMSW response prediction models.

1. The results showed the importance of the inelastic displacements component in evaluating the different DSs associated with backbone curves. However, reliability analyses (using the Mont Carlo simulation or the first-order reliability method) are necessary to codify the proposed model, for different RMSW SFRS categories. Subsequently, calibration factors might need to be introduced for different reliability indices as the key step towards codification of the model.
2. The backbone curve proposed in this dissertation can also be further utilized in numerical models (e.g. OpenSees and etc.) for different flexurally dominated RMSW scenarios. The results of these scenarios can be

considered as a testbed to evaluate the seismic performance of such walls using both pushover and incremental dynamic analysis. This evaluation will aim to assess the seismic performance variability of RMSW for any combination of parameters through performing multiple nonlinear time history analyses under different suits of ground motion records. Also, model sensitivity to both the incremental dynamic- and pushover analysis is needed to identify the most influential parameters (within the range of the investigated ones) on the RMSW response. In addition, uncertainty analyses (e.g. Mont Carlo simulation; point-estimate method; and/or first-order second moment method) is key to estimate the uncertain propagation of such parameters on the RMSW response.

3. Finally, this dissertation used different statistical techniques to assess the capability of available models of simulating the response of flexurally dominated (i.e. slender) shear walls. In future studies, such techniques might be used to assess other response predictive models pertaining to other masonry components [e.g. masonry piers and shear dominated (squat) walls, as well as walls with boundary elements].